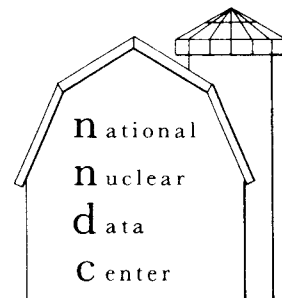# EVALUATION OF NATURAL CHROMIUM NEUTRON CROSS SECTIONS FOR ENDF/B-V

A. PRINCE AND T.W. BURROWS

February 1979

INFORMATION ANALYSIS CENTER REPORT

national
nuclear
data
Center

EVALUATION OF NATURAL CHROMIUM NEUTRON CROSS SECTIONS FOR ENDF/B-V

A. PRINCE AND T.W. BURROWS

February 1979

INFORMATION ANALYSIS CENTER REPORT

DISCLAIMER

ABSTRACT

This report describes the evaluation of natural chromium for ENDF/B-V.

Neutron cross sections and photon production are presented for the energy range 10^{-5} eV to 20 MeV.

An extreme effort was made to incorporate all available new experimental data since the previous ENDF/B-IV evaluation. Particular consideration was also given to consistency between model calculation and experimental data and are described in detail.

Covariance files are given and are based on model code uncertainties along with empirical data.

CONTENTS

LIST OF TABLES

TITLE

LIST OF FIGURES

I. INTRODUCTION

This report describes a re-evaluation of Cr (Nat) for ENDF/B-V and supersedes the ENDF/B-IV, MAT=1191, evaluation by A. Prince (ENDF-246 (1976).[1] Neutron cross section and photon production data are given between 10^{-5} eV and 20 MeV. The cross sections included are total, elastic, non-elastic, inelastic capture, (n,p), (n,d), (n,t), (n,^{3}He), (n,α), (n,2n), (n,3n), (n,nα), (n,np), and gas production. The photon data include multiplicities and transition probabilities, photon production cross sections, and secondary energy spectra.

The major differences in this re-evaluation are the inelastic excitations, the n-particle cross sections, and the photon production cross sections, which are based on new experimental data. The analysis of these data required a higher level of sophistication in the model code treatment and the results are reported herein.

II. CALCULATIONS AND COMPARISON WITH EXPERIMENT

A. Resonance Region

The resonance parameters and background used in determining the total, elastic, and capture cross sections up to 642.85 keV are the same as ENDF/B-IV.[1] The 0.0253 eV values are σ_{tot}=7.446 b, σ_{elas}=4.342 b, σ_{ny}=3.104 b, and the capture resonance integral at a 0.5 eV cutoff is 1.652 b.

Figures 1 and 2 show the total cross section for natural chromium from 10^{-4} eV to 650 keV.

B. Continuum Region

1. **Total Cross Section.** The amount of experimental data on the total cross section at energies above the resonance region is voluminous; however no significantly new experiments have been reported since the ENDF/B-IV[1] evaluation. Thus, the data of Perey et al.[2] (as in ENDF/B-IV) were spline fitted in this region which exhibit rapid fluctuations (E<5.0 MeV). Beyond this region up to 20.0 MeV, optical model calculations were used. Figures 3 to 12 show the fits and calculations compared to the experimental data.

The potential used in the optical model calculations had the conventional form given below. The method used in determining the numerical values of the parameters used in the potential has been given in ref. 3.

$$V(r) = -V_R f(R_R a_R r) - iW_v f(R_I a_I r) + i4a_I W_s f'(R_I a_I r)$$

$$+V_{so}\left(\frac{\hbar}{m_\pi c}\right)^2 \frac{1}{r} f'(R_{so} a_{so} r)\bar{\sigma}\cdot\bar{\ell} \ .$$

where

$$f(R_I a_I r) = \left[1 + \exp\frac{r - R_I}{a_I}\right]^{-1} ,$$

and:

V_R = depth of the real potential,

W = depth of the imaginary potential (v = vol, s = surf),

V_{so}= depth of the spin-orbit potential,

R_R = radius of the real nuclear potential

R_I= radius of the imaginary nuclear potential,

a_R = diffuseness paramenter of the real potential,

a_I = diffuseness parameter of the imaginary potential,

a_{so}= diffuseness parameter of the spin-orbit potential,

m_π = pion mass,

σ = Pauli's spin operator, and

l = orbital angular momentum operator.

In order to obtain the contribution of the direct inelastic scattering component (see Section 5), a vibrational model undergoing dynamic deformations about a spherical shape was assumed. Thus, the radius in Eq. (1) was expressed as:

$$R = R(\theta,\phi) = R_0 \left[1 + \sum_{\lambda\mu} \alpha_{\lambda\mu}(\theta\ \phi) \right] \quad , \tag{2}$$

where

$\alpha_{\lambda\mu}$ may be described in terms of the deformation parameter β. The optical model parameters derived for the chromium isotopes are given below (all E in MeV and in the laboratory system).

^{52}Cr

V_R = (50.9617-0.574 E) MeV

W_S = (6.18+0.4195 E + 0.0089 E^2) MeV

W_V = (0.0) MeV

V_{so}= (7.35) MeV

r_R = (1.2647-0.00527 E) fm

R_S = (1.3202-0.00527 E) fm

r_{so}= r_R

a_R = (0.7692-0.00528 E) fm

a_S = (0.4638-0.00318 E) fm

a_{so}= a_r

^{50}Cr

V_R = (51.6137-0.584 E) MeV

W_S = (6.2984+0.4192+0.0086 E^2) MeV

W_V = (0.0) MeV

V_{so} = (7.6) MeV

r_R = (1.2584-0.0037 E) fm

r_s = (1.3142-0.0037 E) fm

r_{so} = r_R

a_R = (0.7640-0.005 E) fm

a_{so} = a_R

^{54}Cr

V_R = (48.8352-0.544 E) MeV

W_S = (5.871+0.4217 E + 0.0099 E^2) MeV

W_V = (0.0) MeV

V_{so} = (6.89) MeV

r_R = (1.2658-0.0039 E) fm

r_s = (1.3210-0039 E) fm

r_{so} = r_R

a_R = (0.7756-0.00564 E) fm

a_s = (0.466-0.0034 E) fm

a_{so} = a_R

^{53}Cr

V_R = (47.3319-0.516 E) MeV

W_S = (5.716+0.4294 E + 0.0114 E^2) MeV

W_V = (0.0) MeV

V_{so} = (6.75) MeV

r_R = (1.2628-0.0039 E) fm

r_s = (1.3182-0.0039 E) fm

r_{so} = r_R

^{53}Cr (cont)

$$a_R = (0.7729-0.0058 \ E) \ \text{fm}$$

$$a_S = (0.4649-0.0035 \ E) \text{fm}$$

$$a_{so} = a_R$$

While the optical model calculations were carried out over the entire energy range, only the calculated total cross sections for E>5.0 MeV were used. These cross sections are shown in Figs. 11 and 12. However, all of the calculated angular distributions were used for generating the Legendre coefficients for File 4. Likewise, the transmission coefficients calculated from these potentials were also used to describe the inelastic and n-particle cross sections (see the following Sections).

2. **Non-Elastic Cross Section.** The non-elastic cross section, up to about 5.0 MeV, is due primarily to $\sigma_{nn'}$ and $\sigma_{n\gamma}$.

Slightly above this energy, the n,p and n,α contributions become significant. At still higher energies, the n,2n and other reactions must be considered.

Direct measurements of σ_{non} are practically non-existent. There is a rather old set of experimental data by Taylor et al.,[4] who carried out spherical shell transmission measurements in the energy range of 3.5 to 14.1 MeV. There is one other experimental measurement at E = 2.5 MeV (σ_{non} = 1.4±0.3 b) reported by Strizhak.[5]

Up to E = 4.0 MeV, the non-elastic cross section was determined from the experimental data on $\sigma_{nn'}$ and $\sigma_{n\gamma}$, with σ_{non} = $\sigma_{n\gamma}$ for E < 650 keV. In evaluating σ_{non} for the higher energies, a combination of the experimental direct measurements of Taylor et al.[4] and the σ_{tot} and σ_{el} measurements of Kinney and Perey[6] were used in conjunction with the optical model calculations.

A comparison of the evaluated, experimental, and model calculations are shown in Fig. 13. In this figure σ_{non} is 3.8 mb at 650 keV, a value too small to be seen on a linear-linear plot.

3. **Elastic Cross Section.** For energies between the resonance region and 1.5 MeV. The ANL groups [7-9] have produced quite a bit of angular data. At higher energies, the data are rather sparse with the major portion coming from Refs. 10 to 12. Thus, as in ENDF/B-IV, the additional angular distributions necessary to fill the gaps were described by optical model calculations.

In the highly-structured region, the total elastic cross section was determined by subtracting the non-elastic from the total cross section. For energies E>5.0 MeV, a combination of model calculations and experimental data on the non-elastic were used.

The comparisons between the evaluated elastic cross section and the experimental angle-integrated data are shown in Figs. 14 to 23.

In Figs. 24 to 32, the optical model calculations of the differential scattering are compared to some experimental results. These calculations were used to generate the Legendre coefficients in File 4.

4. <u>Radiative Capture Cross Section.</u> Above the resolved energy region ($\tilde{E}>0.7$ MeV), the capture cross sections were determined from calculations using COMNUC[13] for the compound nucleus capture, taking into account $\sigma_{nn'}$ competition, and FISPRO[14] for the direct and collective capture. At energies E>10 MeV, the capture cross section resulting from compound nuclear processes was negligible and the calculated direct and collective results were normalize to th 14 MeV experimental point of Cvelbar et al.[15]

This direct and collective calculation resulted in a slight peaking of the cross section at E_n=17 MeV, as seen in Fig. 33. A similar peak, at about the same energy, was reported by Nishimura et al.,[16] however, their results are high by about a factor of two. This could be due to the fact that they did not normalize to the 14 MeV data point Cvelbar.[15]

5. <u>Inelastic Scattering Cross Sections.</u> As mentioned earlier, one of the <u>major</u> changes in the ENDF/B-V Cr evaluation occurs in the inelastic cross section. These modifications results from primarily two sources, namely, recent measurements and new level structure data.

In ENDF/B-IV, the evaluation was primarily based on the data of Van Patter et al.,[17] who analyzed differential gamma-ray spectra from the (n,n'γ) reaction and converted the data to inelastic scattering cross sections. Other experimental data were also used.[18-22] These experiments produced neutron inelastic scattering data for some individual levels of chromium for neutron incident energies, E_n < 4.0 MeV. Kinney and Perey[6] made measurements for natural Cr between 4.07 and 8.56 MeV and ^{52}Cr for energies between 6.44 and 8.56 MeV. These latter experimental data were very significant in determining not only the level excitations for the low-lying levels in ^{52}Cr and Cr(Nat) at the higher energies, but also in establishing the importance of the direct inelastic contributions.

However, the more recent experimental data of the Lowell group,[23,24] with improved measurement techniques, showed that more low energy (E<4 MeV) level excitation cross sections could be resolved. The ENDF/B-IV evaluation, based on the previous measurements were only in fair agreement with the Lowell results, differing as much as 30% in some cases.

The Lowell group measured absolute 125 degree differential gamma-ray production cross sections for neutron scattering in natural chromium, for neutrons in the 0.84 to 3.97 MeV region. From these measurements, they inferred neutron inelastic scattering cross sections for several individual states in ^{50} ^{52} ^{53} ^{54}Cr. It was observed that the excitation fuhctions displayed considerable structure and provided a possible explanation for the rather large inconsistencies that appear among the previous measurements.

These fluctuations had also been observed by the measurements at Karlsruhe[25] and by Tessler and Glickstein[26] and are believed to be the reason for the high discrepancy existing between the various experimental data.

The ENDF/B-IV Cr evaluation relied on the data of Refs. 17 to 22, where, according to the Lowell group, the energy increments for excitation functions were much broader than the structure expected from the neutron energy spread. Therefore, all the level excitations in the Cr isotopes were re-evaluated in terms of the Lowell results. The energy levels associated with the chromium isotopes are given in Table 1.

Table 1
Energy Level Schemes Used for H-F Inelastic Scattering Calculations

Cr-50		Cr-52		Cr-53		Cr-54	
E(MeV)	J^{π}	E(MeV)	J^{π}	E(MeV)	J^{π}	E(meV)	J^{π}
0.000	0^+	0.000	0^+	0.000	$3/2^-$	0.000	0^+
0.783	2^+	1.434	2^+	0.564	$1/2^-$	0.835	2^+
1.879	4^+	2.370	4^+	1.006	$5/2^-$	1.827	4^+
2.922	2^+	2.647	0^+	1.287	$7/2^-$	2.619	2^+
3.160	2^+	2.768	4^+	1.539	$7/2^-$	2.829	0^+
3.320	4^+	2.965	2^+	1.973	$9/2^-$	3.074	2^+
3.693	2^+	3.114	6^+	2.171	$1/2^-$	3.437	2^+
3.787	5^+	3.162	2^+	2.233	$7/2^-$	3.487	4^+
3.895	0^+	3.414	4^+	2.321	$3/2^-$	3.800	4^+
4.524	3^-	3.471	3^+	2.455	$1/2^-$	4.015	0^+
4.653	2^+	3.617	5^+	2.661	$5/2^-$	4.129	3^-
		3.771	2^+	2.670	$1/2^-$	4.573	0^+
		3.947	1^+	2.711	$1/2^-$		
		4.015	5^+	2.775	$5/2^-$		
		4.039	4^+	2.995	$5/2^-$		
		4.563	3^+	3.132	$9/2^-$		
		4.630	4^+	3.153	$3/2^+$		
		4.837	4^+	3.186	$3/2^-$		
		5.097	4^+	3.268	$3/2^+$		
		5.292	2^+	3.352	$7/2^-$		
		5.585	0^+				
		5.737	0^+				
		6.070	2^+				
		6.154	2^+				
		6.490	3^+				
		6.820	2^+				
		7.070	3^-				
		7.900	3^-				

As with the previous evaluation, it was necessary to carry out Hauser-Feshbach calculations for the discrete and continuum inelastic cross sections to fill the gaps and also compare with the experimental data. The latter analysis provided a reasonable substantiation of the various model parameters used in the calculations.

The anisotropy observed in the differential inelastic scattering data of the ORNL group dictated that a coupled-channel analysis also be carried out for the low-lying collective levels. It was assumed that the higher states are weakly coupled to the ground state so their contributions to the direct inelastic excitation were taken to be negligible.

    a. <u>Comparison of Calculations with Experimental Data</u>. Model calculations, based on the Hauser-Feshbach formalism modified to account for width fluctuations, provided data for both the discrete and continuum inelastic cross sections for the Cr isotopes. The analysis was carried out using a

combination of the statistical model codes COMNUC[13] and the early version of Uhl's code[27](a) (now called STAPRE[27](b)).

In order to obtain meaningful comparisons of the theoretical calculations with experiment, certain corrections had to be considered. First the calculations for the inelastic cross sections for the individual isotopes, when weighted by their respective abundances, had to be renormalized so as to be in agreement with the total inelastic cross section of natural Cr, which, in turn, had to made consistent with the predictions in the non-elastic, i.e.,

$$\sigma_{nn'}(tot) = \sigma_{non} - (\sigma_{n,\gamma} + \sigma_{n,3n} + \Sigma\sigma_{nx} + \Sigma\sigma_{nxn'} + \Sigma\sigma_{nn'x}) \qquad (3)$$

where:

$$x = p,d,t,{}^3He,{}^4He.$$

Also, the inconsistency between the Hauser-Feshbach calculations of the inelastic scattering and the coupled-channel calculations was removed by introducing a reduction factor R given by:

$$R = \frac{\sigma_{expt'l} - \sigma_{direct\ inelastic}}{\sigma_{expt'l}} \qquad (4)$$

where it has been assumed that the difference between the experimental inelastic cross section and the direct inelastic cross section is the true compound inelastic cross section.

While all the levels shown in Table 1 were used in calculating the excitation functions for the various isotopes, only the first low-lying levels of ^{50}Cr (0.7831 MeV) and ^{54}(0.8348 MeV) were put into ENDF/V as discrete. The rest of the level excitations for these two isotopes were put into the continuum. This was necessary since the present ENDF format allows for only 40 discrete levels.

On the other hand, all the levels for ^{52}Cr up to and including the one at 5.097 MeV, and all those for ^{53}Cr were taken into consideration, giving a total of 38 excitations in the discrete region for ^{52}Cr and ^{53}Cr.

The various calculations were run with pre-equilibrium fractions using the Uhl code. More will be said about this later in the discussion of the n-particle cross sections.

In the case of inelastic scattering at low energies, i.e., below the continuum threshold (E< 1.86 MeV), the Uhl code greatly underestimated the compound-elastic contribution. The failure of the early version [27](a) of the code to take width fluctuations into account and the coarse grid of the generated internal table of transmission coefficients caused this underestimation. However, after adjustment of the compound elastic from the COMNUC results, the agreement with experimental data was greatly improved.

The foregoing analysis of the isotopic Cr inelastic cross sections was abundance weighted (see Table 2) to provide the inelastic contributions for natural Cr. These results are presented in Figs. 34 to 50, where the comparisons with the Lowell data are shown. It should be noted that the structure in the evaluated data (e.g., Figs. 34-36, 38, 40) arises not so much from the calculations but shape-fitting and renormalization to the experimental results.

Table 2
Natural Abundance and Mass of Cr Isotopes

Isotopes	% Abundance	Mass (amu)	S_n (MeV) [a]
50	4.35	49.946049	9.262
52	83.79	51.940510	7.940
53	9.50	52.940651	9.720
54	2.36	53.938881	6.246

[a] S_n = Binding energy of last neutron in compound nucleus.

The most important level due to its large contribution, is the 1.434 MeV level of ^{52}Cr. The amount of experimental data for this level provided adequate confirmation for both its magnitude and shape (see Fig. 39).

The total inelastic scattering for natural chromium is shown in Fig. 51 from threshold to 4.0 MeV and Fig. 52 to 20.0 MeV. This evaluated curve includes the abundance weighted discrete and continuum contributions of all four isotopes.

The wide gap in the experimental data for $E_n > 3.5$ MeV required a careful consideration of the competing processes (n,2n), (n,3n), (n-particle) so that an adequate interpretation of the total inelastic cross section would result in the high energy region. The various experimental results around 14.0 MeV were of particular importance in satisfying these criteria.

A good agreement having been established between the optical model calculations and the experimental results of Taylor el al.[3] for the non-elastic cross sections, the contributions for all competing processes were subtracted such that Eq. (3) was satisfied for all significant reactions below 20.0 MeV. Table 3 shows all these reactions which includes those used in the evaluated file.

A few details of the various experimental points at 14 MeV are worth mentioning since their interpretation played a very important role in fixing the value of the cross section at this energy.

Salnikov and Lovchikova[28] analyzed the energy spectra of the inelastically-scattered neutrons at various angles, and thus, obtained the differential inelastic cross section. They reported a value of $\sigma_{nn'} = 880 \pm 40$mb.

Fujita el al.[29] also measured the continuous spectra of inelastically-scattered neutrons using a time-of-flight method. They made their measurement at only one angle ($\theta = 110°$) and assumed isotropic scattering. Their value of $\sigma_{nn'} = 1.27 \pm 0.13$ b was not used in the evaluation since it is at great variance with other measurements at this energy. The probable reason for this value is due to the fact that they assumed isotropic scattering and ignored certain n, particle reactions which emitted neutrons.

Tagesen and Hille,[30] along with Breunlich and Stengel,[31] detected the gamma-rays resulting from the de-excitation of the excited states similar to the method of Van Patter et al.[17] Tagesen and Hille[30] established an upper bound of $\sigma_{nn'} = 870 \pm 80$ mb, based on certain observations of the n,2n reaction. They also carried out an absolute determination of the inelastic cross section achieving a value in agreement with $\sigma_{nn'} = 740$ mb $\pm 20\%$ reported by Morgan et al.[32]

Table 3
Q Values for Possible Neutron-Induced Reactions
in Cr for $E_n \leq 20.0$ MeV

Reaction	Cr-50 -Q(MeV)	Cr-52 -Q(MeV)	Cr-53 -Q(MeV)	Cr-54 -(MeV)	ENDF MT
(n,p)	0.257	3.196	2.640	6.220	103
(n,^{3}He)	8.628	10.844	12.412	14.325	106
(n,n'd)	18.920	19.335	16.222	18.631	
(n,n'^{4}He)	8.555	9.353	9.150	7.927	22
(n,^{4}He,n')	8.555	9.353	9.151	7.927	2
(n,p,^{4}He)	10.139	12.562	10.374	14.031	
(n,2n)	12.939	12.041	7.940	9.720	16
(n,d)	7.364	8.282	8.911	10.135	104
(n,^{4}He)	-0.322	1.211	-1.794	1.554	107
(n,n't)	23.200	22.409	21.017	19.685	
(n,p,n')	9.588	10.507	11.136	12.360	28
(n,^{4}He,p)	10.140	12.562	10.374	14.031	
(n,3n)	23.581	21.302	19.981	17.660	17
(n,t)	12.662	13.077	9.965	12.374	105
(n,n'p)	9.590	10.507	11.136	12.360	28
(n,n'^{3}He)	20.255	21.788	18.784	22.132	
(n,2p)	8.204	12.190	12.323	16.863	
(n,d,n)	18.919	19.335	16.222	18.631	

Breunlich and Stengel[31] quoted a value of $\sigma_{nn'}= 790\pm112$ mb of which, based on an assumption by Uhl,[33] 100 mb is due to the direct inelastic scattering process. Colli and Marcazzan[34] have also reported that at 14 MeV precompound emission might account for as much as 30% of the inelastic cross section.

The combined results of the (n,2n) and (n,particle) cross sections were determined to be about 0.58 b at 14.0 MeV (see Section 6). From a value of $\sigma_{non}=1.31$ b, the total inelastic scattering cross sections turned out to be 0.73 b which is in excellent agreement with the aforementioned experimental results. This agreement at 14.0 MeV provides a rather high level of confidence for the total inelastic scattering in the higher energy region.

b. <u>Differential Inelastic Scattering</u>. As mentioned earlier since the ORNL data on the inelastic angular distributions showed some anisotropy, it seemed advisable to carry out coupled-channel calculations. These calculations were carried out using a modified version of JUPITOR.[35]

Figures 53 to 58 show the comparison between the compound differential inelastic and the direct differential inelastic (coupled-channel calculations) of the 1.434-MeV (2+) and 2.369-MeV (4+) levels in ^{52}Cr. The sum of the compound and direct contribution produces the total differential inelastic cross section. The experimental data is that of Kinney and Perey.[6] Note the symmetry about 90° in the compound inelastic process (Hauser-Feshbach

calculations) as compared to the high forward peaking in the direct process. This forward peaking accounts for some asymmetry about 90° in the calculations as to be expected; however, the Kinney and Perey[6] data do not show this since their measurements ranged only from 35.7 to 135.4 degrees.

The measurements at 14.0 MeV,[36] shown in Fig. 59, definitely shows the high degree of anisotropy in the differential inelastic which is assumed to be due primarily to the direct excitation of these levels. The coupled-channel calculations, while producing a satisfactory shape, slightly under-estimated the magnitude of the cross section by about 20%. However, it should be mentioned that this experimental data of Stelson et al.[36] are for natural Cr which means that the data for the 1.434-MeV level possibly contain a con-tribution from the 1.287-MeV level in ^{53}Cr. The solid curves in Fig. 59 have been normalized to the experimental data at 60°. These calculated inelastic angular distributions have been incorporated into File 4 in the form of Legendre coefficients.

6. <u>Neutron Emission and n-Particle Cross Section</u>. The relative sparsity of experimental data on the various reactions, such as the (n,2n), (n,3n), (n,p), (n,α), etc., made this evaluation highly dependent on model calculations. As noted in the previous Section, the statistical model code of Uhl[27(a)] played a vital role in calculating these reaction cross sections. For those reactions which could not be handled by the code, namely (n,t) and (n,^{3}He), the evaporation code THRESH[37] was used.

Calculations were carried out for all energetically possible re-actions (see Table 3) on the four stable isotopes of chromium. As an example of the various reaction channels considered in the Uhl code calculations, a schematic of the reaction ^{54}Cr(n,3n) is given in Fig. 60. The squares in relief show the various compound nuclei considered at each step of the calcu-lation. Other residual nuclei for which data must be provided are also in-dicated.

The transmission coefficients employed as input to the Uhl code were generated by the code ABACUS-2.[38] The neutron optical model parameters neces-sary for the various residual nuclei were generated by the method mentioned earlier.[3]

The optical model parameters necessary for proton, neutron, and α-particle emission are given below.

<u>Proton Parameters</u>: F.D. Becchetti and G.W. Greenlees, Phys. Rev. <u>182</u>, 1190 (1969).

$$V_R = 54.0-0.32\ E + 0.4\ Z/A^{1/3} + 24.0\ (N-Z)/A$$

$$r_R = 1.17\ fm$$

$$a_R = 0.75\ fm$$

$$W_V = 0.22\ E - 2.7\ \text{or zero, whichever is greater}$$

$$W_{SF} = 11.8-0.25\ E + 12.0\ (N-Z)/A\ \text{or zero, whichever is greater}$$

$$r_I = 1.32\ fm$$

$$a_I = 0.51+0.7\ (n-Z)/A\ fm$$

$$V_{so} = 6.2$$

$$r_{so} = 1.01 \text{ fm}$$
$$a_{so} = 1.01 \text{ fm}$$

Where E is the incident laboratory energy, (in MeV).

Deuteron Parameters: F. Hinterberger, Nucl. Phys. A111, 265 (1968).

$$V = 100 + 2.5 \, Z/A^{1/3} - 0.5 \, E$$
$$r_v = 1.05 \text{ fm}$$
$$a_v = (0.71 + 0.04 \, A^{1/3}) \text{ fm}$$
$$W = (5.0 + 2.0 A^{1/3}) \text{ MeV}$$
$$r_W = 1.28 \text{ fm}$$
$$a_W = 0.71 + 0.02 \, A^{1/3}$$
$$V_{so} = 6.0 \text{ MeV}$$
$$r_c = 1.3 \text{ fm}$$
$$r_{so} = r_v$$
$$a_{so} = a_v$$

Where E is the incident laboratory energy, (in MeV).

Alpha Parameters: R. Bock, Nucl. Phys. A92, 539 (1967).

$$V_R = 183.7 \text{ MeV}$$
$$r_R = 1.4 \text{ fm}$$
$$a_R = 0.564 \text{ fm}$$
$$W_{vol} = 26.6 \text{ MeV}$$
$$r_w = r_R$$
$$a_w = a_R$$
$$r_c = 1.3 \text{ fm}$$

It should be noted that as a preliminary step to substantiate these global optical-model parameters, a comparison of the experimental angular distribution and polarization data to the calculations was performed. Where specific experimental data on chromium did not exist, the comparison was made with experimental data in the region around chromium.

Also incorporated in the statistical model calculations were a "best-set" of level-density parameters, based on the work of Dilg et al.,[39] which reproduced the available experimental data (see Tables 4 to 8).

A summary of the level-density parameters, based on the back-shifted Fermi gas model,[39] are presented below.

Level-Density Parameters:

$$\sigma_{rigid} \approx 0.0150 \, A^{5/3} \, t \quad (t = \text{thermodynamic temperature})$$

$$at^2 - t = U - \Delta \quad (\text{Effective excitation energy})$$

Average Parameters for 40<A<63.

$$\sigma = \sigma_{rigid}$$

$$r_o = 1.25 \text{ fm}$$

$$a \ (\text{MeV}^{-1}) = 2.40 + 0.067 \ A$$

$$\Delta \ (\text{MeV}) = 130 \ A^{-1} + P$$

$$P = \begin{cases} 2 \ \delta \ A^{-1/2} & \text{doubly even} \\ \delta \ A^{-1/2} & \text{odd mass} \\ \mu \ A^{-1} & \text{doubly odd} \end{cases}$$

$$\delta = 12.8 \text{ MeV}$$

$$\mu = 29.4 \text{ MeV}$$

In the attempt to fit the experimental data in a constant manner, the adjustment of 'a' was constrained to +12% of the above value and of Δ to ±1.0MeV. These constraints were made on the basis of Dilg's quoted mean deviations of 6% and 0.5 MeV, respectively. The authors attempted to fit the available experimental data on reactions for all four isotopes simultaneously.

Discrete level information along with spins, parities were obtained from Refs. 40 and 41. The nuclear reaction Q-values (Table 3) were taken from Ref. 42.

All calculations were run with assumed pre-equilibrium fractions of 0%, 20%, and 40%. After comparison with the experimental cross sections, arbitrary fractions of 0% for incident energies below 12 MeV and 20% above (up to 20.0 MeV) were chosen.

Prior to a specific comparison of the calculations with experimental data, it is useful to discuss the problems associated with the version of Uhl's code [27](a) employed and the problems encountered in attempting to reconcile the various data available for the most abundant isotope ^{52}Cr.

As mentioned above, the lack of width fluctuations and the coarse grid of the generated internal table of transmission coefficients in the version of Uhl's code used caused problems in the case of inelastic scattering below E=1.86 MeV. This coarse grid also caused problems in almost all the calculations near the reaction threshold. Also, as with most statistical model codes, Uhl's code cannot account for such phenomenon as the Giant Resonance. In ^{52}Cr, this may be important since the Giant Resonance would be expected at $E_n \approx 8$ MeV, where the ^{52}Cr(n,p) cross section is rapidly rising. However, no data existed in this region which could have given us an estimate of the Giant Resonance effect, if any.

For ^{52}Cr, experimental data exist for the (n,2n), (n,p) and (n,α) reactions for $E_n \geq 14$MeV. Detailed comparisons will be made between the calculations and each set of reaction data below. At this point, an inter-comparison of the available data (see Tables 5 and 6 and Figs. 62, 64, 69) will be made and a discussion of the problems associated with fitting these data, presented. While the calculations reproduce the total inelastic and the (n,p) cross sections fairly well, they overpredict the (n,2n) and (n,α) cross sections. An attempt to fit the (n,2n) and (n,α) data resulted in over prediction of the (n,p) and total inelastic. If the experimental data for the

(n,p), (n,2n), (n,α), and total inelastic were appropriately summed, it will be found that the total nonelastic cross section thus calculated is substantially less than the measured value (see Fig. 13). This would indicate that one or more of the data sets are in error. Since the (n,2n) and (n,α) data in this region were each based on one measurement, Ref. 46 and Ref. 66, respectively, the evaluators placed less weight on these data.

a. Comparison of Calculations with Experimental Data

i. n,2n Cross Sections. As pointed out at the Lowell Conference[43] and Ref. 1 at the time of the ENDF/B-IV evaluation, no data existed for the n,2n reaction in natural chromium, thus the results were highly dependent on model code interpretation. The calculations were carried out for each of the four isotopes and combined with the experimental data of Refs. 44 to 51.

Figure 61 comparies the results for ^{50}Cr (n,2n). As can be seen the agreement with experimental data is rather poor. However, it should be noted that the Bormann data at the higher energies does not portray the shape one would expect for this threshold reaction. It has been pointed out that many experimenters using neutron generators quote a neutron energy which is 200 to 300 keV higher than the actual energy. If this is the case here, then such a shift would slightly improve the fit.

Similarly in Fig. 62, the comparison for ^{52}Cr(n,2n), while fitting the data very well for E<16MeV, shows a deviation beyond this energy. A possible cause for the variance could be the contamination of the neutron spectra above 17 MeV by neutrons from the D(d,n) reaction due to buildup of deuterium on the source target.

Unfortunately, the Bormann data[46] is the only experiment in this range for the ^{50}Cr and ^{52}Cr isotopes, which eliminates any possible comparison with others.

Despite this lack of agreement between the calculations and data for the aforementioned isotopes, the results of the model calculations on ^{53}Cr and ^{54}Cr were combined with ^{50}Cr and ^{52}Cr to yield the n,2n reaction for natural Cr. When these results were compared (see Fig. 63), with the recent data of Frehaut and Mosinski[52] (which we obtained after the evaluation), the agreement was very good. In fact, except for a minor difference near threshold, the ENDF/B-IV data also is in rather goo agreement with the Frehaut data.

One cannot rule out the fact that this harmony between the calculations and experiment might well be fortuitous in that the ^{53}Cr and ^{54}Cr calculations could be causing cancellation effects (e.g., overpredicting and underpredicting), thus leading to such a concurrence.

ii. n,p Cross Sections. With the exception of ^{52}Cr, only a very small number of experiments exist for the n,p reaction in the Cr isotopes and most of them are clustered about 14.0 MeV point. The (n,p) data are based on Refs. 51 and 53 to 64.

Figure 64 shows the calculated values compared to the experimental data for ^{52}Cr(n,p). Since the relatively large amount at "14 MeV" cannot be clearly seen in Fig. 64, the "14 MeV" results are summarized in Table 6. The agreement is fair between 14 to 17 MeV; however, it is rather high in the 12 to 14 MeV region. Changing the model parameters to fit the (n,p) data in this region would manifest itself in an increased n,2n reaction over the entire range; and an underprediction of the n,p reaction above 14 MeV. As seen in

Figs. 61 and 62, the n,2n cross section is already on the high side.

A recent communication from D.L. Smith and J.W. Meadows[65] indicates the possibility that the present evaluation may be overestimating the ^{52}Cr(n,p) cross section in the 6- to 9-MeV region. A possible explanation of this discrepancy would be the effect of the Giant Resonance. As noted above, the Uhl code does not take this effect into account and at the time of the evaluation we had no experimental data in this energy region.

Fig. 65 shows the difference between ENDF/B-IV and -V for the (n,p) cross section of natural Cr. The large difference is caused by the difference in the evaluation of the ^{52}Cr(n,p). For ENDF/B-IV, the shape of the ^{52}Cr(n,p) was calculated using the evaporation model code THRESH and normalized to the "best value" cited by Kenna and Harrison[44]. As has been noted above, the present evaluation, ENDF/B-V, is heavily based on an early version of the statistical model code of Uhl[27(a)]. While the parameters were adjusted in an attempt to fit all experimental data, the final results for the (n, particle) cross sections were not renormalized. There is the possibility that the ^{52}Cr(n,p) cross section is overestimated due to the relatively heavy weight placed on the data of Kern et al.;[54] however, as we noted in the introduction to this section, any reduction in the ^{52}Cr(n,p) cross section would result in an overestimation of the total inelastic, n,2n, and n,α cross sections of ^{52}Cr.

iii. <u>(n,^{4}He) Cross Section.</u> Up until recently only one measurement existed for this reaction and this was for ^{54}Cr.[66]

Dolya et al.[67] at the 1973 Kiev Conference reported on their direct measurement at 14.7 MeV of the (n,α) cross section for all four chromium isotopes. These were angular distribution experiments ranging from 0 to 150 degrees, whose integrated cross sections produced the following:

$$^{50}\text{Cr}(\sigma_{na} = 121.0 \pm 8.5 \text{ mb})$$
$$^{52}\text{Cr}(\sigma_{na} = 40.2 \pm 3.6 \text{ mb})$$
$$^{53}\text{Cr}(\sigma_{na} = 45.1 \pm 3.7 \text{ mb})$$
$$^{54}\text{Cr}(\sigma_{na} = 37.2 \pm 3.0 \text{ mb})$$

These data were used to normalize the model calculations in ENDF/B-IV. In the present evaluation, ENDF/B-V, these data were included in the data set that we attempted to fit by adjusting the model code parameters. However, since it is not clear whether these measurements are of the n,α cross sections or of the total α-production cross sections, some care must be used in considering these values. In Tables 4, 5, 7, and 8 and in Figs. 68 to 72, it is assumed that these measurements are for the total α-production.

The resulting calculations for the (n,α) cross sections and ^{4}He production cross sections for each isotope were weighted by abundance and summed to provide the cross sections for natural chromium (Fig. 72).

iv. <u>Other n-Particle Reactions.</u> The amount of experimental data on reactions such as (n,t), (n,d), (n,np), etc. is very very meager and the evaluation is highly model dependent. However, due to the high threshold for these reactions (see Table 3), they are expected to be of the order of a few millibarns even at 20.0 MeV.

Figures 66 and 67 present the evaluated reaction cross sections for the (n,t) and (n,^{3}He) reactions which are the same as those given in ENDF/B-IV.

Table 4
Selected ^{50}Cr Cross Sections

	E_n (MeV)	Calculated σ (mb)	Experimental σ (mb) Original	Renormalized[a]	Ref.
^{50}Cr(n,p)	14.0	351	277±21	256+19	1
^{50}Cr(n,np)	14.0	406	153+21	141+19	1
^{50}Cr p-production	15.0	811	830+100		3
^{50}Cr d-production	15.0	4.6	12±4		3
^{50}Cr α-production	14.7	102	121±8		2
	15.0	105	94±15		3

[a]Renormalized to ^{54}Fe(n,p) cross sections from ENDF/B-IV Dosimetry File edited by B. Magurno (BNL-NCS-50466, April 1975).

1. D.L. Allan, Nucl. Phys. 24, 274 (1961).
2. G.P. Dolja, YK-11, 9 (1973).
3. S.M. Grimes, R.C. Haight, K.R. Alvar, H.H. Barschall and R.R. Borchers. Reprint UCRL-81802 (1978). To be published in Rev. C. Data received after evaluation.

Table 5
Selected ^{52}Cr Cross Sections

	E_n (MeV)	Calculated σ (mb)	Experimental σ (mb) Original	Renormalized	Ref.
^{52}Cr inelastic	14.0	805	740±180		1
	14.4	710	727±100		2
^{52}Cr(n,p)					
^{52}Cr p-production	15.0	165	180±25		4
^{52}Cr d-	15.0	0	8±3		4
^{52}Cr α-production	14.7	69	40±4		3
	15.0	85	36±6		4

1. S. Tagesen, Acta Phys. Austriaca 23, 31 (1966).
2. S. Breunlich and G. Stengel, Zeit. Natur. A26, 451 (1971).
3. G.P. Dolja, YK-11, 9 (1973).
4. S.M. Grimes, R.C. Haight, K.R. Alvar, H.H. Barschall, and R.R. Borchers. Preprint UCRL-81802 (1978). To be published in Phys. Rev. C. Data received after evaluation.

Table 6

Comparison of "14-MeV" ^{52}Cr(n,p) Cross Sections

En(MeV)	Calculated σ(mb)	Experimental[a] σ(mb)	Renormalized*	Reference
14.1	136	130±30[b]		1
14.1	136	67±10[c]		2
14.8	124	82.7±9		3
14.4	131	115±25		4
14.6	128	96.1±3	95.2±3.0	5
14.7±0.3	126	94±10	105±11	6
14.8±0.2	124	115±15	118±15	7
14.01	137	133.3±15		
14.28	133	109.3±12		8
14.52	128	100±12[d]		
14.99	121	107±12[e]		
14.8	124	118±16	116±16	9
14.8±0.1	124	82.8±5.8	86±6	10
14.8	124	105±10	104±10	11
14.5	128	78±10		12
14.8±0.5	124	73±5	56±4	13
14.7±0.3	126	80±6	76±6	14
14.7	126	82	78.5	15
		Reduced χ^2=26.5	62.5	

[a] All measurements were activation measurements except as noted.

[b] CounterTelescope

[c] Emulsion

[d] Unweighted average of three activiation measurements.

*Where author has given sufficient information on the activation standard, the data have been renormalized to standard values obtained from the ENDF/IV dosimetry file.

1. D.V. Aleksandrov, L.I. Klochkova, and B.S. Kourigin. At. Energia 39,(2), 137 (1975).
2. D.L. Allan, Nucl. Phys. 24, 274 (1961).
3. D.M. Chittenden and D.G. Gardner. Arkansas Report (1961).

4. I.G. Clator. Diss. Abst. _30_, 2850 (1969). Priv. Comm. from T. Clator (1969).
5. J. Dressler, J. Araminowicz, and U. Garuski. INR-1464, 12 (1973).
6. P. Holmberg, R. Rieppo, J.K. Keinaenen, and M. Valkonen. J. Inorg. Nucl. Chem. _36_, 715 (1974).
7. L. Husain and P.K. Kuroda. J. Inorg. Nucl. Chem. _29_, 2665 (1967).
8. B.D. Kern and W.E. Ferguson. Nucl. Phys _10_, 226 (1959).
9. C.S. Khurana and I.M. Covil. Nucl. Phys _69_, 153 (1965).
10. B. Mitra and A.M. Ghose. Nucl. Phys _83_, 157 (1966).
11. S.K. Mukherjee, A.K. Ganguly, and N.K. Majumder. Proc. Phys. Soc. (London) _77_, 508 (1961).
12. E.B. Paul and R.L. Clarke. Can. J. Phys. _31_, 267 (1953).
13. R. Prasad and D.C. Sarkar. Nuoud Cimento A3(3), 467 (1971).
14. S.M. Qaim and N.I. Molla. Ninth Symposium on Fusion Technology (Garmish, 1976), p. 589.
15. J.F. Strain and W.J. Ross, ORNL-3672 (1965).

Table 7
Selected ^{53}Cr Cross Sections

	E_n (MeV)	Calculated σ(mb)	Experimental σ(mb) Original	Renormalized[a]	Ref.
^{53}Cr(n,p)	14.0	39	48±7	44±6	1
	14.7±0.3	38.6	40±7		2
	14.8	38.5	37±4		3
	14.8±0.2	38.5	44±5	45±5	4
	14.8±0.6	38.5	36±6		5
		Reduced χ^2 =0.80		0.68	
^{53}Cr(n,np)	14.7±0.3	11	7.3±0.7		6
	14.8±0.2	12			4
^{53}Cr α-production	14.7	44	45±4		7

[a]Where sufficient information on the standards has been given, the data have been renormalized to cross sections obtained from ENDF/B-IV Dosimetry File edited by B. Magurno (BNL-NCS-50466, April 1975).
1. D.L. Allan, Nucl. Phys. 24, 274 (1961).
2. P. Holmberg, J. Inorg. Nucl. Chem. 36, 715 (1974).
3. D.M. Chittendon, Report (Arkansas, Jan. 1961).
4. L. Husain, J. Inorg. Nucl. Chem. 29, 2665 (1967).
5. R. Prasad and D.C. Sarkar, Nouvo. Cimuto 3A, 467 (1971).
6. L.D. Webber, Bull. Am. Phys. Soc. 13, 1663 (1968).
7. G.P. Dolja, YK-11 9 (1973).

Table 8
Selected ^{54}Cr Cross Sections

	E_n (MeV)	Calculated σ(mb)	Experimental σ(mb) Original	Renormalized[a]	Ref.
^{54}Cr(n,p)	14.7±0.3	8.3	15±4		1
	14.8±0.2	8.42	13.5±1.5	13.6±1.5	2
^{54}Cr(n,α)	14.7±0.3	17.4	7±4		1
	14.8±0.2	17.9	12.5±1.3	12.6±1.3	2
^{54}Cr α-production	14.7	19	37±3		3

[a]Renormalized to ^{27}Al(n,α) cross sections from ENDF/B-IV Dosimetry File edited by B. Magurno (BNL-NCS-50466, April 1975).
1. P. Holmberg, J. Inorg. Nucl. Chem. 36, 715 (1974).
2. L. Husain, J. Inorg. Nucl. Chem. 29, 2665 (1967).
3. G.P. Dolja, YK-11, 9 (1973).

As mentioned earlier in the (n,n'α) and (n,αn') reactions are probability hidden in the (n,α) data of Dolya.[67]

Figures 68 through 71 show the hydrogen, deuterium and helium gas production for the four stable isotopes of chromium and elemental chromium. Also shown in these figures are the available experimental data. Figure 72 also compares gas production cross sections derived from ENDF/B-IV to present calculations. The present data are marked in File 3 at MT = 203 to 207.

Although there are few fission spectrum average data available, a comparison of the present work and the available experimental data related to gas production in the Cr isotopes was made. The results are shown in Table 9. The three spectral distributions were obtained from Ref. 68.

Table 9
Comparison of Calculated Fission Spectrum Average
Cross Sections to Experimental Values*

Type	Watt	Calculated Maxwell	Cranberg	Experimental	Ref.
				0.14	1
α-prod. Cr(Nat)	0.17	0.18	0.16	0.19[a]	2
				0.17±0.06	3
^{52}Cr(n,p)[b,c]	1.69	1.69	1.57	1.31±0.05	4
^{53}Cr(n,p)[c]	0.41	0.40	0.38	0.44±0.030	4
^{54}Cr(n,p)[c]	6.0×10^{-3}	6.0×10^{-3}	5.2×10^{-3}	$(5.8 \pm 1.0) \times 10^{-3}$	4

*These data were not used to renormalize the differential calculations in File 3.

[a] Mean value of results obtained by using ^{58}Ni(n,p), ^{46}Ti(n,p), and ^{63}Cu(n,α) as monitors.

[b] Rau used activation techniques to measure ^{52}Cr(n,p). For a target he employed natural Cr_2O_3. Therefore, he has really observed ^{52}Cr(n,p) + ^{53}Cr(n,np) + ^{53}Cr(n,pn) + ^{53}Cr(n,d). The calculated values have been corrected for the ^{53}Cr reactions. Also, it appears that he did not correct for the natural abundance of ^{52}Cr, therefore this correction has been applied.

[c] Rau used the ^{58}Ni(n,p), reaction as a standard citing a value of 95 mb.[5] Three recent evaluations give values of 101.5 mb,[6] 104 mb,[7] and 113+3 mb[8] for the ^{58}Ni(n,p) fission spectrum average cross section. We have corrected Rau's results using the evaluation of Fabry.[8]

1. E.P. Lippencott, W.N. McElrow, and H. Farrar IV, 4th Conf. Nuclear Cross Sections and Technology, Washington, D.C., 3-7 March 1975, P. 375.
2. J. Weitmann, N. Davenhog, and S. Farvolden, ANS 13, 558 (1970).
3. N.J. Freeman, J.F. Barry, and N.L. Campbell, JNE 23, 713 (1969).
4. G. Rau, Nuk 9, 228 (1967).
5. F. Hertlein, Ann. Physik 7, 308 (1961).
6. B.A. Magurno (editor), BNL-NCS-50446, 285 (1975).
7. M. Divadeenam, Private Communication, February 23, 1979.
8. A. Fabry, BLG-465 (1972).

7. Miscellaneous Data

a. __Angular Distributions.__ The angular distributions of secondary neutrons were derived as follows. The elastic distribution is the same as ENDF/B-IV. The angular distributions for (n,2n), (n,3n), (n,nα), (n,np) and continuum inelastic (MT = 16, 17, 22, and 91) were assumed to be isotropic. The discrete inelastic angular distributions (MT = 51 to 90) are the results of compound-nucleus Hauser-Feshbach calculations and direct reaction calculations combined to describe angular distributions and of available experimental data.

b. __Secondary Energy Distribution.__ The secondary energy distributions for (n,2n), (n,3n), (n,n'α) and (n,n'p) (MT = 16, 17 22, and 28) are presented as nuclear temperature histograms based on the Gilbert-Cameron formalism.[69] Since the threshold for the (n,3n) reaction is so high, it was necessary to arbitrarily renormalize the temperatures to conserve energy. The continuum inelastic secondary energy distributions are presented as histograms based on the experimental data of Salnikov et al.[28]

c. __Photon Production Data.__ In the evaluation of the photon production data, the procedures for the different energy regions ($E_n \leq$ thermal; E_n = thermal-200 keV, 200-600 keV, 600 keV-1 MeV, and $E_n \geq$ 1 MeV) were different. This approach was necessary since the types of data available for these energy regions differed as did the complexity of the data in File 3. Care was taken to ensure no sharp discontinuities in the total photon production cross section; however, there are probably slight discontinuities in the photon spectra between energy regions caused by the assumptions made.

Three sets of data[70-72] were combined in a consistent manner to obtain the thermal capture-γ spectrum (MF = 15, MT = 102) with the final total multiplicity adjusted to conserve energy. The capture-γ spectrum at 10^{-5} eV was assumed to be the same at thermal and the total multiplicity adjusted to conserve energy.

Between thermal and 200 keV, the spectrum-average capture-γ data of Allen et al.[73] were employed with the assumption that the distribution did not vary with neutron energy and the final total multiplicity adjusted to conserve energy.

In the 200 to 600-keV range the data of Morgan and Newman[74] were assumed to be pure capture. These data were integrated over the photon-energy range and the capture cross section from this evaluation was used to calculate the total multiplicity. The resulting multiplicities and photo-energy spectra were entered in MF = 12, MT = 15, MT = 102.

In the 600-keV to 1-MeV region, the data of Morgan and Newman[74] did not have detail corresponding to the capture cross section. It was necessary, therefore, to convert their photon production cross sections to capture-γ multiplicitities. Since inelastic processes begin to enter in this region, the data had to be adjusted for the inelastic contribution prior to conversion to capture-γ multiplicities. The discrete photon production (MF = 12, Mt = 4) was obtained from the total inelastic and inelastic scattering from the first-excited states of ^{50,53,54}Cr (MF = 3, MT = 4, 51, 52, 53). These discrete data were subtracted from the E_n = 600 to 1000 keV photon distributions of Morgan and Newman in an energy-conserving manner. The resulted spectra were assumed to result from capture and the total multiplicities adjusted to conserve energy.

Above 1 MeV, the photon production cross sections (MF = 13, MT = 3) and energy distributions (MF = 15, MT = 3) were obtained from the data of

Morgan and Newman.[74]

Electron production was assumed to be negligible. The photon production angular distributions were assumed to be isotropic.

C. Covariance Files

1. Resonance Parameters (MF = 32). Since the resonance parameters and background used in determining the total, elastic, and capture cross sections up to 642.85 keV are the same as ENDF/B-IV and no uncertainties were assigned,[1] there is no covariance file for the resonance parameters.

2. Cross Sections (MF = 33). Since there were, in general, many channels open and the statistical model code of Uhl[27(a)] does not give the covariance between channels, no attempt was made to estimate the off-diagonal covariance between competing reactions.

The evaluation of chromium was independent of other ENDF/B-V evaluations. Therefore, there are no covariance matrices relating this material to other ENDF materials.

Model code uncertainties were estimated by varying the input parameters. The estimated uncertainties are summerized in the Appendix.

a. Total, Elastic, Non-elastic, and Capture (MT = 1, 2, 3, 102).

These sections being unchanged from ENDF/V-IV, the uncertainties were taken from Table 12 of Reference 1. In the resonance region, the total cross section was derived as the sum of the elastic and capture cross sections and the nonelastic was assumed to be equal to the capture. Above the resonance region, the elastic cross section was obtained by subtracting the nonelastic from the total.

b. Total Inelastic (MT = 4). The total inelastic cross section was completely derived. Between threshold and 3.97 MeV, the total inelastic cross section was derived from the sum of the first 31 discrete levels. Above 3.97 MeV, the total inelastic was assumed to be the difference between the nonelastic and the sum of the reaction channels.

c. (n,2n) Cross Section (MT = 16). Below 15 MeV, the covariance are based on estimates in the model code uncertainty. Above 15 MeV, the co-variances were derived by comparing the calculations and experimental data, both for the natural and for the individual isotopes.

d. (n,3n), (n,nα), (n,d), (n,t) Cross Sections (MT = 17, 22, 104, 105)

Since there were no experimental data for these reactions, the co-variance matrices are based on the estimates of the model uncertainty.

e. (n,α) Cross Section (MT = 28). Between 13.5 and 15.0 MeV, the covariance matrix represents a comparison between calculations and experiment. The remainder of the matrix represents the uncertainty in the model calculations.

f. Discrete Inelastic Cross Sections (MT = 51-90). The covariance matrices represent a comparison between calculations and available experimental data. Where no experimental data were available, the representation is a estimate of the model code uncertainties.

g. Continuum Inelastic (MT =91). Although the continuum was derived from the difference between the total and discrete inelastic, we have elected to represent the matrix an "evaluated." We chose this representation because

the correlations between the discrete inelastic cross sections have not been included. Without these correlations the continuum inelastic matrix would be distorted if represented as "derived."

h. (n,p) Cross Section (MT = 103). The covariance between 12 and 17 MeV results from a comparison of calculations and experiment. The remainder is a representation of the model uncertainties.

i. (n,α) Cross Section (MT =107). The 14- to 15-MeV region represents a comparison between experiment and calculation; the remainder, model uncertainties.

j. Gas Production Cross Sections (MT = 203-207). Covariance matrices have not been included for gas production. The gas production cross sections were derived from the appropriate (n,particle) cross sections (MT = 103-107) except near 20 MeV where there was a small contribution from more esoteric reactions. The following relationships hold for the gas production uncertainties.

$$(\Delta\sigma)^2_{\text{Hydrogen production}} = (\Delta\sigma)^2_{n,np} + (\Delta\sigma)^2_{n,p}$$

$$\Delta\sigma_{\text{Deuteron production}} = \Delta\sigma_{n,d}$$

$$\Delta\sigma_{\text{Tritium production}} = \Delta\sigma_{n,t}$$

$$(\Delta\sigma)^2_{\text{Helium production}} = (\Delta\sigma)^2_{n,n\alpha} + (\Delta\sigma)^2_{n,\alpha}$$

REFERENCES

1. A. Prince, BNL-NCS-50593 (ENDF-246) (1976).
2. F.G. Perey & W.E. Kinney (Priv. Comm.) CSISRS (1973).
3. A. Prince, Proc. Int'l Conf. on the Interactions of Neutrons with Nuclei, Lowell Mass., July 1976 (Vol. 1).
4. H.L. Taylor, et al., Phys. Rev. 100, 174 (1955).
5. V.I. Strizhak, JETP 4, 769 (1957) Eng. Trans.
6. W.E. Kinney & F.G. Perey, ORNL-4806 (1974).
7. A.B. Smith (unpublished) See BNL-400, 3rd Ed., 1970.
8. A.J. Elwyn, et al., Bull. Am. Phys. Soc. 12, 473 (1967).
9. S.A. Cox, Bull. Am. Phys. Soc. 10, 576 (1965).
10. B. Holmqvist, Ark. Fys. 38, 403 (1968).
11. B. Holmqvist & T. Wiedling, AE 366 (1969).
12. B. Holmqvist & T. Wiedling, AE 430 (1971).
13. COMNUC., C. Dunford, AI-AEC 12931 (1970).
14. FISPRO., V. Benzi, et al., CEC(69)24.
15. F. Cvelbar, et al., Nucl. Phys. A130, 401 (1969).
16. K. Nishamura, et al., Helsinki Conf. 1970, IAEA-CN-26/28.
17. D.M. Van Patter, et al., Phys. Rev. 128, 1246 (1962).
18. D.L. Broder, et al., Sov. J. At. En. 16, 113 (1965).
19. Yu, G. Degtyarev & V.N. Protopopov, J. At. En. 23, 1350 (1967).
20. Yu. G. Degtyarev & V.N. Protopopov, Bull. Acad. Sai, USSR, Phys., Series 35 (11) 2123 (1971).

21. A.I. Abramov, Sov. J. At. En. 12, 65 (1962).

22. N.P. Glazkov, Sov. J. At. En. 15, 416 (1963).

23. G.P. Couchell, (Priv. Comm.) 1978, Lowell Tech. Mass.

24. P.T. Karatzes, et al., NSE 67, 34 (1978).

25. F. Voss, et al., Proc. Conf. on Nuclear Cross Sections & Technology, NBS 425, 916 (1975).

26. G. Tessler & S.S. Glickstein, ibid (p. 934).

27.(a) M. Uhl, Acta Phys. Austria 31, 245 (1970).

27.(b) M. Uhl & B. Strohmaier, IRK 76/01, Inst. fur Radiumforschung and Kernphysik der Osterreichischen, Vienna, 1976.

28. D.A. Salnikov & G.N. Lovchikova, Helsinki Conf. (1970), IAEA-CN26/79 (Also see BNL TR-545, 1970).

29. I. Fujita, et al., J. Nucl. Sci. & Tech. 9 (5), 301, (1972).

30. S. Tagesen & P. Hille, Acta Phys. Austria 23, 31 (1966).

31. W. Breunlich & G. Stengel, A. Naturforsch 26A, 451 (1971).

32. I.L. Morgan, et al., TID 20658 (unpublished).

33. M. Uhl, Nuc. 1. Phys. A184, 253 (1972).

34. L.M. Colli & G.M. Marcazzan, Riv. d. Nouvo Cim. 3 (4) 535, 1973.

35. JUPITOR I, T. Tamura, ORNL-4152 (1967).

36. P.H. Stelsen, et al., Nucl. Phys. 68, 97 (1965).

37. THRESH, S. Pearlstein, J. Nucl. En. 27, 81 (1973).

38. ABACUS 2, E.H. Auerbach, BNL-6562 (1962) unpublished.

39. W. Dilg, et al., Nucl. Phys. A217, 269 (1973).

40. Nuclear Level Schemes, A=45 through

41. Nuclear Data A3, 367 (1967).

42. Nuclear Data Tables A. Vol. 11 (2,3) 1972), N.B. Gove & A.W. Wapstra, Academic Press, N.Y., 1972.

43. T.W. Burrows & A. Prince, Proc. Int'l Conf. on the Interactions of Neutrons with Nuclei, Lowell, Mass., 1976.

44. B.T. Kenna & P.E. Harrison, SLA-73-0637 (1973).

45. M. Bormann, et al., Nucl. Phys. A115, 309 (1968).

46. M. Bormann, CSISR (unpublished) 1965.

47. S.M. Qaim, et al., Proc. Int'l Conf. Canterbury (1971).

48. Z.T. Boedy, INDC(HUN)-10, Jan. 1973.

49. L.A. Rayburn, Phys. Rev. 122, 168 (1961).

50. G.N. Maslov, et al., Jadernye Konstanty 9, 50 (1972).

51. P. Holmberg, et al., J. Inorg. Nucl. Chem 36 (4) 715, 1974.

52. J. Frehaut & G. Mosinski, 5th Int'l Symposium on the Interaction of Fast Neutrons with Nuclei, Gaussis, DDR 1975.

53. L. Husain & P.K. Kuroda, J. Inorg. Nucl. Chem 29, 2665 (1967).

54. B.D. Kern, et al., Nucl. Phys. 10, 226 (1959).

55. I.G. Clator, Priv. Comm. (1969).

56. E.B. Paul and R.L. Clark, Can. J. Phys. 31, 267 (1953).

57. D.L. Allan, Nuc. 1 Phys. 24, 274 (1961).

58. B. Mitra and A.M. Ghose, Nucl. Phys. 83, 157 (1966).

59. J.K. Mukherjee, Proc. Phys. Soc. (London) 77, 508 (1961).

60. J. Dressler, et al., INR-1464, 12 (1973).

61. C.J. Khurana & I.M. Gavil, Nucl. Phys. 69, 153 (1965).

62. D.V. Aleksandrov, et al., Sov. J. At. En. 39, 736 (1976).

63. R. Prasad & D.C. Sarker, Nuovo, Cimento 3H, 467 (1971).

64. W.N. Levkovskii, Sov. J. Nucl. Phys. 18 (4), 361 (1974).
65. D.L. Smith and J.W. Meadows, ANL (Priv. Comm. 1979).
66. L. Husain, J. Inorg. & Nucl. Chem 29, 2665 (1967).
67. G.P. Dolya, et al., Kiev. Conf. (USSR) YK-11, 9 (1973).
68. J.A. Grundl, "Fission Neutron Spectra; Macroscopic and Ingegral Results," Neutron Standards & Flux Normalization, edited by A.B. Smith, p. 417 (Conf.-701002, 1970).
69. A. Gilbert & A.G.W. Cameron, Can. J. of Phys. 43, 1446 (1965).
70. D.L. Broder, et al., Sov. J. Nucl. Phys. 13, 129 (1971).
71. V.J. Orphan, et al., GA-10248 (1970).
72. D.C. Kocher, Nucl. Data Sheets 18, 463 (1976).
73. B.J. Allen, et al., AAEC/E-200 (1969).
74. G.L. Morgan & E. Newman, ORNL-TM-5098 (1976).

APPENDIX

Estimated Uncertainties in the Evaluated
Cross Sections for Natural Chromium

MT	Reaction	Energy Range (eV)	Uncertainty (%)
1	Total	$10^{-5} - 6.5 \times 10^5$	$(\Delta\sigma_1)^2 = (\Delta\sigma_2)^2 + (\Delta\sigma_{102})^2$
		$6.5 \times 10^5 - 2.0 \times 10^7$	20.0
2	Elastic	$10^{-5} - 10^{-2}$	10.0
		$10^{-2} - 10^{-1}$	5.0
		$10^{-1} - 6.5 \times 10^5$	15.0
		$6.5 \times 10^5 - 2.0 \times 10^7$	$(\Delta\sigma_2)^2 = (\Delta\sigma_1)^2 + (\Delta\sigma_3)^2$
3	Nonelastic	$1.0^{-5} - 6.5 \times 10^5$	$\Delta\sigma_3 = \Delta\sigma_{102}$
		$6.5 \times 10^5 - 1.0 \times 10^6$	20.0
		$1.0 \times 10^6 - 2.0 \times 10^6$	15.0
		$2.0 \times 10^6 - 5.0 \times 10^6$	10.0
		$5.0 \times 10^6 - 1.0 \times 10^7$	5.0
		$1.0 \times 10^7 - 1.5 \times 10^7$	8.0
		$1.5 \times 10^7 - 2.0 \times 10^7$	10.0
4	Total Inelastic	$7.0 \times 10^5 - 3.97 \times 10^6$	$(\Delta\sigma_4)^2 = \sum\limits_{i=51}^{81} (\Delta\sigma_i)^2 + \sum\limits_{i=102}^{107} (\Delta\sigma_i)^2$
		$3.97 \times 10^6 - 2.0 \times 10^7$	$(\Delta\sigma_4)^2 = (\Delta\sigma_3)^2 + (\Delta\sigma_{16})^2 + (\Delta\sigma_{17})^2$ $+(\Delta\sigma_{22})^2 + (\Delta\sigma_{28})^2 + \sum\limits_{i=102}^{107} (\Delta\sigma_i)^2$
16	(n,2n)	$8.09 \times 10^6 - 9.5 \times 10^6$	20
		$9.5 \times 10^6 - 1.1 \times 10^7$	17
		$1.1 \times 10^7 - 1.25 \times 10^7$	10
		$1.25 \times 10^7 - 1.5 \times 10^7$	6.5
		$1.5 \times 10^7 - 1.6 \times 10^7$	1.6
		$1.6 \times 10^7 - 1.7 \times 10^7$	15
		$1.7 \times 10^7 - 2.0 \times 10^7$	16.0
17	(n,3n)	$1.8 \times 10^7 - 2.0 \times 10^7$	20
22	(n,nα)	$8.08 \times 10^6 - 2.0 \times 10^7$	20
28	(n,np)	$1.0 \times 10^7 - 1.35 \times 10^7$	20
		$1.35 \times 10^7 - 1.4 \times 10^7$	12
		$1.4 \times 10^7 - 1.45 \times 10^7$	10

Estimated Uncertainties in the Evaluated
Cross Sections for Natural Chromium (cont.)

MT	Reaction	Energy Range (eV)	Uncertainty (%)
28		$1.45 \times 10^7 - 1.5 \times 10^7$	9.4
		$1.5 \times 10^7 - 1.8 \times 10^7$	12
		$1.8 \times 10^7 - 2.0 \times 10^7$	20
	Direct Inelastic		
51		$5.75 \times 10^5 - 8.8 \times 10^5$	20
		$8.8 \times 10^5 - 1.13 \times 10^6$	10
		$1.13 \times 10^6 - 1.24 \times 10^6$	16.
		$1.24 \times 10^6 - 1.65 \times 10^6$	10.
		$1.65 \times 10^6 - 1.75 \times 10^6$	14.
		$1.75 \times 10^6 - 1.95 \times 10^6$	10
		$1.95 \times 10^6 - 2.16 \times 10^6$	13.0
		$2.16 \times 10^6 - 2.21 \times 10^6$	11.
		$2.21 \times 10^6 - 3.57 \times 10^6$	13
		$3.57 \times 10^6 - 3.77 \times 10^6$	14.
		$3.77 \times 10^6 - 3.87 \times 10^6$	17.
		$3.87 \times 10^6 - 3.97 \times 10^6$	21
		$3.97 \times 10^6 - 5.0 \times 10^6$	15.
		$5.0 \times 10^6 - 1.0 \times 10^7$	20
		$1.0 \times 10^7 - 2.0 \times 10^7$	30
52		$7.98 \times 10^5 - 8.4 \times 10^5$	20.
		$8.4 \times 10^5 - 1.24 \times 10^6$	14.
		$1.24 \times 10^6 - 1.65 \times 10^6$	9.3
		$1.65 \times 10^6 - 1.75 \times 10^6$	13.
		$1.75 \times 10^6 - 1.85 \times 10^6$	10.
		$1.85. 10^6 - 1.95 \times 10^6$	7.1
		$1.95 \times 10^6 - 2.76 \times 10^6$	9.6
		$2.76 \times 10^6 - 2.97 \times 10^6$	12.
		$2.97 \times 10^6 - 3.02 \times 10^6$	13.
		$3.02 \times 10^6 - 3.07 \times 10^6$	16.
		$3.07 \times 10^6 - 3.17 \times 10^6$	14.
		$3.17 \times 10^6 - 3.27 \times 10^6$	19.

Estimated Uncertainties in the Evaluated
Cross Sections for Natural Chromium (cont.)

MT	Reaction	Energy Range (eV)	Uncertainty (%)
52		$3.27 \times 10^6 - 1.0 \times 10^7$	25.
		$1.0 \times 10^7 - 2.0 \times 10^7$	30.
53		$8.51 \times 10^5 - 1.03 \times 10^6$	33.
		$1.03 \times 10^6 - 1.13 \times 10^6$	14.
		$1.13 \times 10^6 - 1.24 \times 10^6$	63
		$1.24 \times 10^6 - 1.34 \times 10^6$	38.
		$1.34 \times 10^6 - 1.44 \times 10^6$	14.
		$1.44 \times 10^6 - 1.49 \times 10^6$	33.
		$1.49 \times 10^6 - 1.54 \times 10^6$	10.
		$1.54 \times 10^6 - 1.60 \times 10^6$	19.
		$1.60 \times 10^6 - 1.65 \times 10^6$	14.
		$1.65 \times 10^6 - 1.85 \times 10^6$	19.
		$1.85 \times 10^6 - 2.21 \times 10^6$	16.
		$2.21 \times 10^6 - 2.26 \times 10^6$	9.7
		$2.26 \times 10^6 - 2.31 \times 10^6$	12.
		$2.31 \times 10^6 - 2.46 \times 10^6$	8.5
		$2.46 \times 10^6 - 2.66 \times 10^6$	11.
		$2.66 \times 10^6 - 2.92 \times 10^6$	14.
		$2.92 \times 10^6 - 2.97 \times 10^6$	20.
		$2.97 \times 10^6 - 3.17 \times 10^6$	14.
		$3.17 \times 10^6 - 3.27 \times 10^6$	20.
		$3.27 \times 10^6 - 3.47 \times 10^6$	22.
		$3.47 \times 10^6 - 3.57 \times 10^6$	29.
		$3.57 \times 10^6 - 3.97 \times 10^6$	33.
		$3.97 \times 10^6 - 2.0 \times 10^7$	38.
54		$1.02 \times 10^6 - 1.13 \times 10^6$	25.
		$1.13 \times 10^6 - 1.24 \times 10^6$	24.
		$1.24 \times 10^6 - 1.34 \times 10^6$	15.
		$1.44 \times 10^6 - 1.49 \times 10^6$	7.7
		$1.49 \times 10^6 - 1.55 \times 10^6$	10.
		$1.55 \times 10^6 - 1.60 \times 10^6$	12.

MT	Reaction	Energy Range (eV)	Uncertainty (%)
54		$1.60 \times 10^6 - 1.65 \times 10^6$	11.
		$1.65 \times 10^6 - 1.75 \times 10^6$	14.
		$1.75 \times 10^6 - 1.85 \times 10^6$	19.
		$1.85 \times 10^6 - 2.05 \times 10^6$	12.
		$2.05 \times 10^6 - 2.16 \times 10^6$	9.7
		$2.16 \times 10^6 - 3.02 \times 10^6$	13.
		$3.02 \times 10^6 - 3.17 \times 10^6$	22.
		$3.17 \times 10^6 - 3.27 \times 10^6$	16.
		$3.27 \times 10^6 - 3.37 \times 10^6$	23.
		$3.37 \times 10^6 - 3.47 \times 10^6$	24.
		$3.47 \times 10^6 - 3.57 \times 10^6$	27.
		$3.57 \times 10^6 - 3.77 \times 10^6$	19.
		$3.77 \times 10^6 - 3.87 \times 10^6$	22.
		$3.87 \times 10^6 - 3.97 \times 10^6$	25.
		$3.97 \times 10^6 - 5.0 \times 10^6$	21.
		$5.0 \times 10^6 - 2.0 \times 10^7$	20.
55		$1.31 \times 10^6 - 1.44 \times 10^6$	15.
		$1.44 \times 10^6 - 1.49 \times 10^6$	11.
		$1.49 \times 10^6 - 1.55 \times 10^6$	18.
		$1.55 \times 10^6 - 1.60 \times 10^6$	12.
		$1.60 \times 10^6 - 1.65 \times 10^6$	18.
		$1.65 \times 10^6 - 1.75 \times 10^6$	30.
		$1.75 \times 10^6 - 1.85 \times 10^6$	26
		$1.85 \times 10^6 - 1.95 \times 10^6$	30
		$1.95 \times 10^6 - 2.05 \times 10^6$	17.
		$2.05 \times 10^6 - 2.16 \times 10^6$	11.
		$2.16 \times 10^6 - 2.76 \times 10^6$	12.
		$2.26 \times 10^6 - 2.76 \times 10^6$	14.
		$2.76 \times 10^6 - 2.97 \times 10^6$	17.
		$2.97 \times 10^6 - 3.17 \times 10^6$	19.
		$3.17 \times 10^6 - 3.57 \times 10^6$	21

Estimated Uncertainties in the Evaluated
Cross Sections for Natural Chromium (cont.)

MT	Reaction	Energy Range (eV)	Uncertainty (%)
55		$3.57 \times 10^6 - 5.0 \times 10^6$	33
		$5.0 \times 10^6 - 1.0 \times 10^7$	10.
		$1.0 \times 10^7 - 2.0 \times 10^7$	20.
56		$1.46 \times 10^6 - 1.49 \times 10^6$	40.
		$1.49 \times 10^6 - 1.54 \times 10^6$	40.
		$1.54 \times 10^6 - 1.60 \times 10^6$	15
		$1.60 \times 10^6 - 1.65 \times 10^6$	7.1
		$1.65 \times 10^6 - 1.75 \times 10^6$	10.
		$1.75 \times 10^6 - 2.86 \times 10^6$	7.1
		$2.86 \times 10^6 - 3.07 \times 10^6$	7.3
		$3.07 \times 10^6 - 3.37 \times 10^6$	10.
		$3.37 \times 10^6 - 3.57 \times 10^6$	13.
		$3.57 \times 10^6 - 3.77 \times 10^6$	14.
		$3.77 \times 10^6 - 5.0 \times 10^6$	18.
		$5.0 \times 10^6 - 1.0 \times 10^7$	15
		$1.0 \times 10^7 - 2.0 \times 10^7$	20
57		$1.57 \times 10^6 - 1.61 \times 10^6$	57
		$1.61 \times 10^6 - 1.75 \times 10^6$	50
		$1.75 \times 10^6 - 1.85 \times 10^6$	35
		$1.85 \times 10^6 - 1.95 \times 10^6$	29.
		$1.95 \times 10^6 - 2.05 \times 10^6$	33.
		$2.05 \times 10^6 - 2.21 \times 10^6$	22.
		$2.21 \times 10^6 - 2.26 \times 10^6$	17.
		$2.26 \times 10^6 - 2.46 \times 10^6$	11.
		$2.46 \times 10^6 - 5.0 \times 10^6$	14.
		$5.0 \times 10^6 - 1.5 \times 10^7$	15.
		$1.5 \times 10^7 - 2.0 \times 10^7$	20.
58		$2.01 \times 10^6 - 2.16 \times 10^6$	33.
		$2.16 \times 10^6 - 2.26 \times 10^6$	20.
		$2.26 \times 10^6 - 2.36 \times 10^6$	27.
		$2.36 \times 10^6 - 2.46 \times 10^6$	36.

Estimated Uncertainties in the Evaluated
Cross Sections for Natural Chromium (cont.)

MT	Reaction	Energy Range(*eV)	Uncertainty (%)
58		$2.46 \times 10^6 - 2.56 \times 10^6$	57.
		$2.56 \times 10^6 - 2.76 \times 10^6$	28.
		$2.76 \times 10^6 - 2.87 \times 10^6$	20.
		$2.87 \times 10^6 - 2.92 \times 10^6$	28.
		$2.92 \times 10^6 - 3.07 \times 10^6$	12.
		$3.07 \times 10^6 - 3.17 \times 10^6$	27.
		$3.17 \times 10^6 - 3.57 \times 10^6$	36.
		$3.57 \times 10^6 - 3.67 \times 10^6$	24.
		$3.67 \times 10^6 - 3.77 \times 10^6$	28.
		$3.77 \times 10^6 - 3.87 \times 10^6$	17.
		$3.87 \times 10^6 - 3.97 \times 10^6$	20.
		$3.97 \times 10^6 - 5.0 \times 10^6$	13.
		$5.0 \times 10^6 \quad 1.5 \times 10^7$	20.
		$1.5 \times 10^7 - 2.0 \times 10^7$	30.
59, 60		$2.2 \times 10^6 - 1.5 \times 10^7$	20.
		$1.5 \times 10^7 - 2.0 \times 10^7$	30.
61		$2.3 \times 10^6 - 2.76 \times 10^6$	60.
		$2.76 \times 10^6 - 3.17 \times 10^6$	43.
		$3.17 \times 10^6 - 3.47 \times 10^6$	60.
		$3.47 \times 10^6 - 3.57 \times 10^6$	40.
		$3.57 \times 10^6 - 3.67 \times 10^6$	75.
		$3.67 \times 10^6 - 3.77 \times 10^6$	67.
		$3.77 \times 10^6 - 3.87 \times 10^6$	36.
		$3.87 \times 10^6 - 3.97 \times 10^6$	33.
		$3.97 \times 10^6 - 2.0 \times 10^7$	47.
62		$2.4 \times 10^6 - 2.66 \times 10^6$	20.
		$2.66 \times 10^6 - 2.76 \times 10^6$	13.
		$2.76 \times 10^6 - 2.86 \times 10^6$	7.4
		$2.86 \times 10^6 - 3.02 \times 10^6$	8.3
		$3.02 \times 10^6 - 3.37 \times 10^6$	7.5

Estimated Uncertainties in the Evaluated
Cross Sections for Natural Chromium (cont.)

MT	Reaction	Energy Range (eV)	Uncertainty (%)
62		$3.37 \times 10^6 - 3.77 \times 10^6$	8.2
		$3.77 \times 10^6 - 3.87 \times 10^6$	7.1
		$3.87 \times 10^6 - 1.0 \times 10^7$	16.
		$1.0 \times 10^7 - 1.5 \times 10^7$	20
		$1.5 \times 10^7 - 2.0 \times 10^7$	30
63		$2.5 \times 10^6 - 5.0 \times 10^6$	50
		$5.0 \times 10^6 - 2.0 \times 10^7$	40
64		$2.70 \times 10^6 - 2.97 \times 10^6$	23.
		$2.97 \times 10^6 - 3.17 \times 10^6$	8.1
		$3.17 \times 10^6 - 3.57 \times 10^6$	13.
		$3.57 \times 10^6 - 3.67 \times 10^6$	10.
		$3.67 \times 10^6 - 3.87 \times 10^6$	9.4
		$3.87 \times 10^6 - 5.0 \times 10^6$	10.
		$5.0 \times 10^6 - 1.5 \times 10^7$	20.
		$1.5 \times 10^7 - 2.0 \times 10^7$	30.
65-67, 69		$2.7 \times 10^6 - 1.25 \times 10^7$	50.
71-74, 76-81, 83-90		$5.0 \times 10^6 - 1.25 \times 10^7$	40.
		$1.25 \times 10^7 - 2.0 \times 10^7$	50.
68		$2.8 \times 10^6 - 3.02 \times 10^6$	25.
		$3.02 \times 10^6 - 3.17 \times 10^6$	31.
		$3.17 \times 10^6 - 3.27 \times 10^6$	13.
		$3.27 \times 10^6 - 3.37 \times 10^6$	10
		$3.37 \times 10^6 - 3.47 \times 10^6$	8.1
		$3.47 \times 10^6 - 3.77 \times 10^6$	9.6
		$3.77 \times 10^6 - 3.87 \times 10^6$	21.
		$3.87 \times 10^6 - 3.97 \times 10^6$	12.
		$3.97 \times 10^6 - 5.0 \times 10^6$	15.
		$5.0 \times 10^6 - 1.5 \times 10^7$	20.
		$1.5 \times 10^7 - 2.0 \times 10^7$	30.
70		$3.0 \times 10^6 - 3.08 \times 10^6$	20.
		$3.08 \times 10^6 - 3.17 \times 10^6$	12.

Estimated Uncertainties in the Evaluated
Cross Sections for Natural Chromium (cont.)

MT	Reaction	Energy Range (eV)	Uncertainty (%)
70		$3.17 \times 10^6 - 5.0 \times 10^6$	7.3
		$5.0 \times 10^6 - 1.0 \times 10^7$	15.
		$1.0 \times 10^7 - 2.0 \times 10^7$	20.
75		$3.2 \times 10^6 - 3.37 \times 10^6$	25.
		$3.37 \times 10^6 - 3.47 \times 10^6$	16.
		$3.47 \times 10^6 - 3.67 \times 10^6$	10.
		$3.67 \times 10^6 - 5.0 \times 10^6$	7.8
		$5.0 \times 10^6 - 1.5 \times 10^7$	15.
		$1.5 \times 10^7 - 1.8 \times 10^7$	20.
		$1.8 \times 10^7 - 2.0 \times 10^7$	30.
82		$3.84 \times 10^6 - 3.87 \times 10^6$	40.
		$3.87 \times 10^6 - 5.0 \times 10^6$	32.
		$5.0 \times 10^6 - 2.0 \times 10^7$	40.
91	Continuum Inelastic	$1.9 \times 10^6 - 2.0 \times 10^7$	40.
102	$(n, \gamma$	$1.0 \times 10^{-5} - 1.0 \times 10^{-2}$	13.
		$1.0 \times 10^{-2} - 1.0 \times 10^{-1}$	9.7
		$1.0 \times 10^{-1} - 6.5 \times 10^5$	13.
		$6.5 \times 10^5 - 5.0 \times 10^6$	20.
		$5.0 \times 10^6 - 1.5 \times 10^7$	15.
		$1.5 \times 10^7 - 2.0 \times 10^7$	10.
103	(n, p)	$1.8 \times 10^6 - 1.2 \times 10^7$	20.
		$1.2 \times 10^7 - 1.3 \times 10^7$	14.
		$1.3 \times 10^7 - 1.35 \times 10^7$	8.6
		$1.35 \times 10^7 - 1.45 \times 10^7$	9.6
		$1.45 \times 10^7 - 1.7 \times 10^7$	8.9
		$1.70 \times 10^7 - 2.0 \times 10^7$	20.
104	(n, d)	$7.51 \times 10^6 - 2.0 \times 10^7$	20.
105	(n, t)	$8.80 \times 10^6 - 2.0 \times 10^7$	40.
106	$(n, ^3He)$	$8.80 \times 10^6 - 2.0 \times 10^7$	40.
107	(n, α)	$1.0 \times 10^6 - 1.4 \times 10^7$	20.
		$1.40 \times 10^7 - 1.50 \times 10^7$	6.8
		$1.50 \times 10^7 - 1.90 \times 10^7$	9.8
		$1.90 \times 10^7 - 2.0 \times 10^7$	20.

CHROMIUM (NATURAL) TOTAL CROSS SECTION

E_n = 0.0001 to 0.1 MeV

□ C.T. Hibdon, Phys. Rev. 108, 414 (1957)
∇△ R.E. Cote, et al, Phys. Rev. III, 288 (1958)
— Calculated

TOT

NEUTRON ENERGY (MeV)
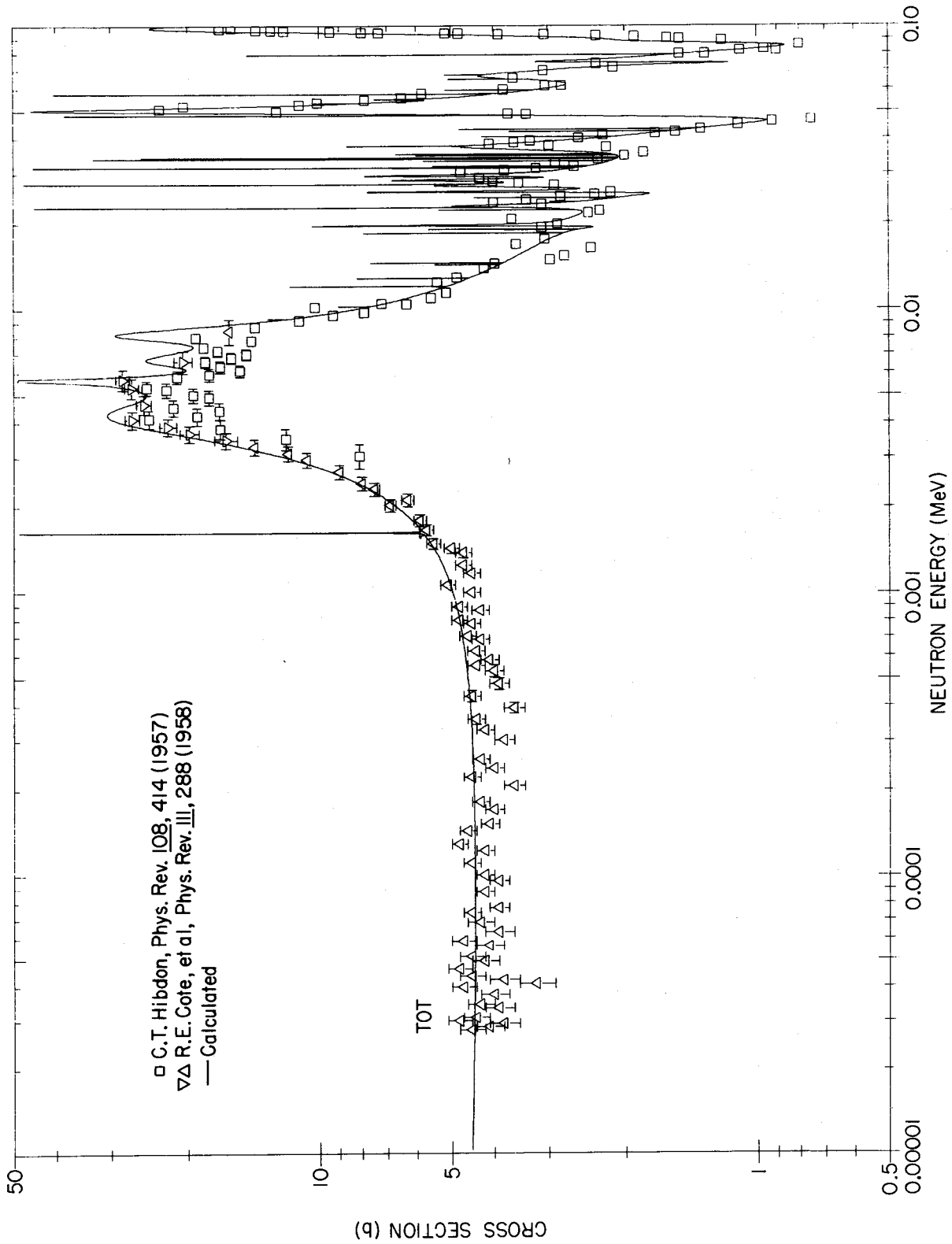
CROSS SECTION (b)

Figure 1.

CHROMIUM (NATURAL) TOTAL CROSS SECTION

E_n = 0.1 to 0.65 MeV

○ S.Cierjacks, et al, KFK-1000 (Suppl.1) 1968
□ J.F.Whalen & J.W.Meadows, ANL 7210 (1966)
△ C.T.Hibdon, Phys. Rev. 108, 414 (1957)
▽◇ J.Cabe et al, Comptes Rendus 258, 1478 (1964)

NEUTRON ENERGY (MeV)

CROSS SECTION (b)

Figure 2.

- 34 -
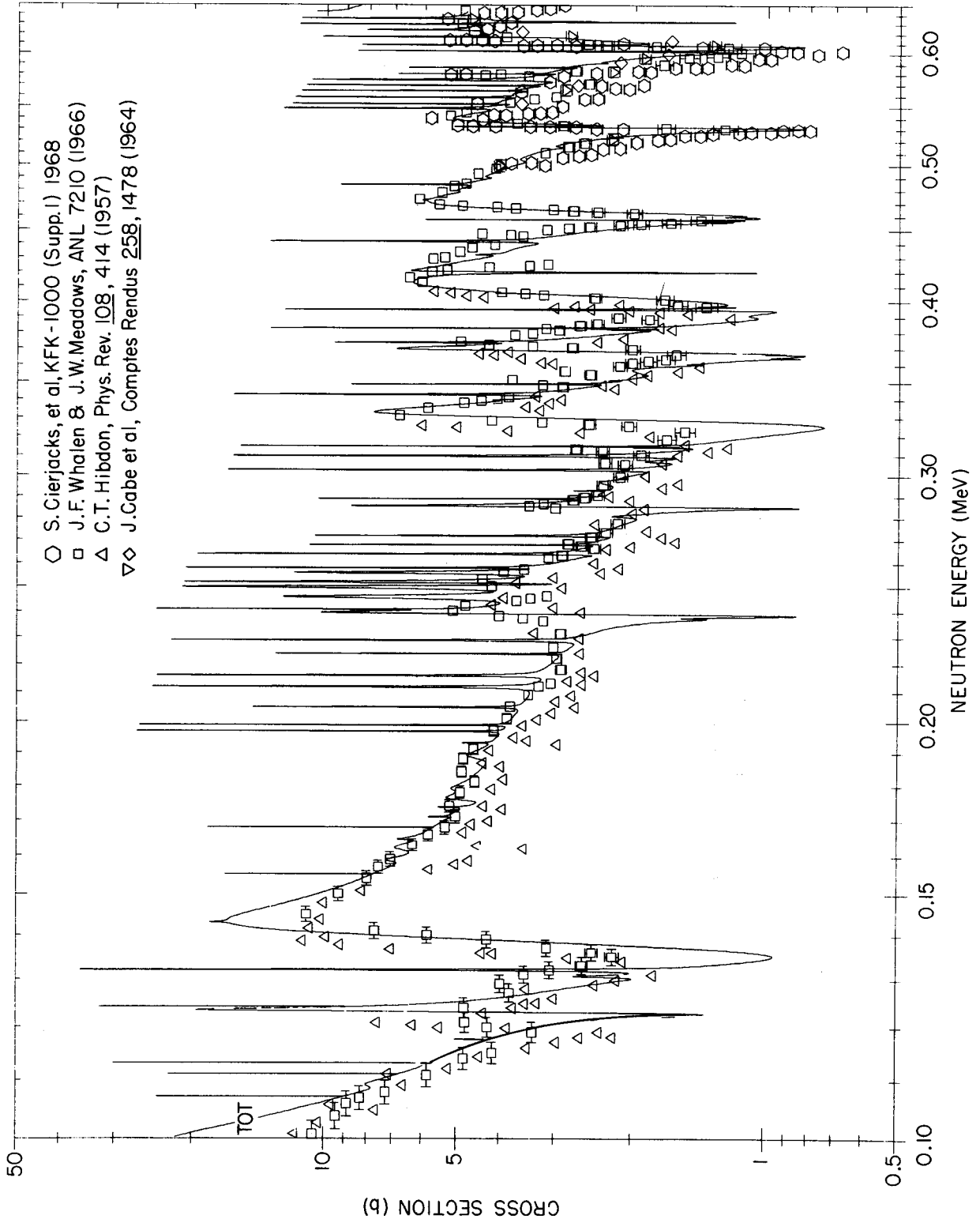
CHROMIUM
TOTAL CROSS SECTION
△ F.G. PEREY et al-ORNL (1973)
0.65 to 0.70 MeV
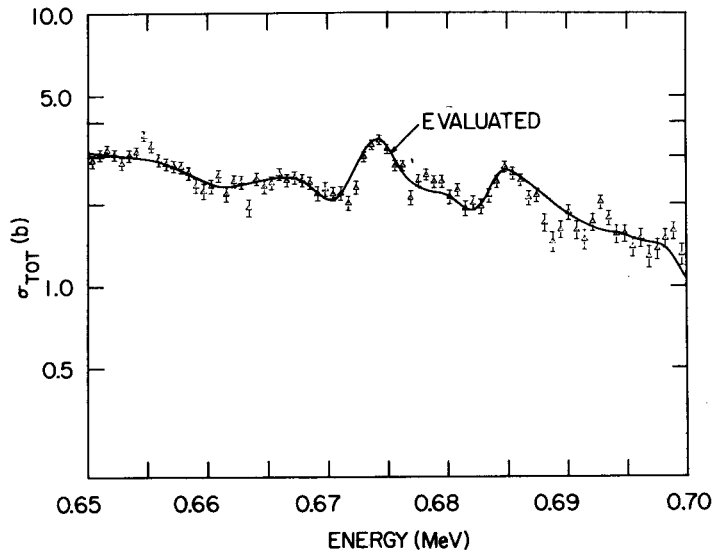
Figure 3.

CHROMIUM
TOTAL CROSS SECTION
△ F.G. PEREY et al-ORNL (1973)
0.70 to 0.90 MeV
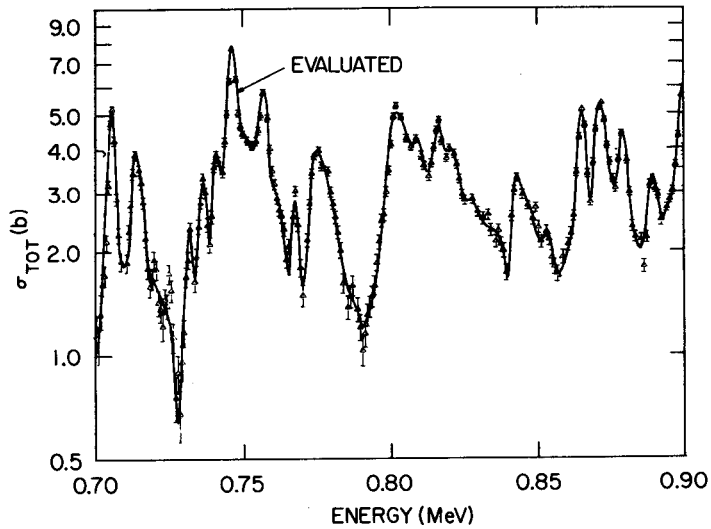
Figure 4.

CHROMIUM
TOTAL CROSS SECTION
△ F.G. PEREY et al-ORNL (1973)
0.90 to 1.20 MeV
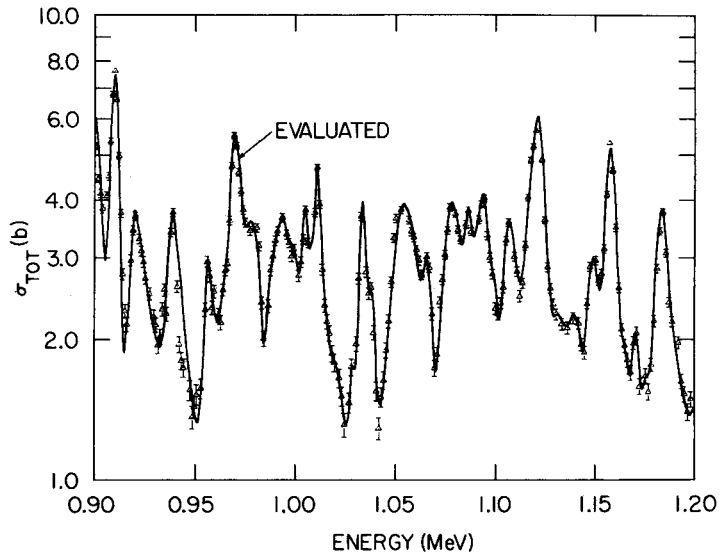
Figure 5.

CHROMIUM
TOTAL CROSS SECTION
△ F.G. PEREY et al-ORNL (1973)
1.2 to 1.5 MeV
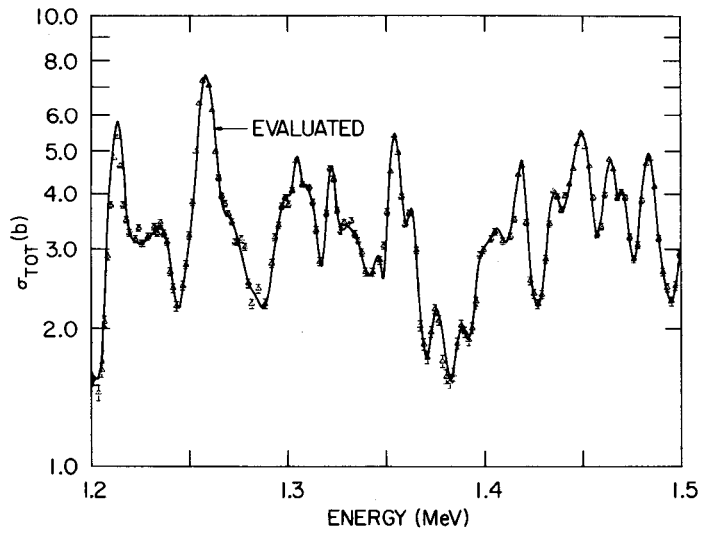
Figure 6.

CHROMIUM
TOTAL CROSS SECTION
Δ F.G. PEREY et al - ORNL (1973)
1.5 to 2.0
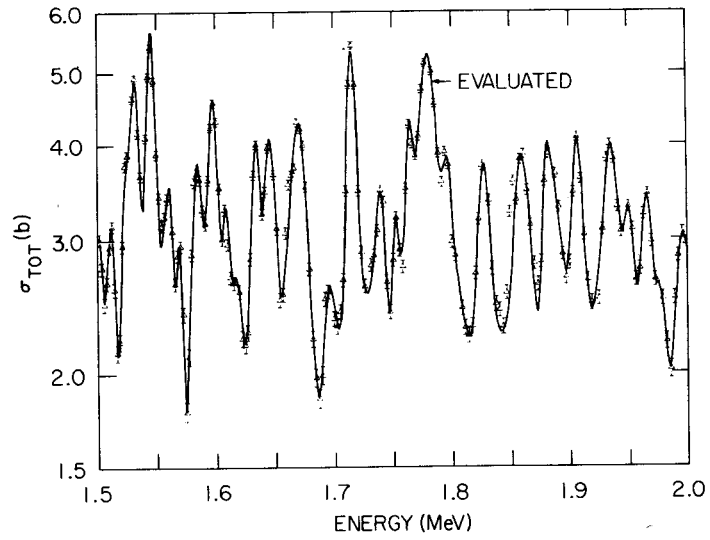
Figure 7.

CHROMIUM
TOTAL CROSS SECTION
Δ F.G. PEREY et al - ORNL (1973)
2.0 to 2.5 MeV
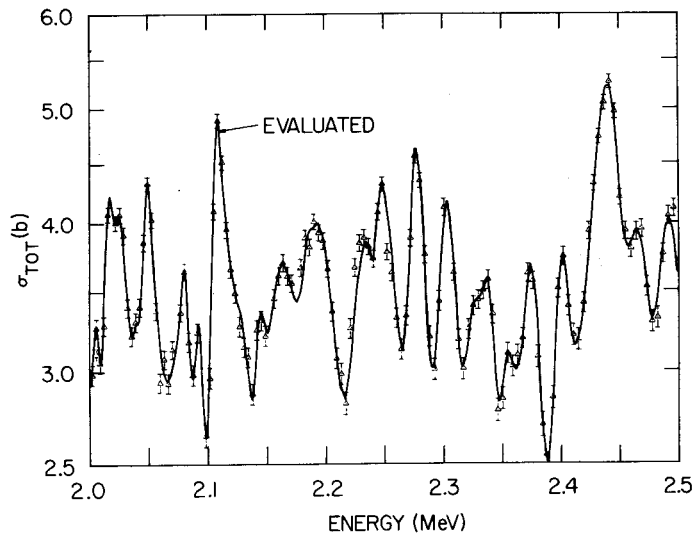
Figure 8.

CHROMIUM
TOTAL CROSS SECTION
△ F.G.PEREY et al - ORNL (1973)
2.5 to 3.0 MeV
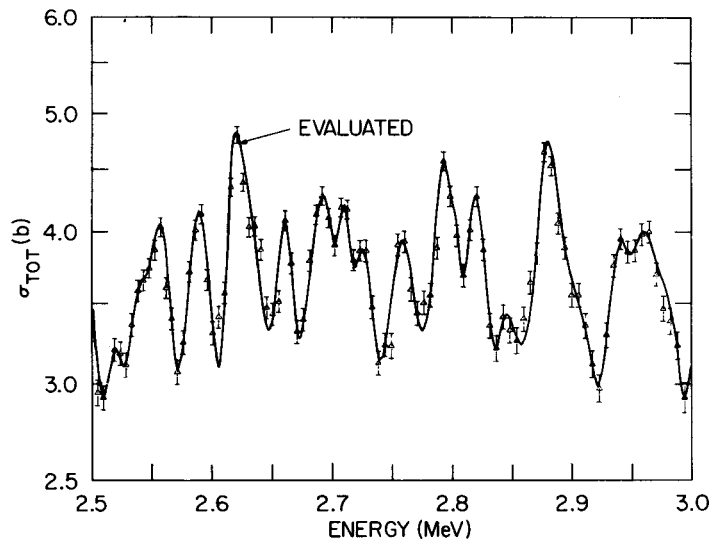
Figure 9.

CHROMIUM
TOTAL CROSS SECTION
△ F.G.PEREY et al - ORNL (1973)
3.0 to 5.0 MeV
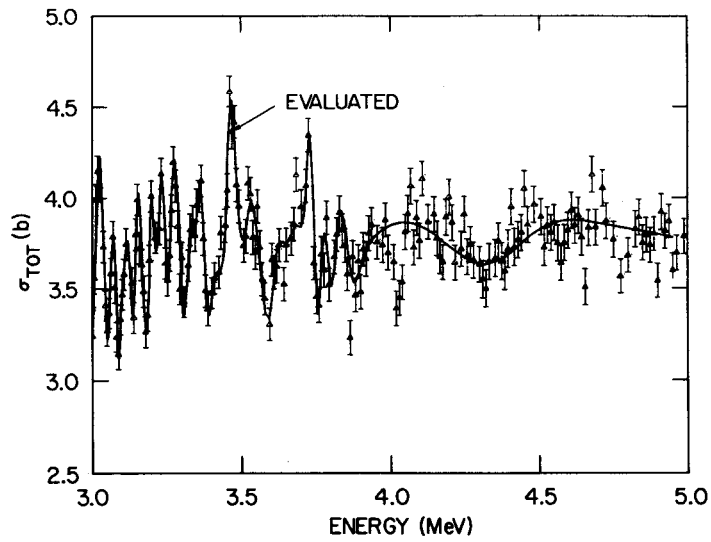
Figure 10.

CHROMIUM
TOTAL CROSS SECTION
△ F.G.PEREY etal-ORNL(1973)
5.0 to 10.0 MeV
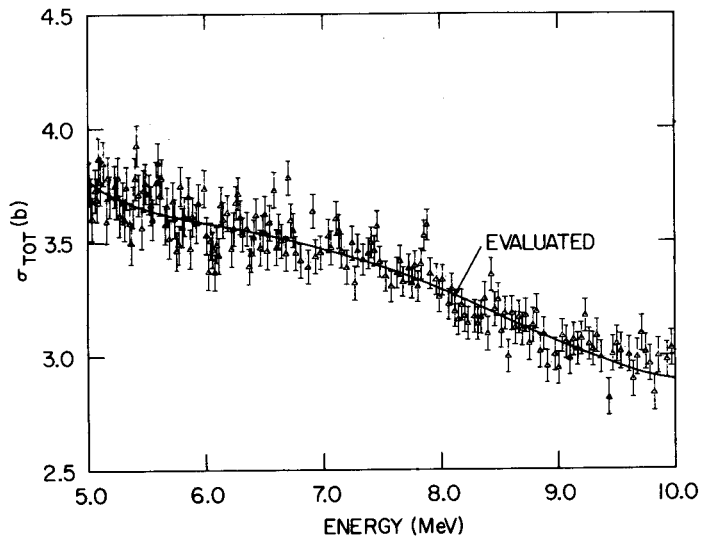
Figure 11.

CHROMIUM
TOTAL CROSS SECTION
△ F.G.PEREY etal-ORNL(1973)
10.0 to 20.0 MeV
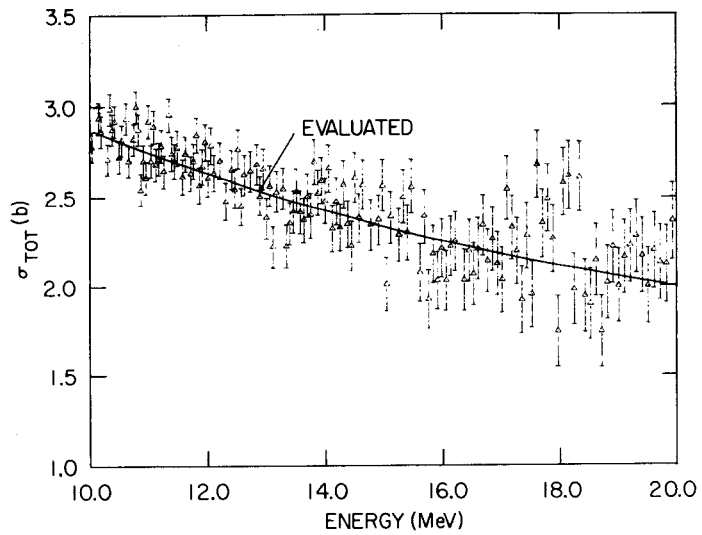
Figure 12.

CHROMIUM
NONELASTIC CROSS SECTION

CROSS SECTION (b)

ENERGY (MeV)

EVALUATED
● H.L. TAYLOR, et al, Phys. Rev. 100, 174 (1955)
□ ($\sigma_T - \sigma_{el}$) — W.E. KINNEY & F.G. PEREY–ORNL 4806 (1974)
△ ($\sigma_T - \sigma_{el}$) — OPTICAL MODEL CALCS. —THIS WORK.
○ {M.V. PASECHNICK–GENEVA CONF 1955 P/714
  {V.I. STRIZHAK – JET P 4, 769 (1957)

Figure 13.

CHROMIUM
ELASTIC CROSS SECTION
0.65 TO 0.7 MeV
□ A.B.SMITH, ANL 1966 (UNPUBLISHED)

Figure 14.
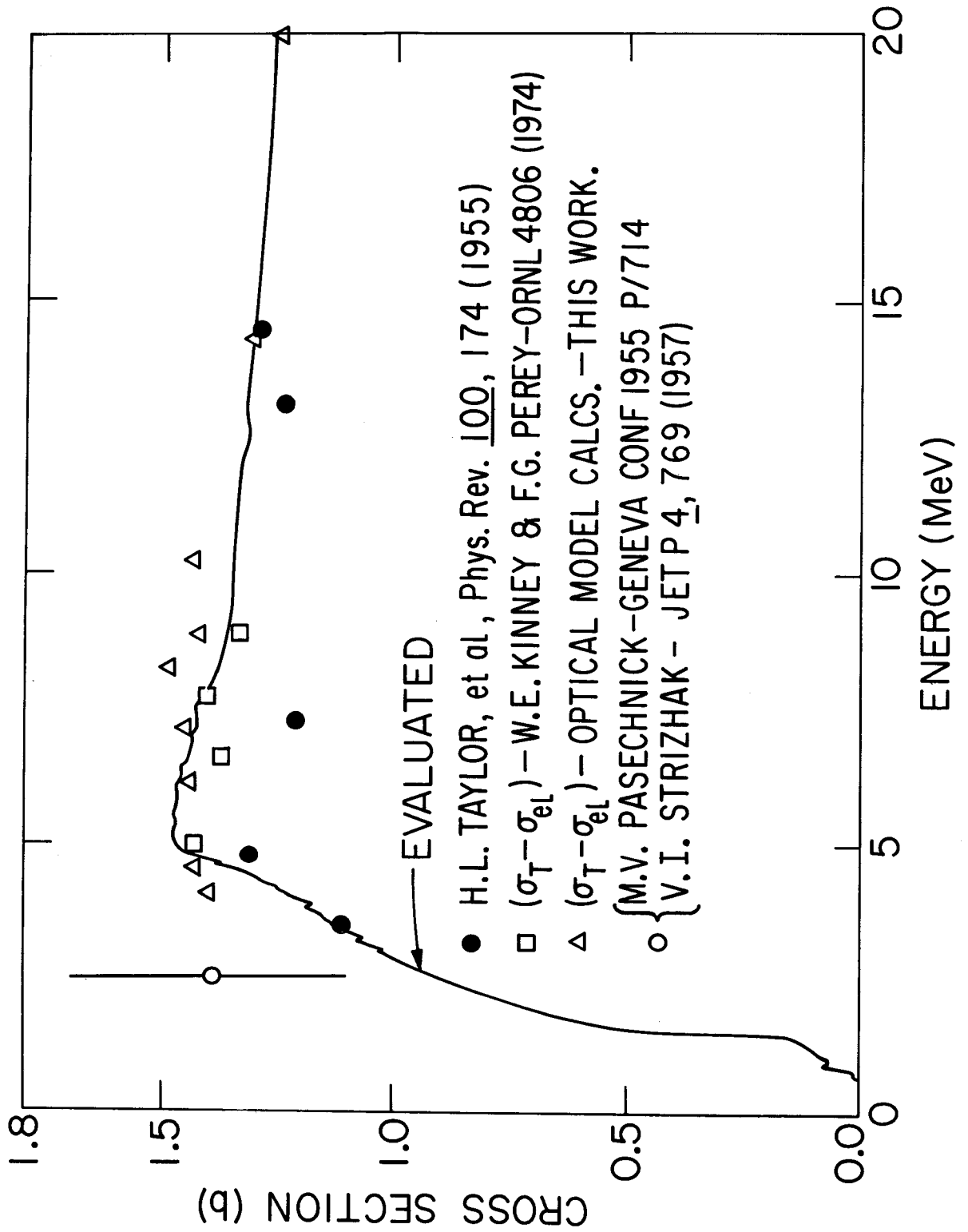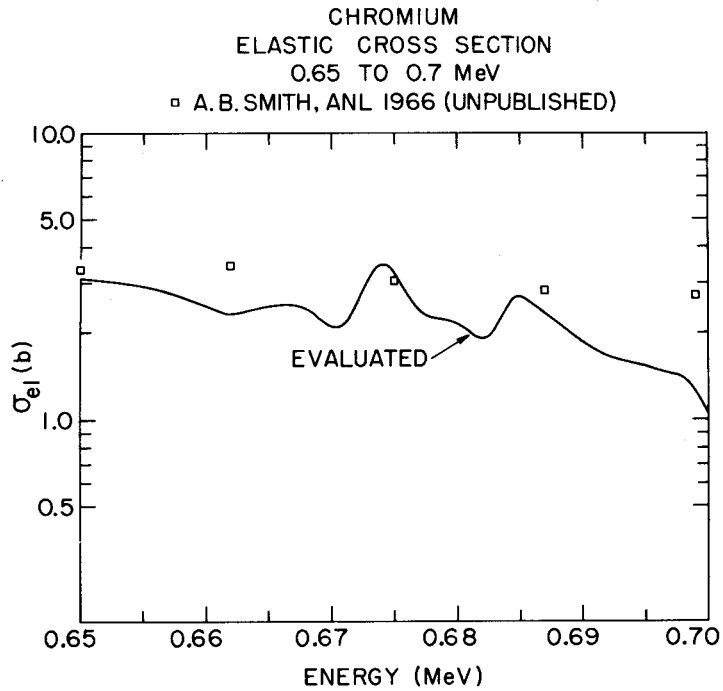
CHROMIUM
ELASTIC CROSS SECTION
0.70 TO 0.9 MeV
□ A.B.SMITH, ANL (1966)
▽ I.A.KORZH, M.T. SKLYAR, J. UFZ $\underline{9}$, 577 (1964)
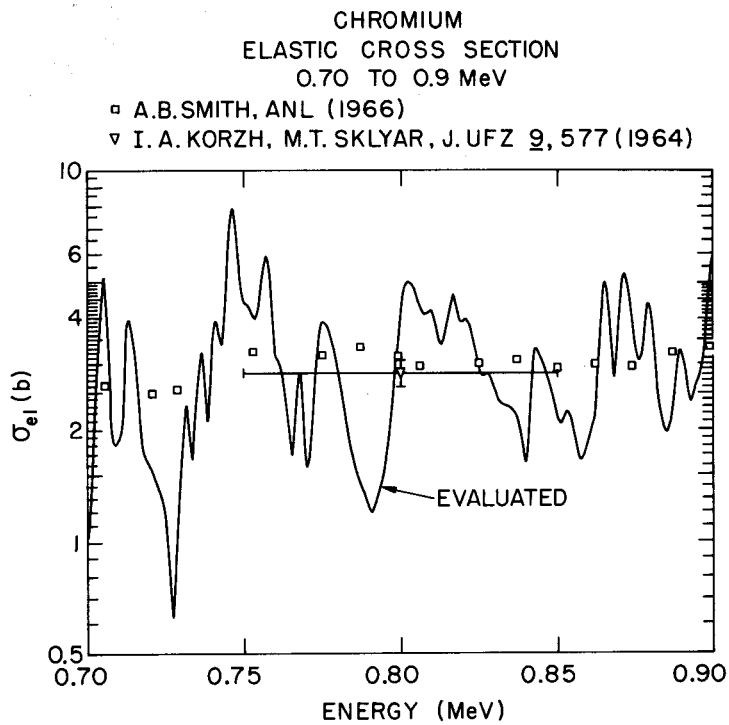
Figure 15.

CHROMIUM
ELASTIC CROSS SECTION
0.90 TO 1.20 MeV
□ A.B. SMITH, ANL (1966)
◊ W.B. GILBOY & J.H. TOWLE, NUCL. PHYS. 42, 86 (1963)
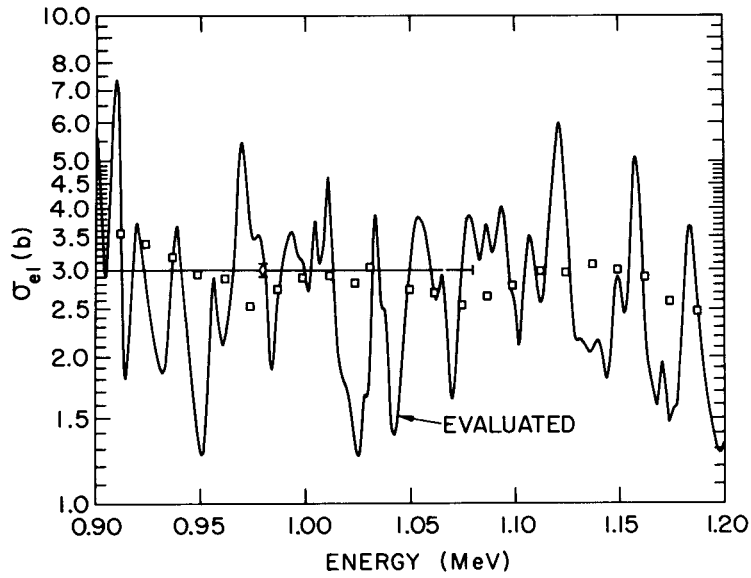
Figure 16.

CHROMIUM
ELASTIC CROSS SECTION
1.20 TO 1.5 MeV
□ A.B. SMITH, ANL (1966)
○ I.A. KORZH, et al, J. UFZ 12,1571 (1967)
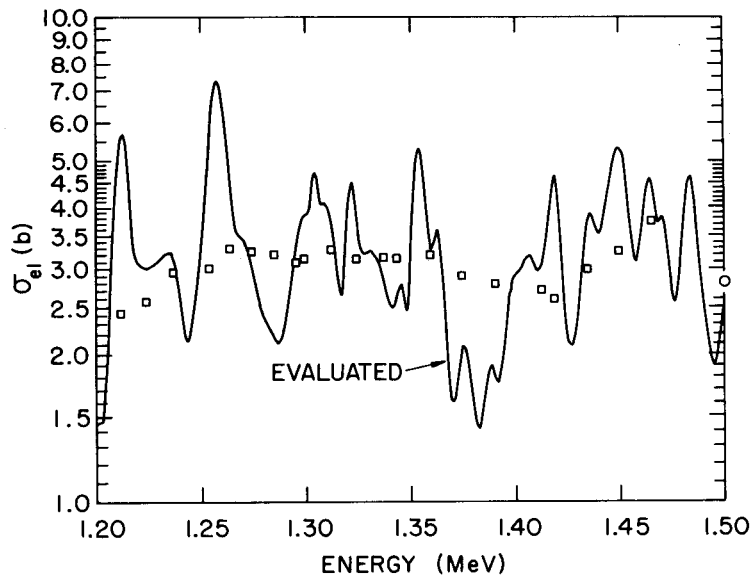
Figure 17.

CHROMIUM
ELASTIC CROSS SECTION
1.5 TO 2.0 MeV
△ I. B.HOLMQVIST & T. WIELDING, AE 385(1970)
○ 2. I. A. KORZH , J. UFZ 12 , 1571 (1967)
◆ 3. L.YA. KASAKOV, ANTWERP CONF. 576 (1965)
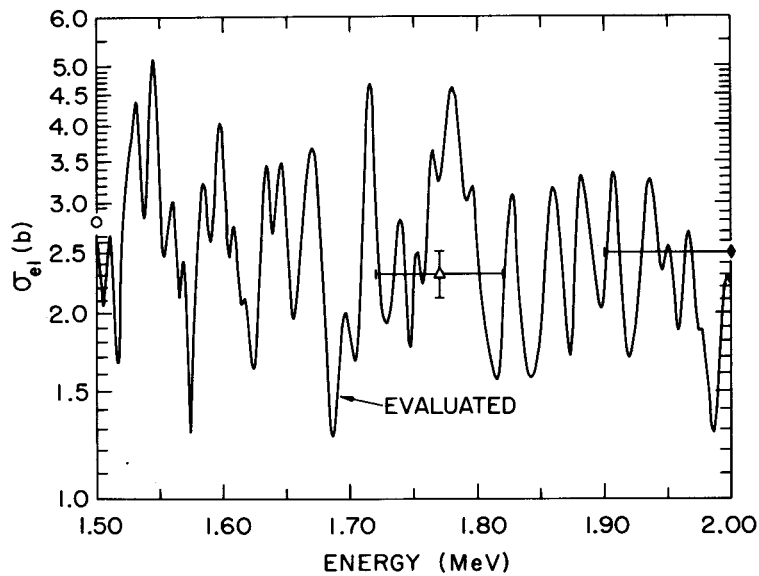
Figure 18.

CHROMIUM
ELASTIC CROSS SECTION
2.0 TO 2.5 MeV
× I. B. HOLMQVIST & T. WIEDLING AE 366(1969)
△ 2. B. HOLMQVIST & T. WIEDLING AE 385(1970)
◆ 3. L. YA. KASAKOV, ANTWERP CONF. 576 (1965)
▫ 4. M.V. PASECHNIK et al, SOV. J.NUCL.PHYS.⊔ 533(1970)

Figure 19.

- 43 -

CHROMIUM
ELASTIC CROSS SECTION
2.5 TO 3.0 MeV
× I. B. HOLMQVIST & T. WIEDLING AE 366 (1969)
△ 2. B. HOLMQVIST & T. WIEDLING AE 385 (1970)
◐ 3. B. HOLMQVIST, ARK. FYS. 38, 403 (1968)
▫ M.V. PASECHNIK et al, SOV. J. NUCL. PHYS. 11, 533 (1970)
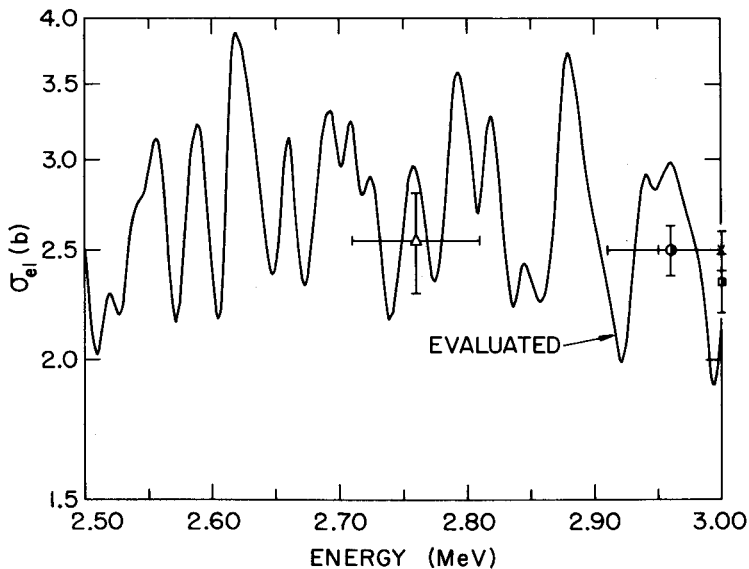
Figure 20.

CHROMIUM
ELASTIC CROSS SECTION
3.0 TO 5.0 MeV
× I. B. HOLMQVIST & T. WIEDLING AE 366 (1969)
◐ 2. B. HOLMQVIST, ARK. FYS. 38, 403 (1968)
● W. E. KINNEY & F. G. PEREY, ORNL 4806 (1974)
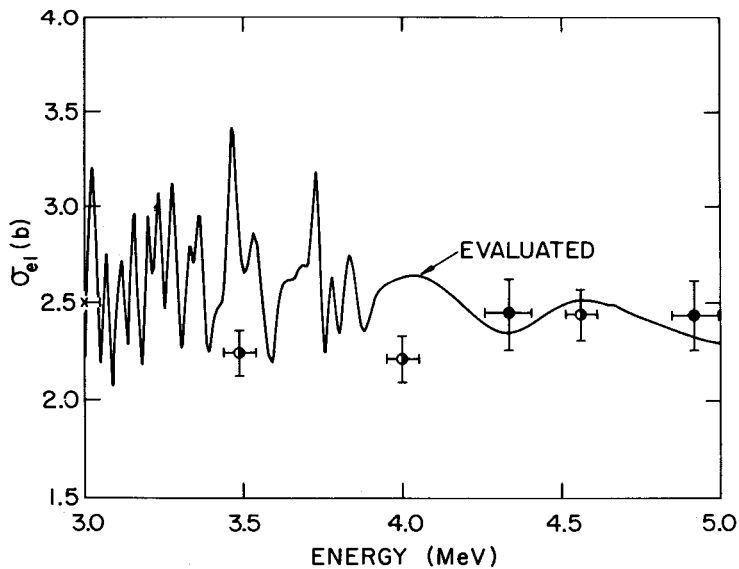
Figure 21.

CHROMIUM
ELASTIC CROSS SECTION
5.0 TO 10.0 MeV
x 1. B. HOLMQVIST & T. WIEDLING AE 366 (1969)
o 2. B. HOLMQVIST, ARK. FYS. 38, 403 (1968)
● W. E. KINNEY & F. G. PEREY, ORNL 4806 (1974)
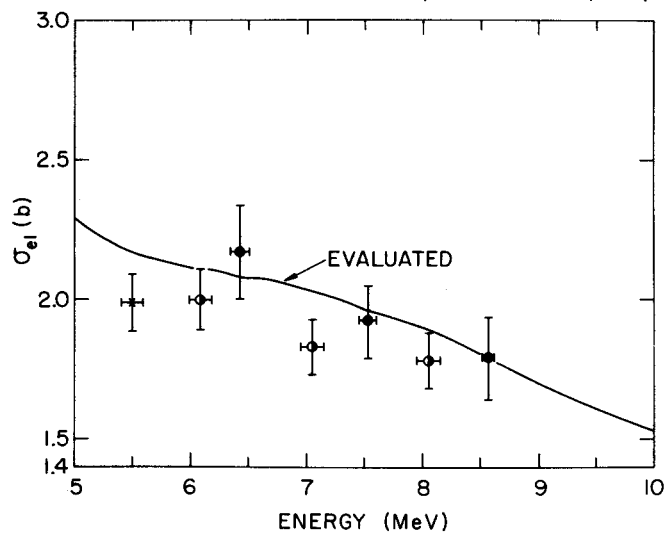
Figure 22.

CHROMIUM
ELASTIC CROSS SECTION
10.0 TO 20.0 MeV
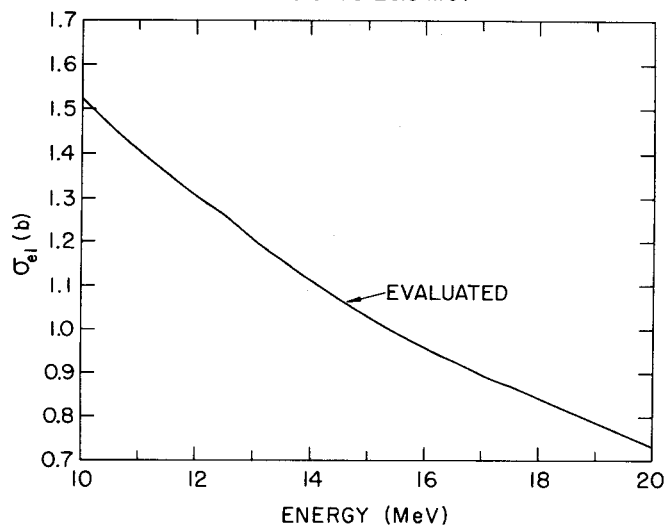
Figure 23.

Cr (NATURAL) DIFFERENTIAL ELASTIC SCATTERING

E_n = 4.0 MeV

○ B. Holmqvist & T. Wiedling,
AE – 430 (1971)

● Wick limit

—— Calculated (^{52}Cr)

$\sigma(\theta)$ (mb/sr)

$\theta_{c.m.}$ (deg)
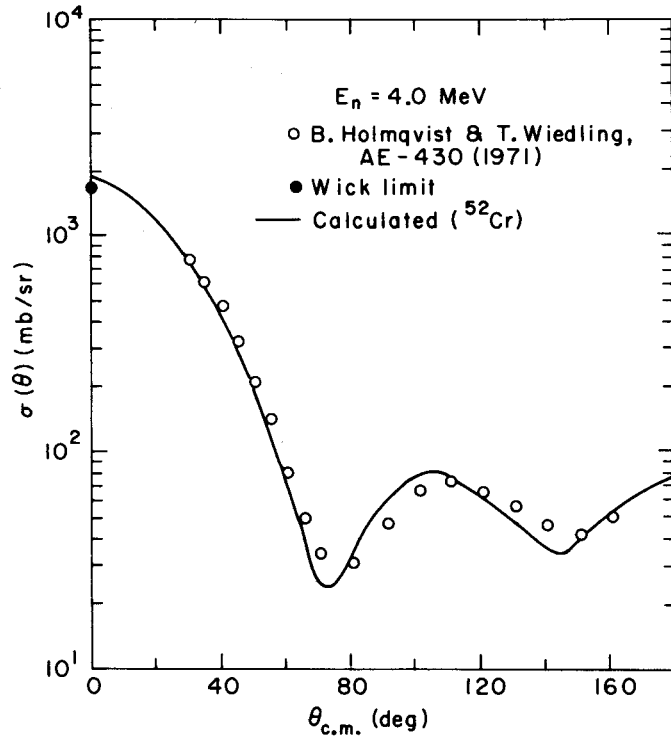
Figure 24.

Cr (NATURAL) DIFFERENTIAL ELASTIC SCATTERING

E_n = 4.56 MeV

□ J. B. Weddell, Phys. Rev. 104,
1069 (1956)

○ B. Holmqvist & T. Wiedling,
AE – 430 (1971)

● Wick limit

——Calculated (^{52}Cr)

$\sigma(\theta)$ (mb/sr)

$\theta_{c.m.}$ (deg)

Figure 25.

- 46 -
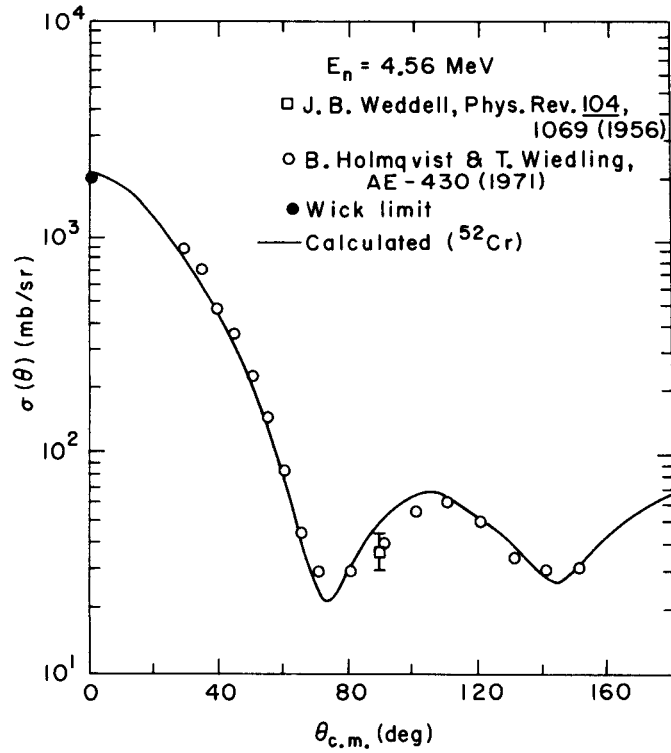
Cr (NATURAL) DIFFERENTIAL ELASTIC SCATTERING
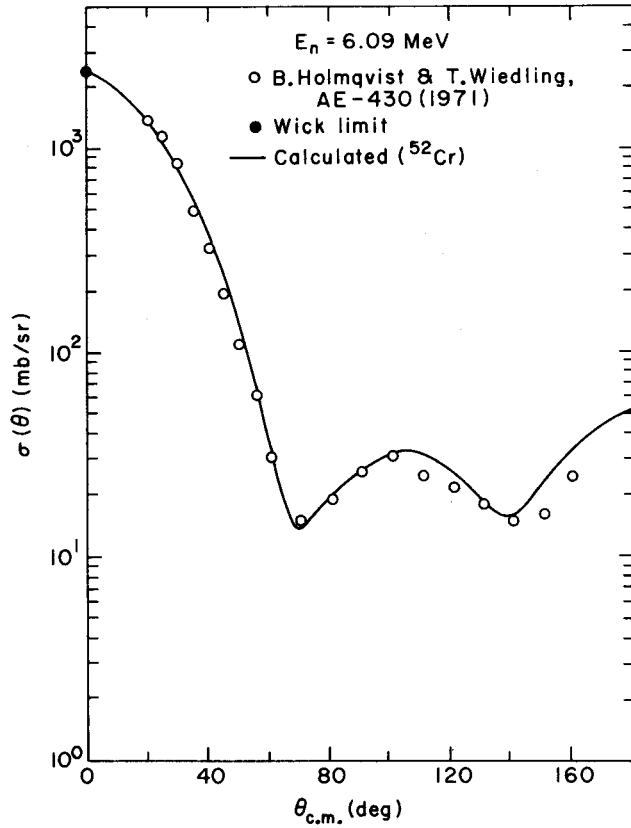
Figure 26.

^{52}Cr DIFFERENTIAL ELASTIC SCATTERING
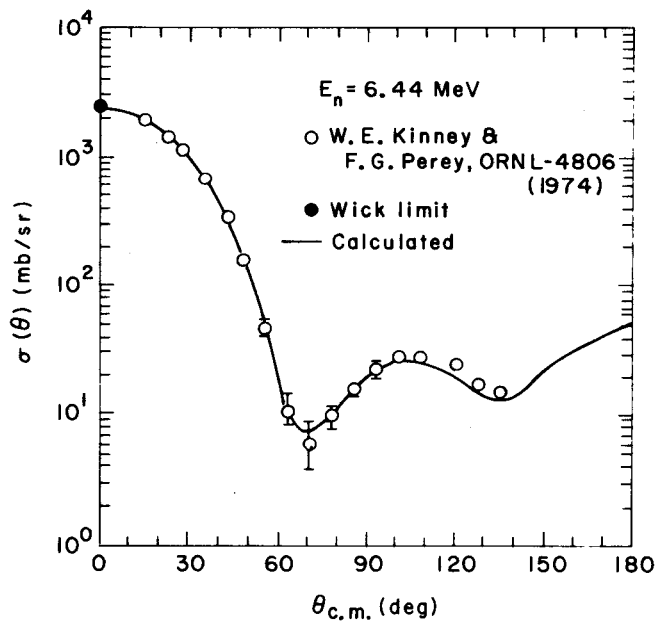
Figure 27.
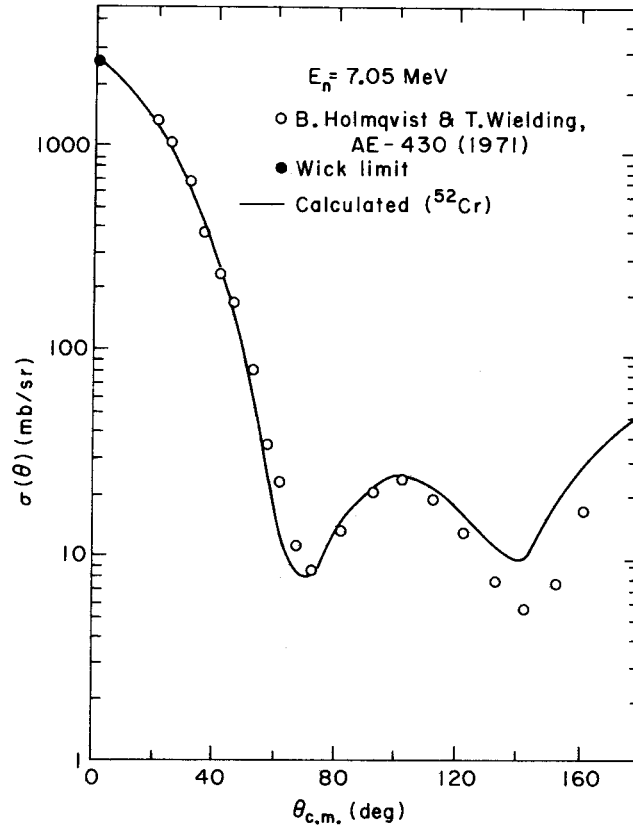
Figure 28.

^{52}Cr DIFFERENTIAL ELASTIC SCATTERING
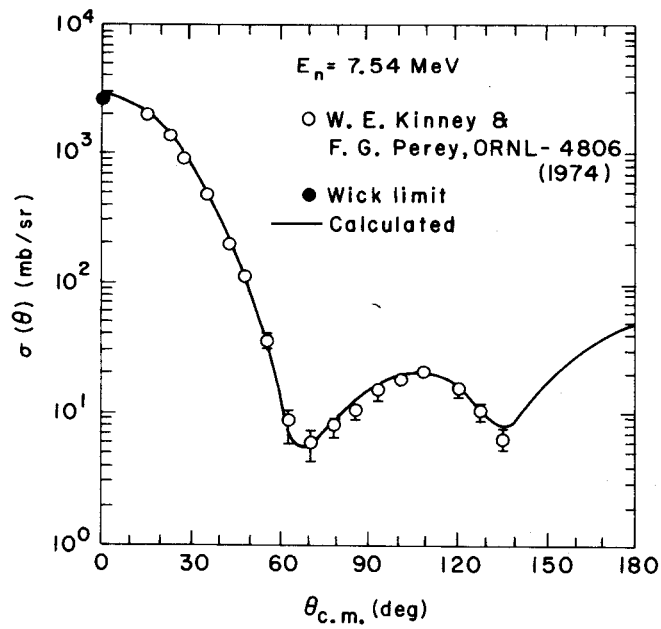
Figure 29.

Cr (NATURAL) DIFFERENTIAL ELASTIC SCATTERING
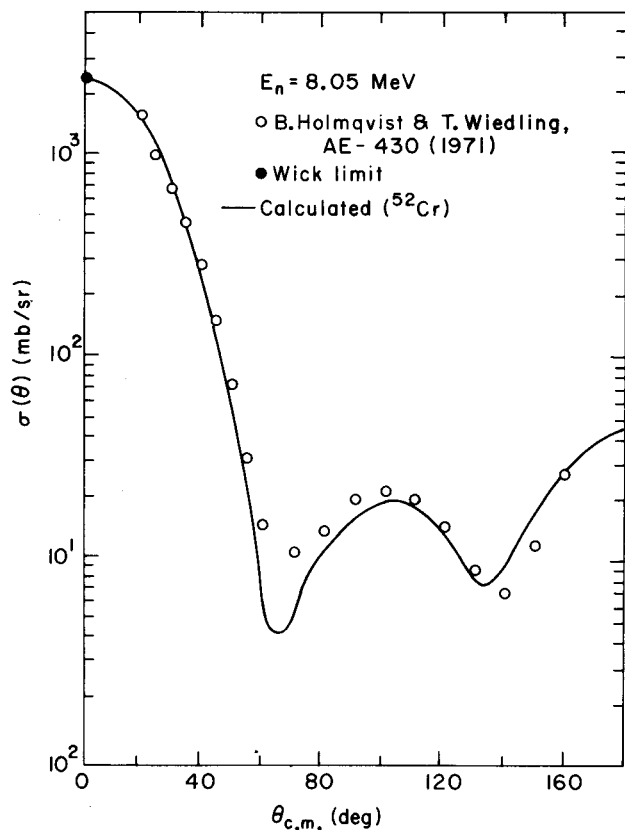
Figure 30.

^{52}Cr DIFFERENTIAL ELASTIC SCATTERING
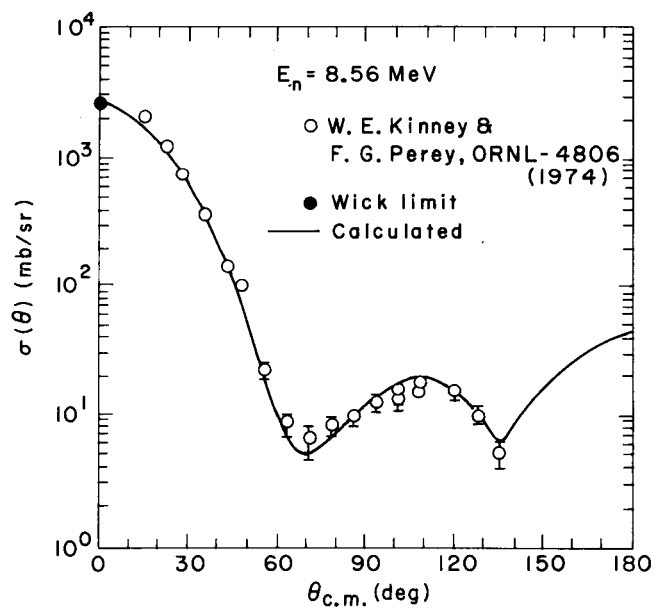
Figure 31.

Cr (NATURAL) DIFFERENTIAL ELASTIC SCATTERING
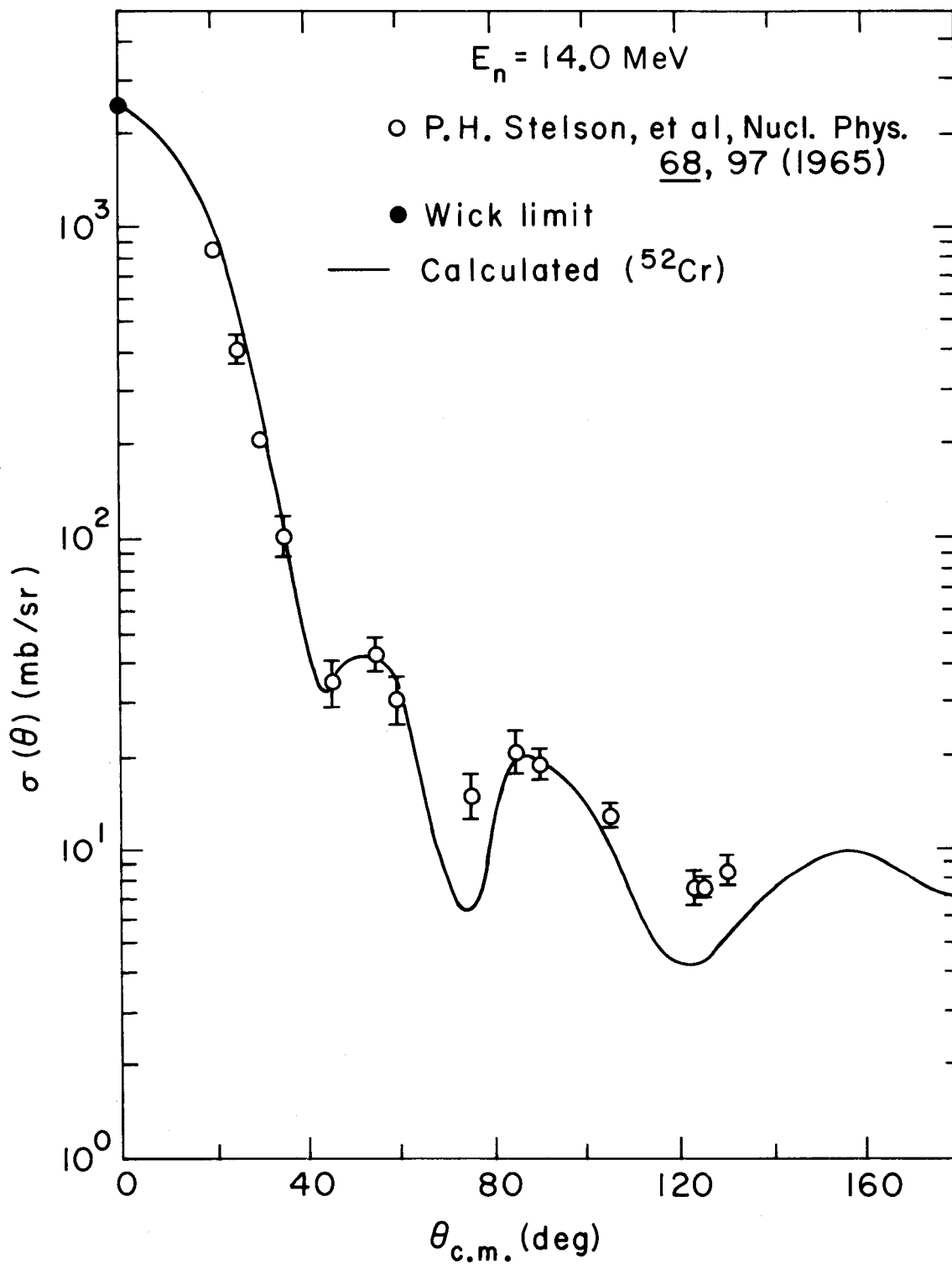
Figure 32.

CHROMIUM
RADIATIVE CAPTURE CROSS SECTION
▲ F. CVELBAR, et al, Nucl. Phys. A 130, 401(1969)

EVALUATED
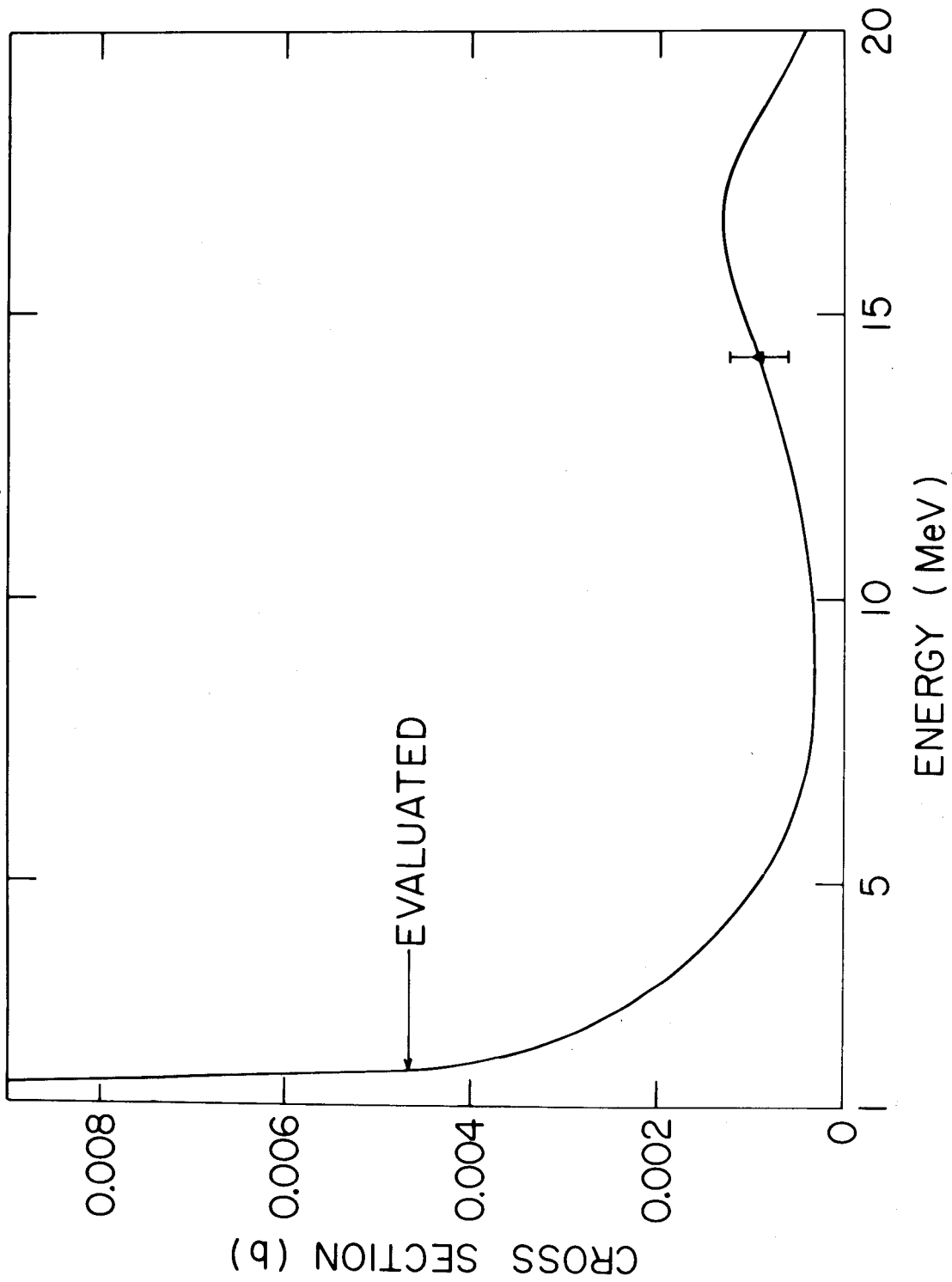
Figure 33.

Cr (Nat) INELASTIC CROSS SECTION
(0.564 MeV LEVEL – ^{53}Cr)

$\triangle$ NSE 67, 34 (1978)
—— ENDF/V

E_n (MeV)

σ (mb)
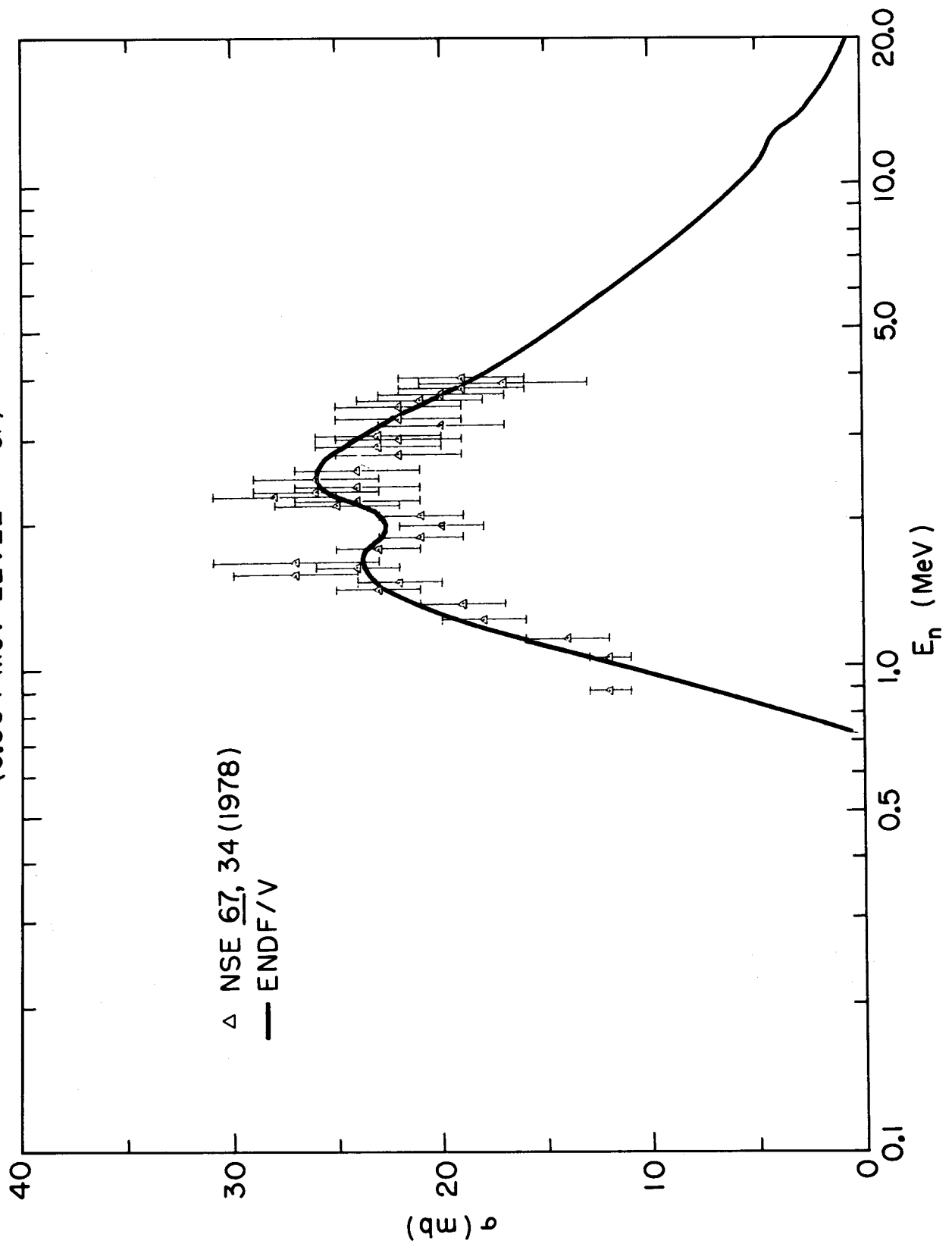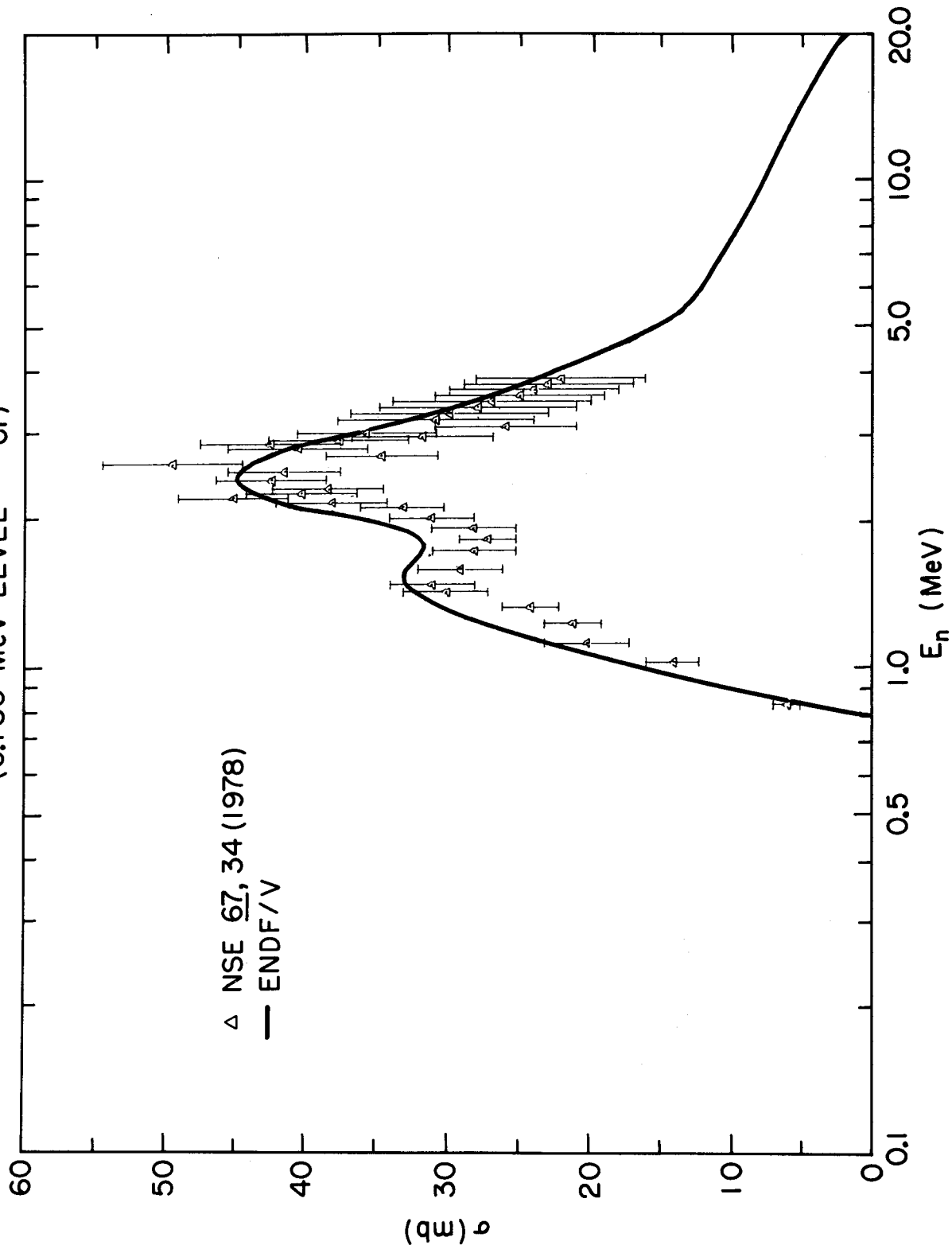
Figure 34.

Figure 35.

Cr (Nat) INELASTIC CROSS SECTION
(0.8348 MeV LEVEL — ^{54}Cr)
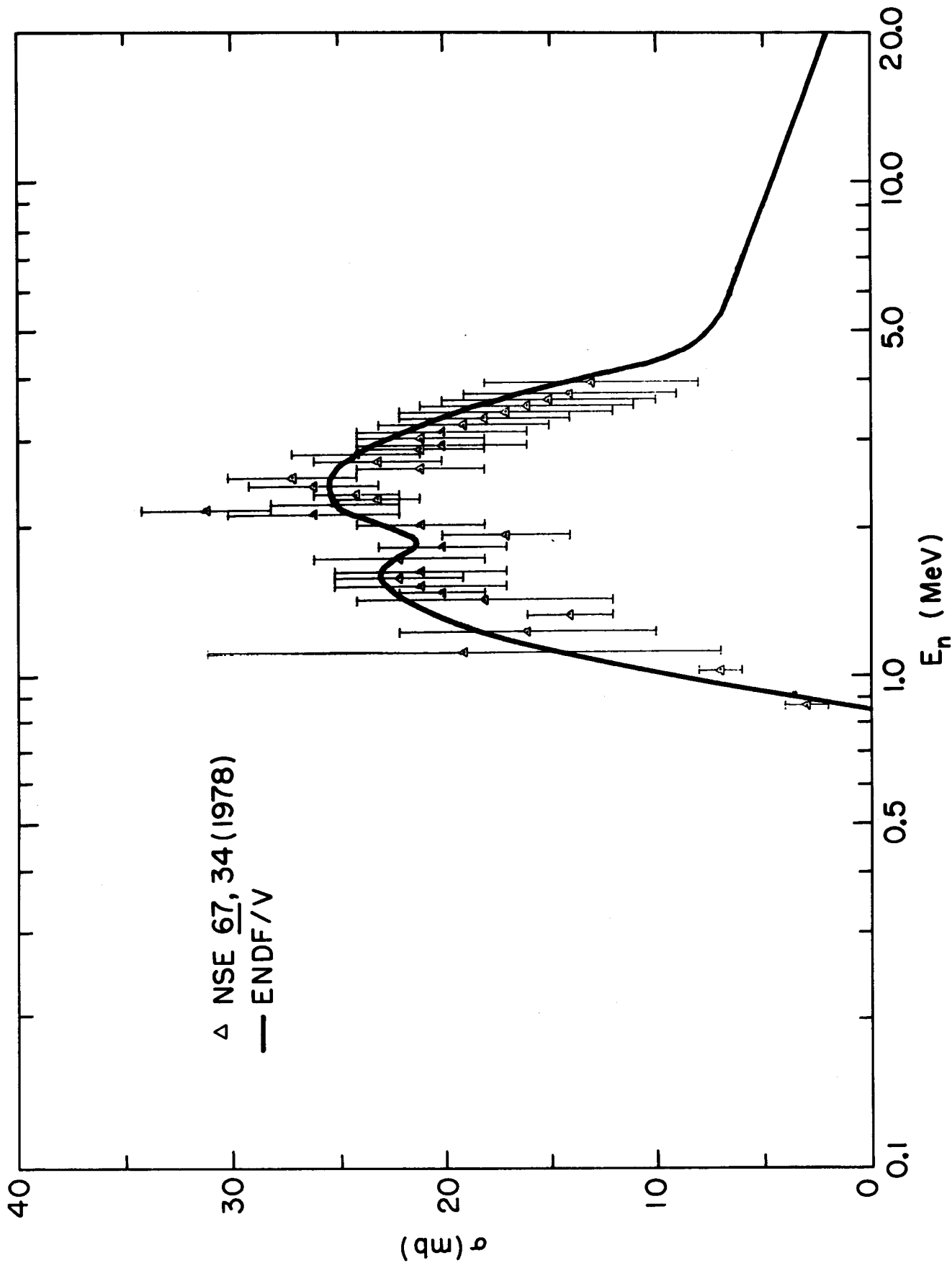
△ NSE 67, 34 (1978)
—— ENDF/V
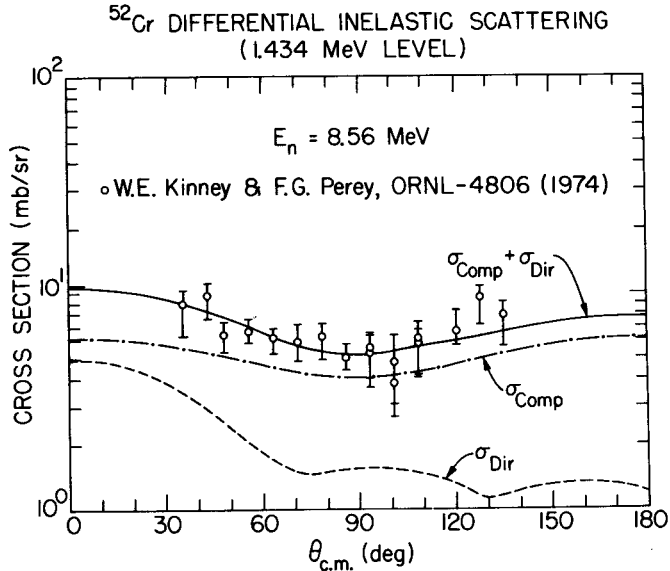
E_n (MeV)
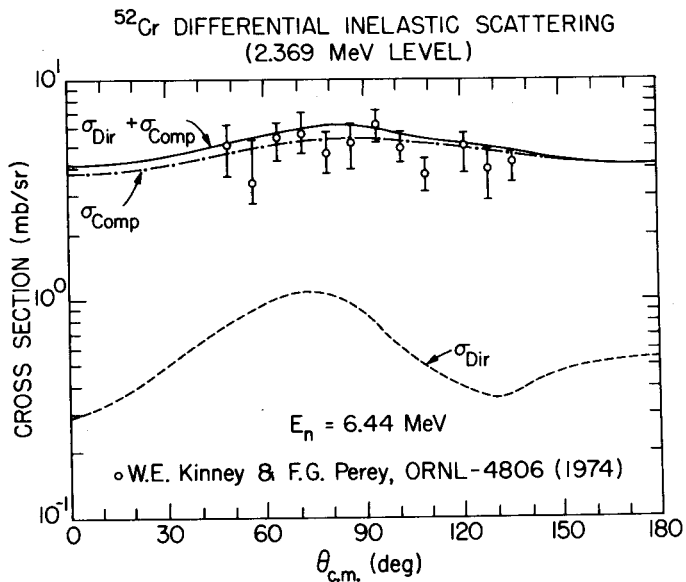
σ (mb)
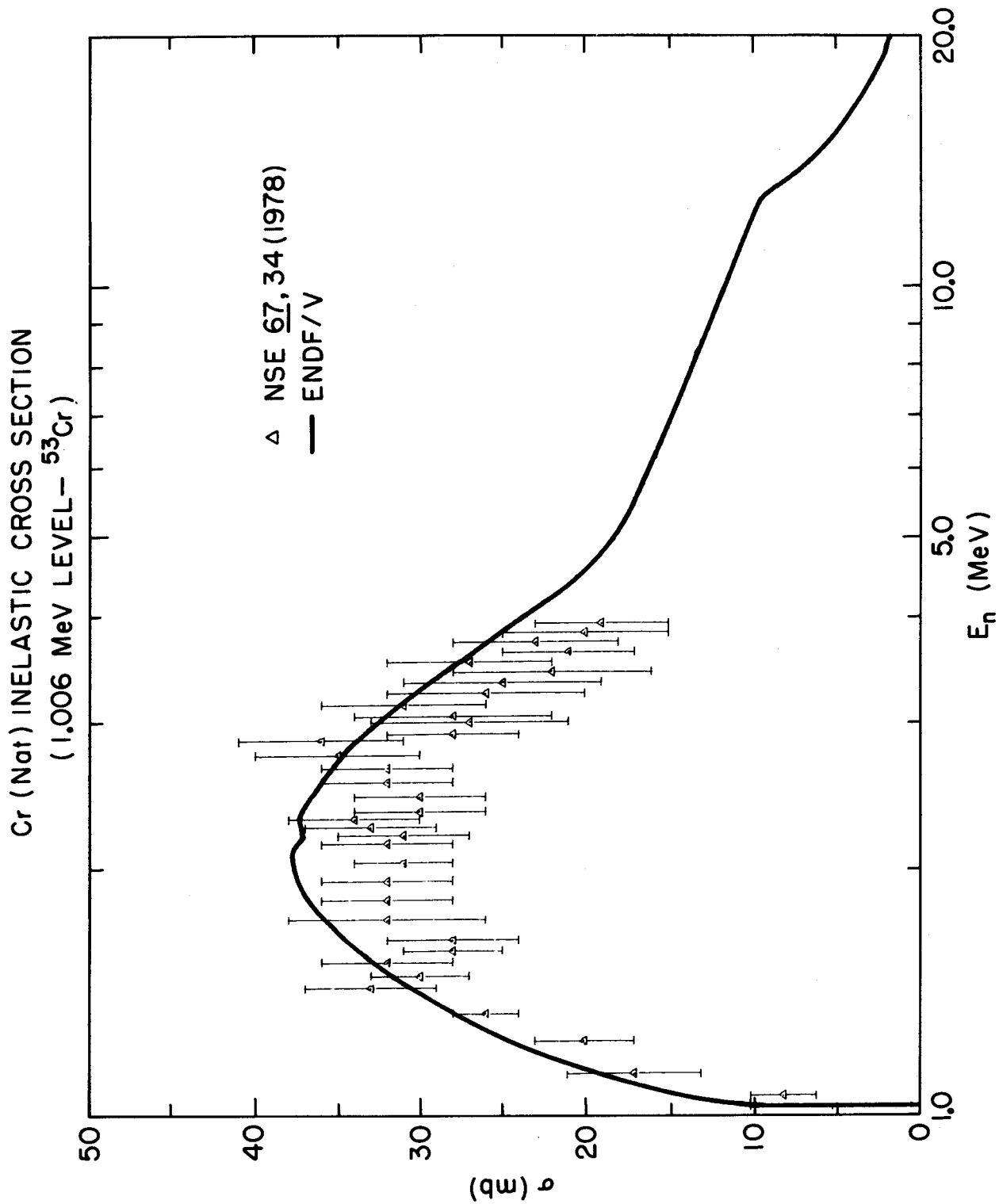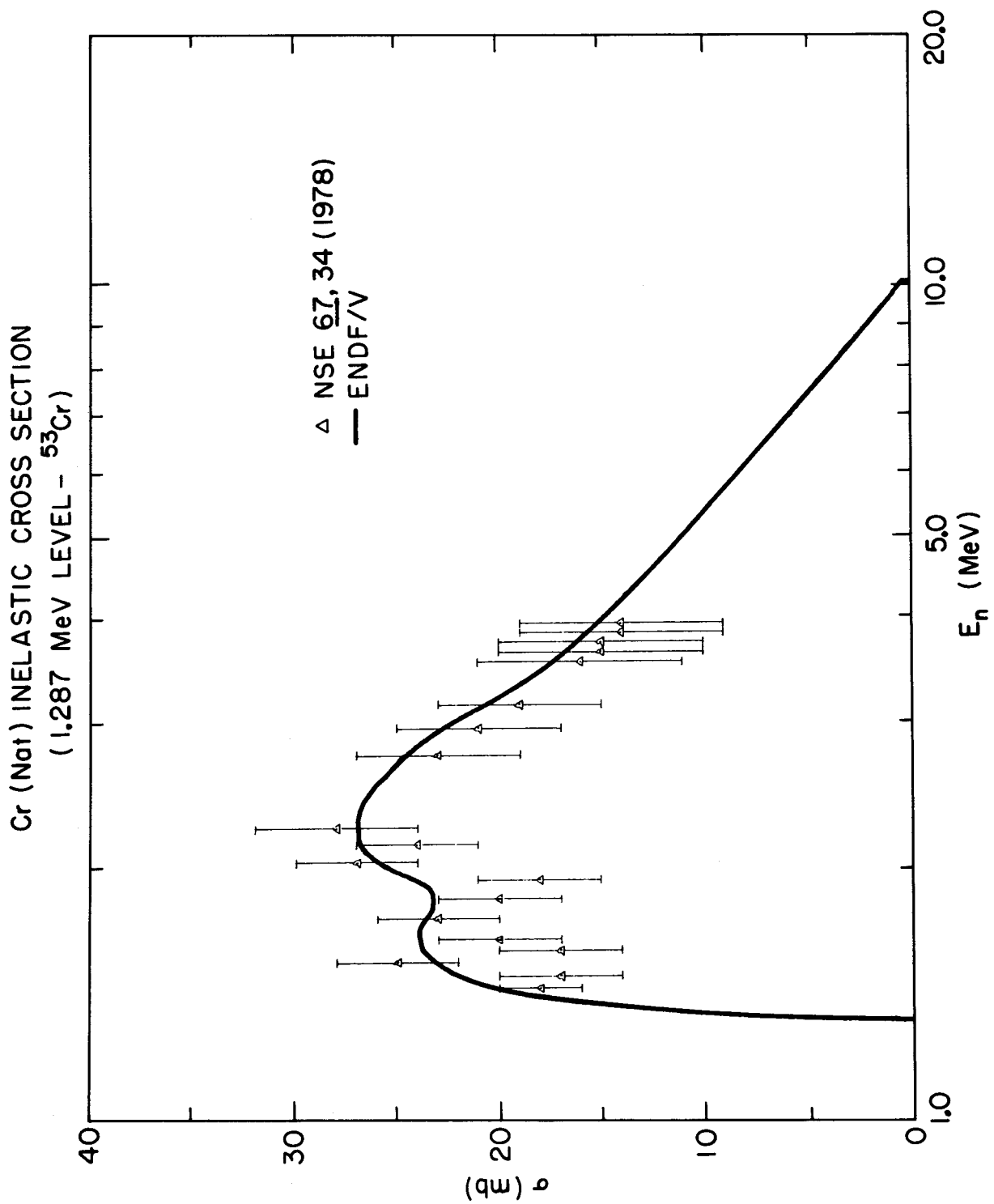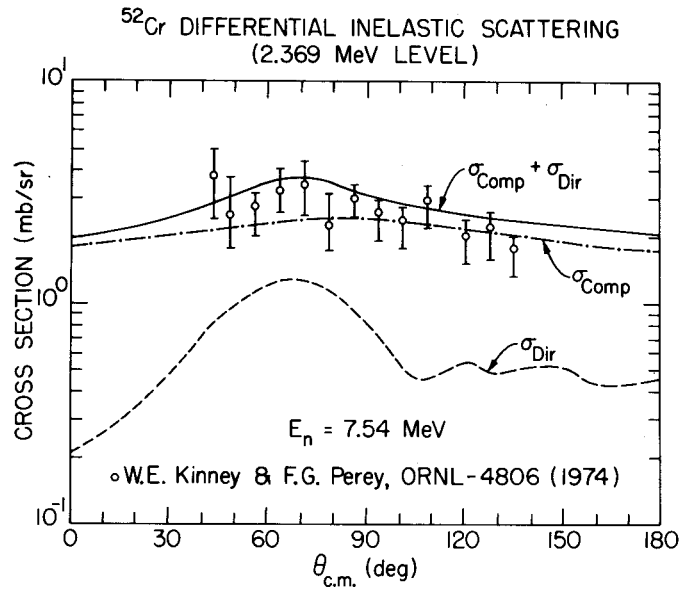
Figure 36.
- 54 -

Figure 37.

Figure 38.
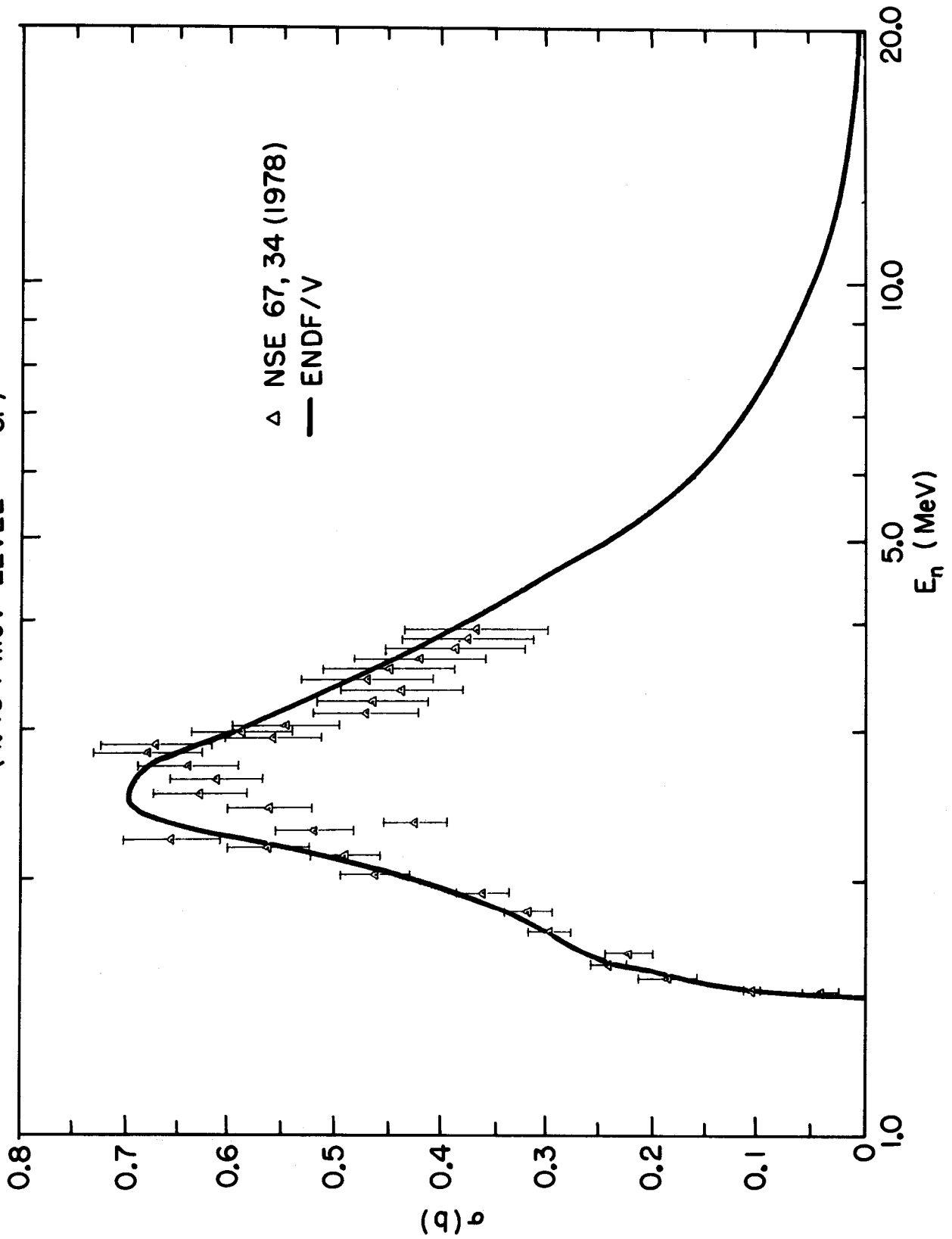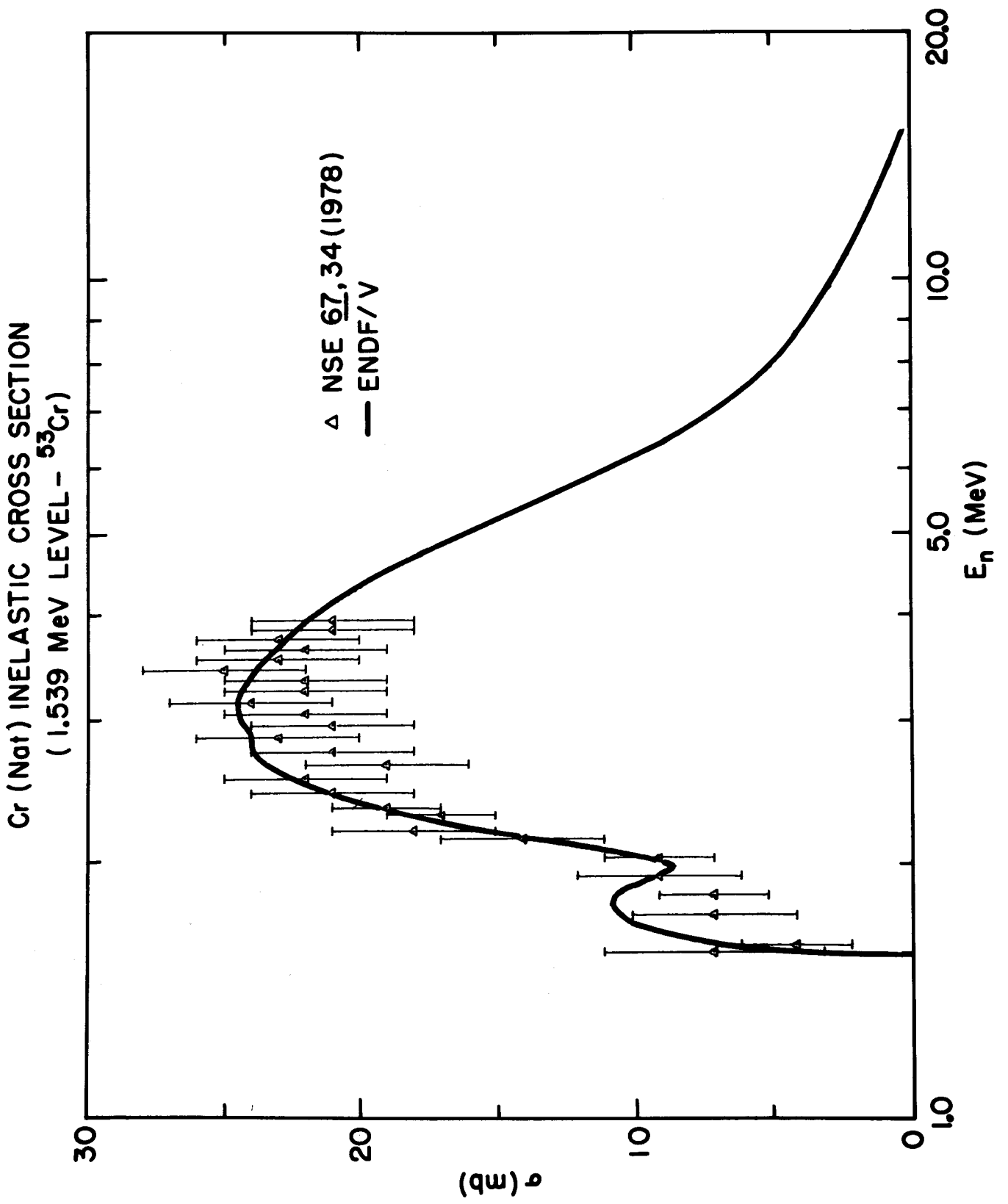
Figure 39.

Figure 40.
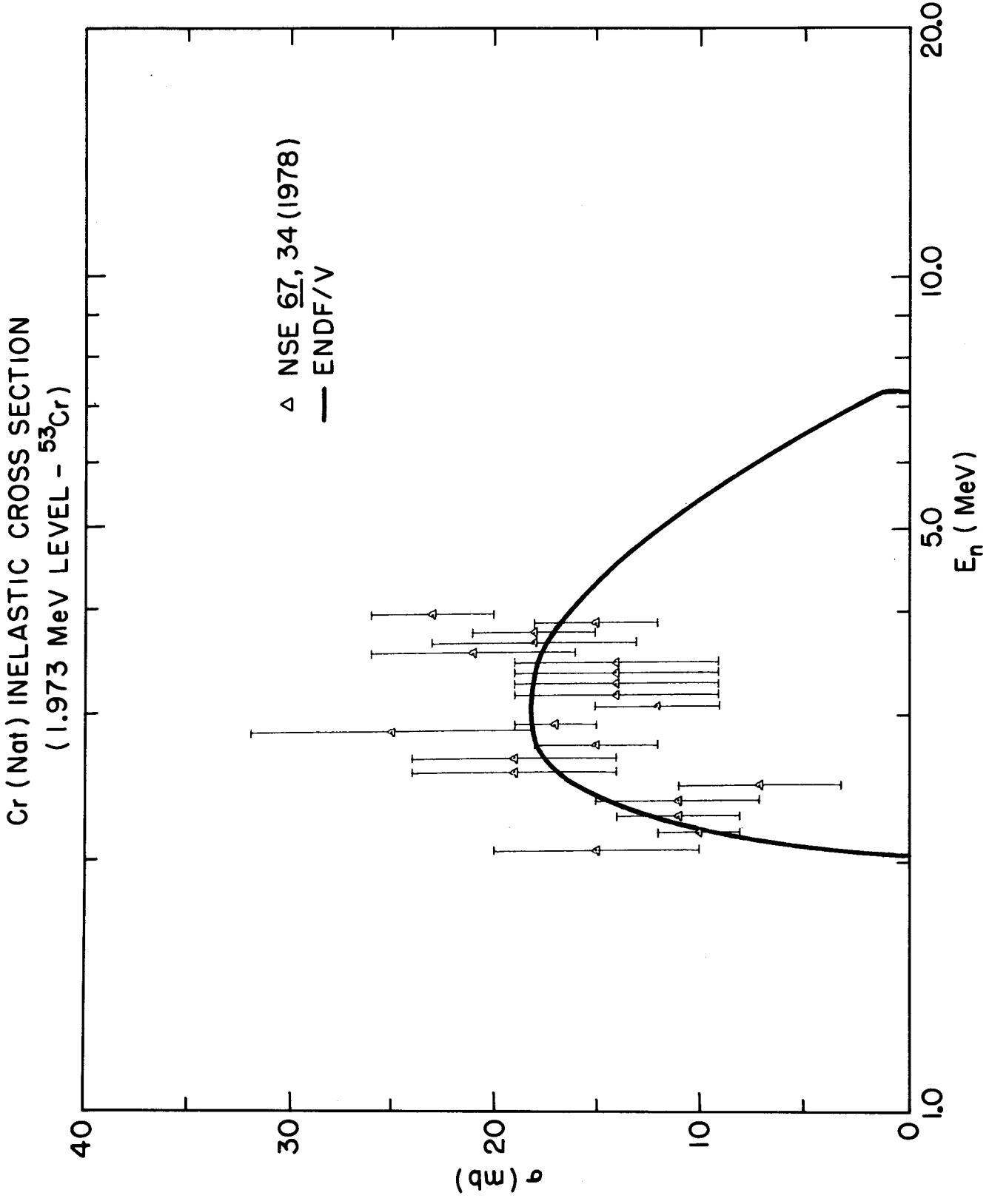
Figure 41.

Figure 42.

Cr (Nat) INELASTIC CROSS SECTION
(2.370 MeV LEVEL – ^{52}Cr)

$\triangle$ NSE $\underline{67}$, 34 (1978)
—— ENDF/V

E_n (MeV)

σ (mb)
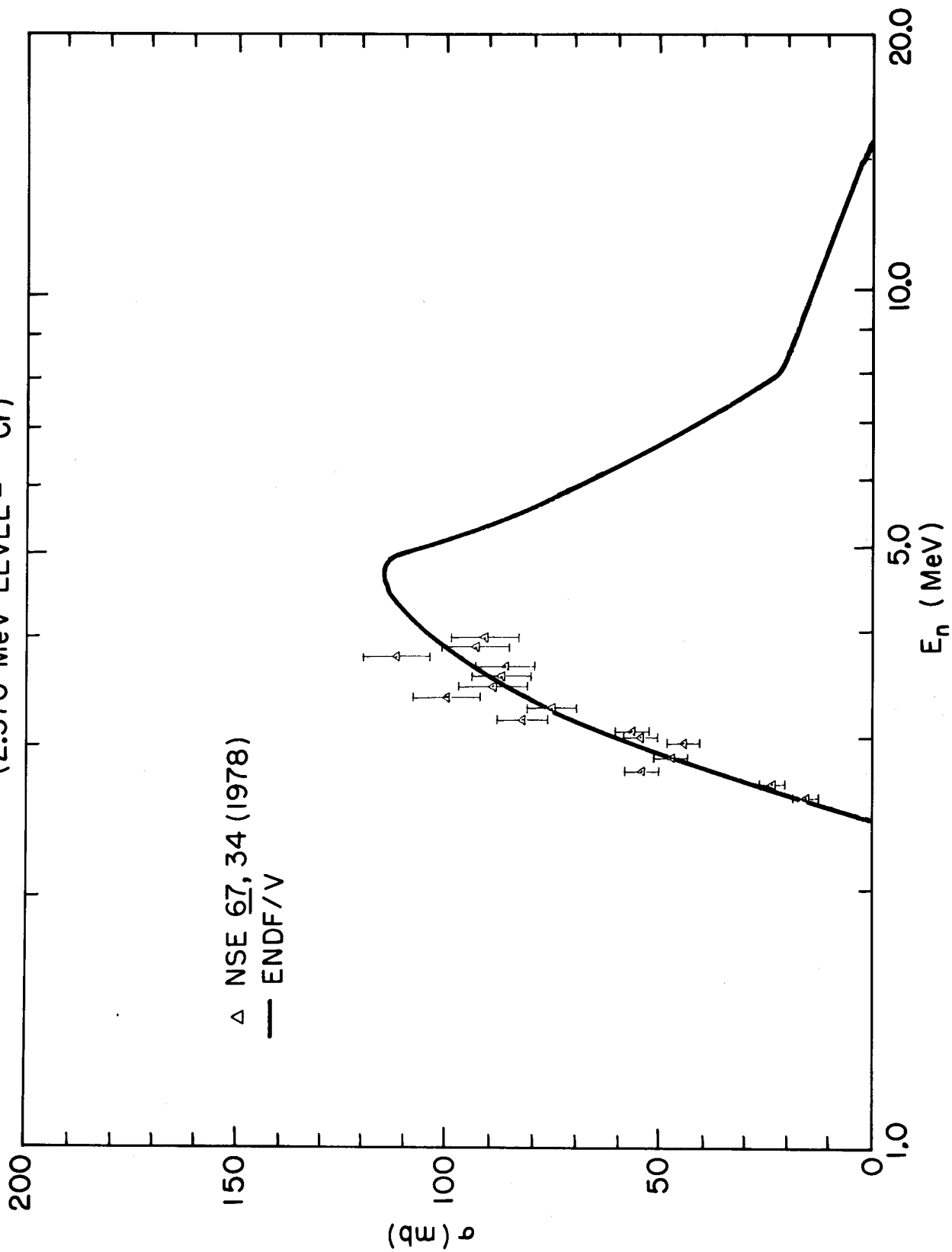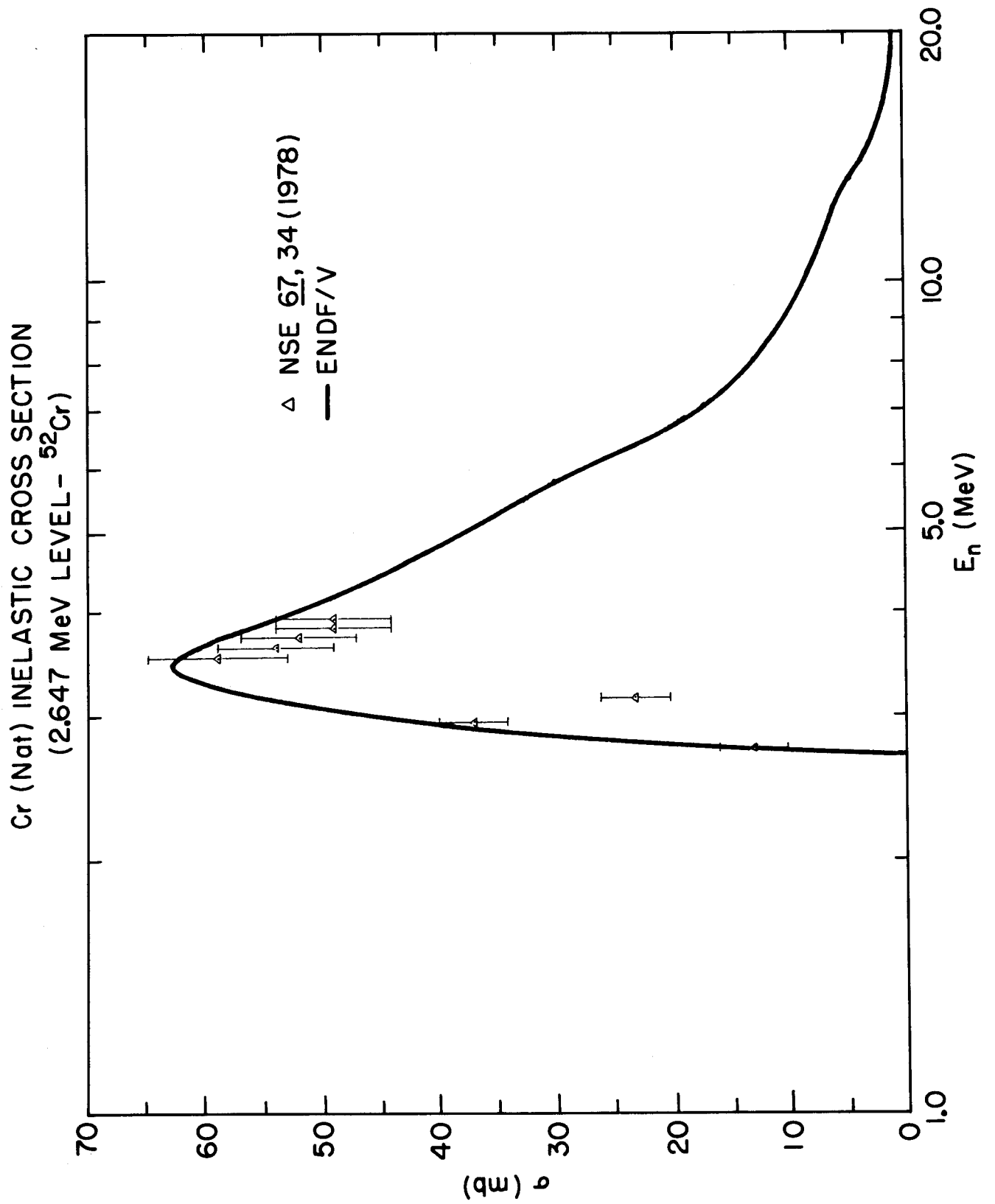
Figure 43.

Figure 44.
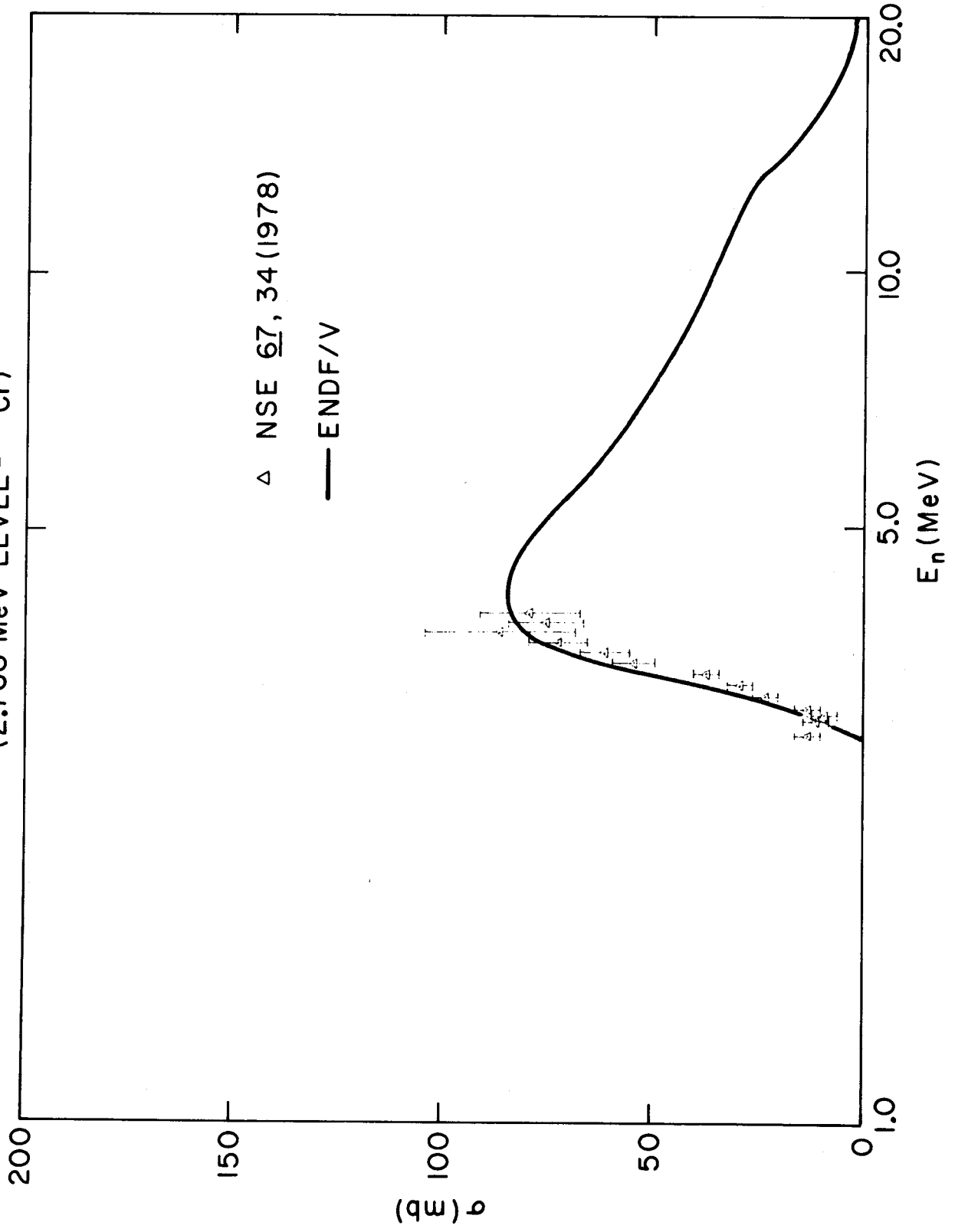
Figure 45.

Cr (Nat) INELASTIC CROSS SECTION
(2.965 MeV LEVEL – ^{52}Cr)

△ NSE 67, 34(1978)
— ENDF/V

E_n (MeV)

σ (mb)
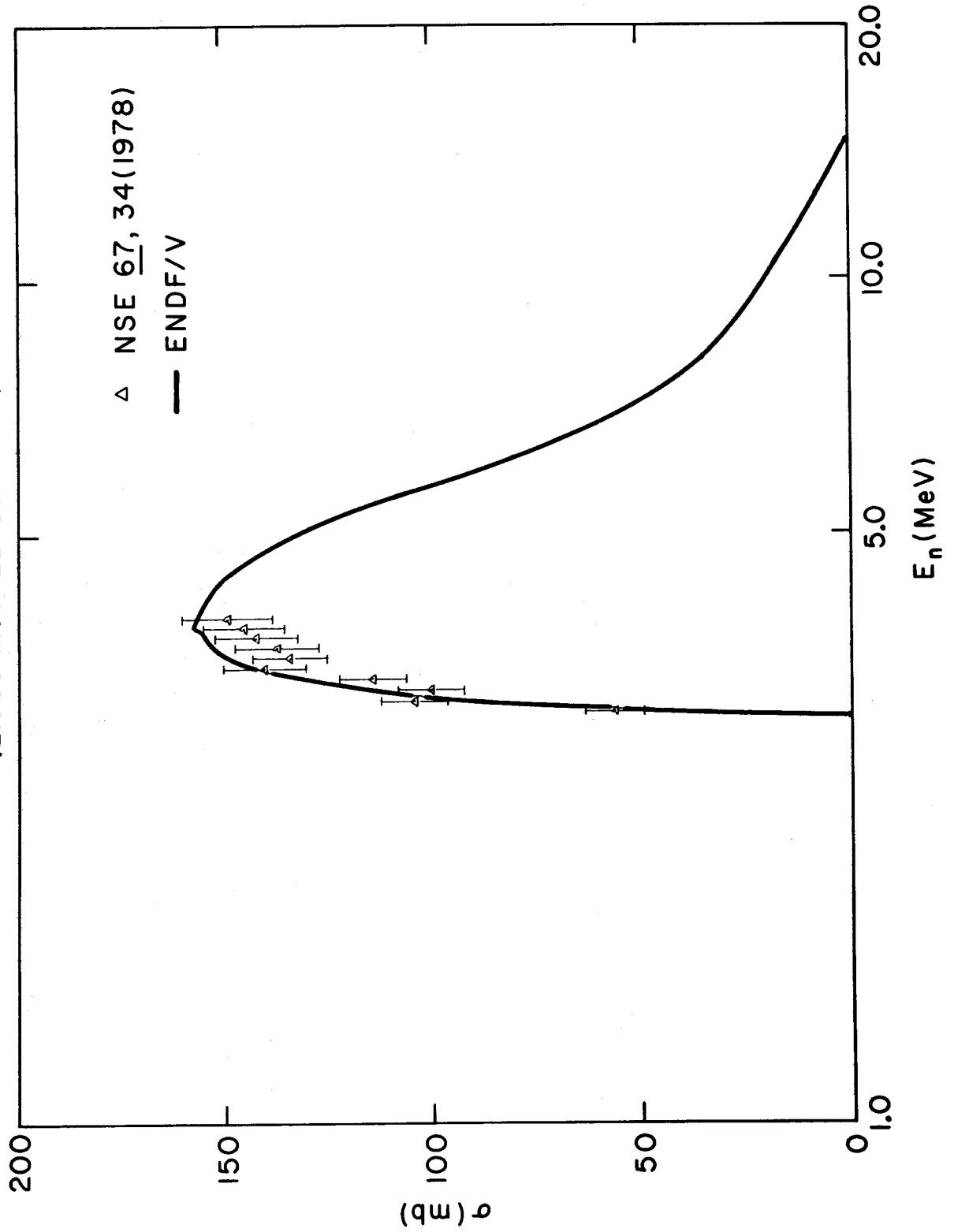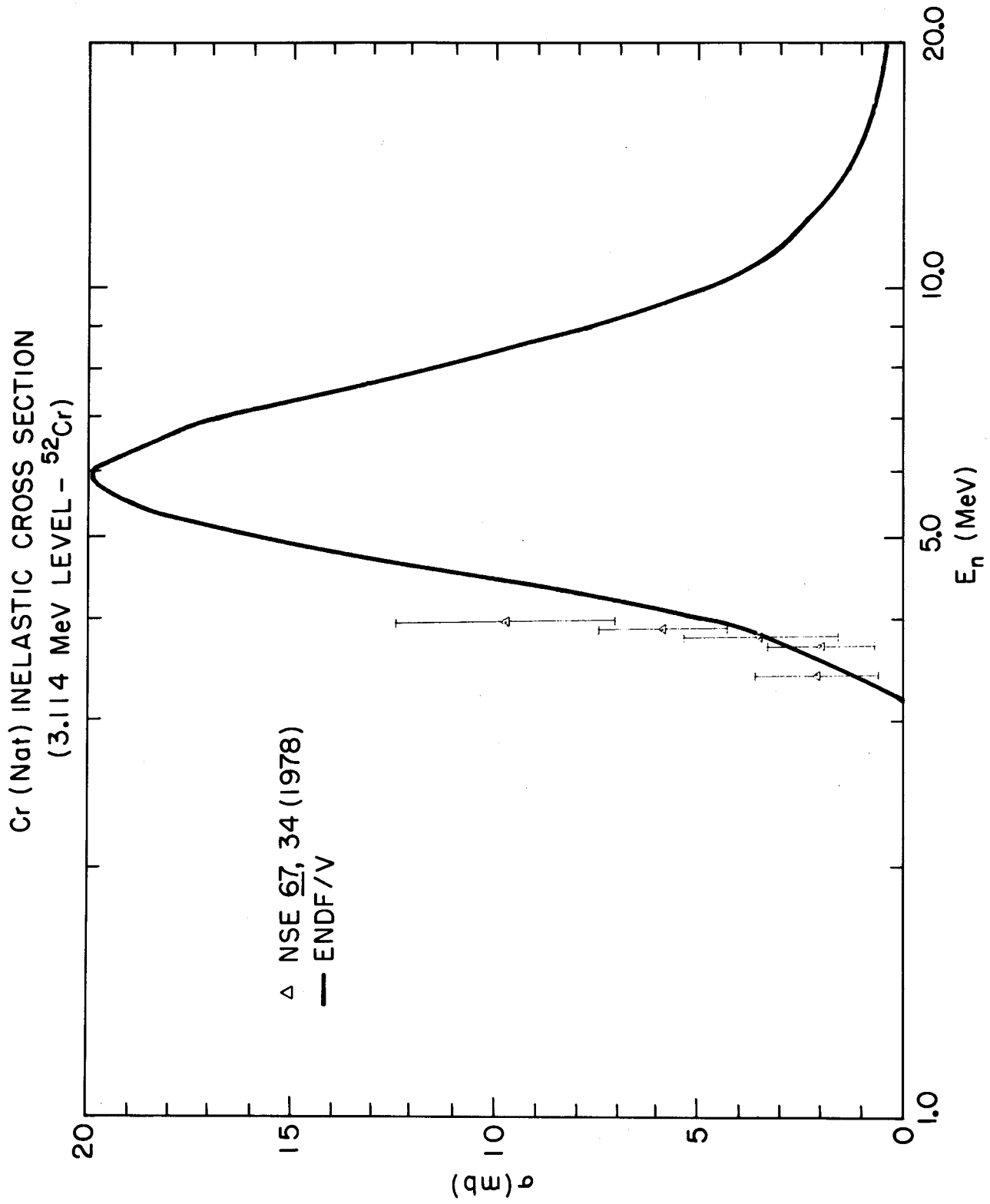
Figure 46.

Figure 47.

Cr (Nat) INELASTIC CROSS SECTION
(3.162 MeV LEVEL – ^{52}Cr)

△ NSE 67, 34 (1978)
—— ENDF/V
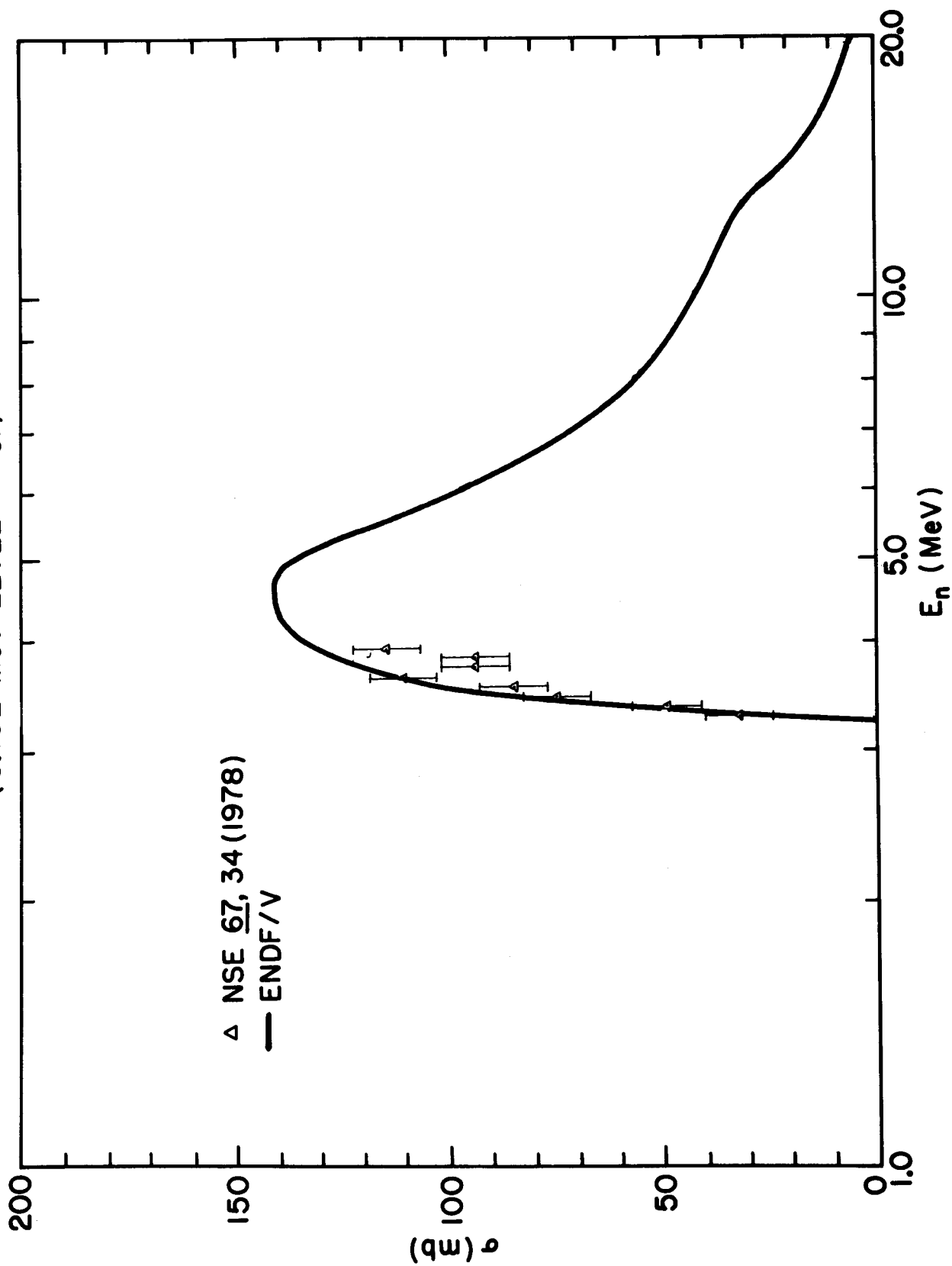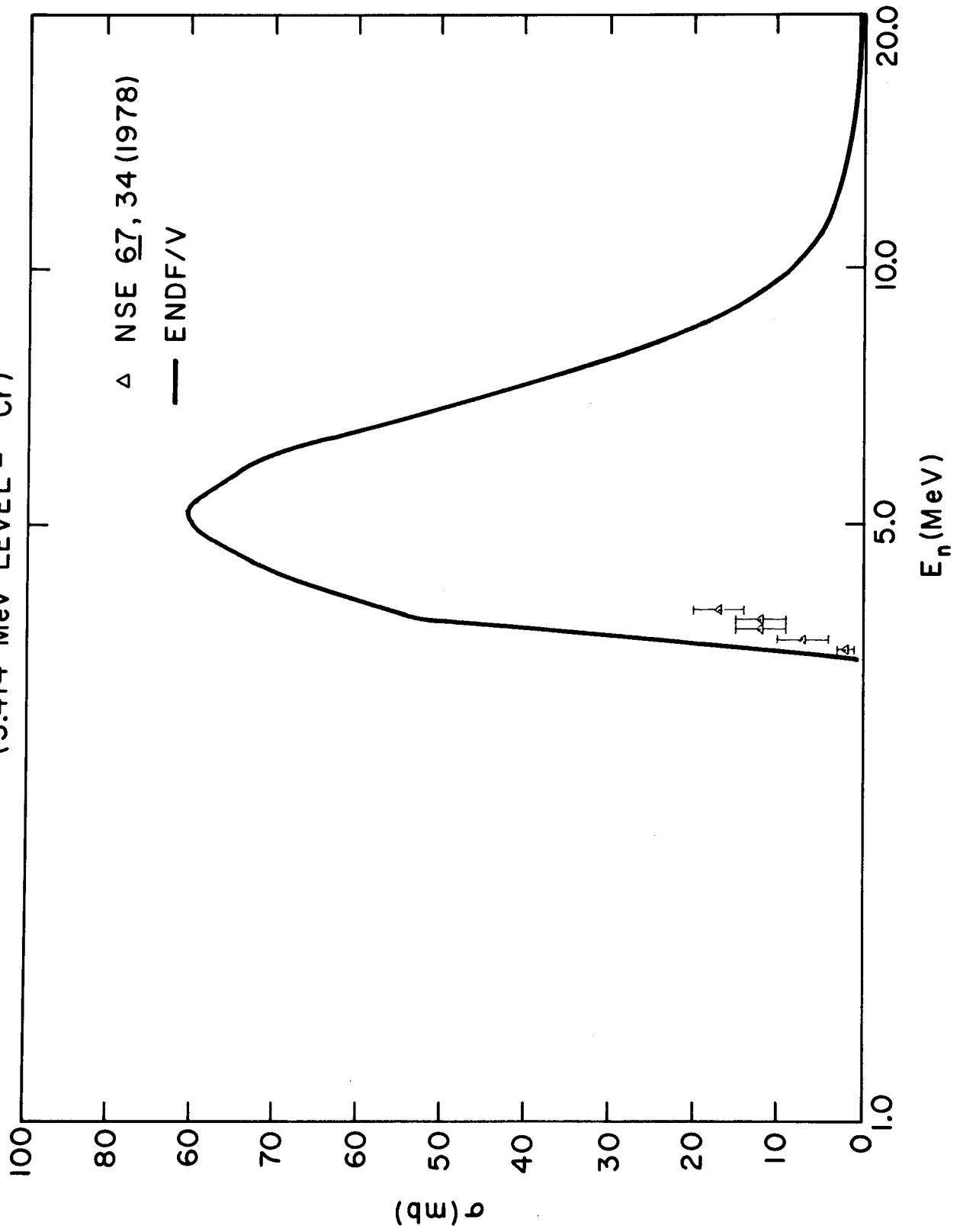
Figure 48.

Figure 49.

Cr (Nat) INELASTIC CROSS SECTION
(3.771 MeV LEVEL – ^{52}Cr)

△ NSE 67, 34 (1978)

—— ENDF/V

σ (mb)

E_n (MeV)

Figure 50.

Figure 51.

Figure 52.

^{52}Cr DIFFERENTIAL INELASTIC SCATTERING
(1.434 MeV LEVEL)

E_n = 6.44 MeV

○ W.E. Kinney & F.G. Perey, ORNL-4806 (1974)

$\sigma_{Comp} + \sigma_{Dir}$

σ_{Comp}

σ_{Dir}

Figure 53.

^{52}Cr DIFFERENTIAL INELASTIC SCATTERING
(1.434 MeV LEVEL)

E_n = 7.54 MeV

○ W.E. Kinney & F.G. Perey, ORNL-4806 (1974)

$\sigma_{Comp} + \sigma_{Dir}$

σ_{Comp}

σ_{Dir}

Figure 54.

- 71 -

^{52}Cr DIFFERENTIAL INELASTIC SCATTERING
(1.434 MeV LEVEL)

$E_n = 8.56$ MeV

○ W.E. Kinney & F.G. Perey, ORNL-4806 (1974)

$\sigma_{Comp} + \sigma_{Dir}$

σ_{Comp}

σ_{Dir}

CROSS SECTION (mb/sr)

$\theta_{c.m.}$ (deg)

Figure 55.

^{52}Cr DIFFERENTIAL INELASTIC SCATTERING
(2.369 MeV LEVEL)

$\sigma_{Dir} + \sigma_{Comp}$

σ_{Comp}

σ_{Dir}

$E_n = 6.44$ MeV

○ W.E. Kinney & F.G. Perey, ORNL-4806 (1974)

CROSS SECTION (mb/sr)

$\theta_{c.m.}$ (deg)

Figure 56.

^{52}Cr DIFFERENTIAL INELASTIC SCATTERING
(2.369 MeV LEVEL)

$\sigma_{Comp} + \sigma_{Dir}$

σ_{Comp}

σ_{Dir}

$E_n = 7.54$ MeV

∘ W.E. Kinney & F.G. Perey, ORNL-4806 (1974)

CROSS SECTION (mb/sr)

$\theta_{c.m.}$ (deg)

Figure 57.

^{52}Cr DIFFERENTIAL INELASTIC SCATTERING
(2.369 MeV LEVEL)

$\sigma_{Comp} + \sigma_{Dir}$

σ_{Comp}

σ_{Dir}

$E_n = 8.56$ MeV

∘ W.E. Kinney & F.G. Perey, ORNL-4806 (1974)

CROSS SECTION (mb/sr)

$\theta_{c.m.}$ (deg)

Figure 58.

- 73 -

Cr (NATURAL) DIRECT INELASTIC SCATTERING

$E_n = 14.0$ MeV

Expt'l pts. P.H.Stelson, et al, Nucl. Phys. 68, 97 (1965)

4.34 (3⁻) LEVEL

x 10

1.434 (2⁺) LEVEL

$\sigma(\theta)$ (mb/sr)

$\theta_{c.m.}$ (deg)
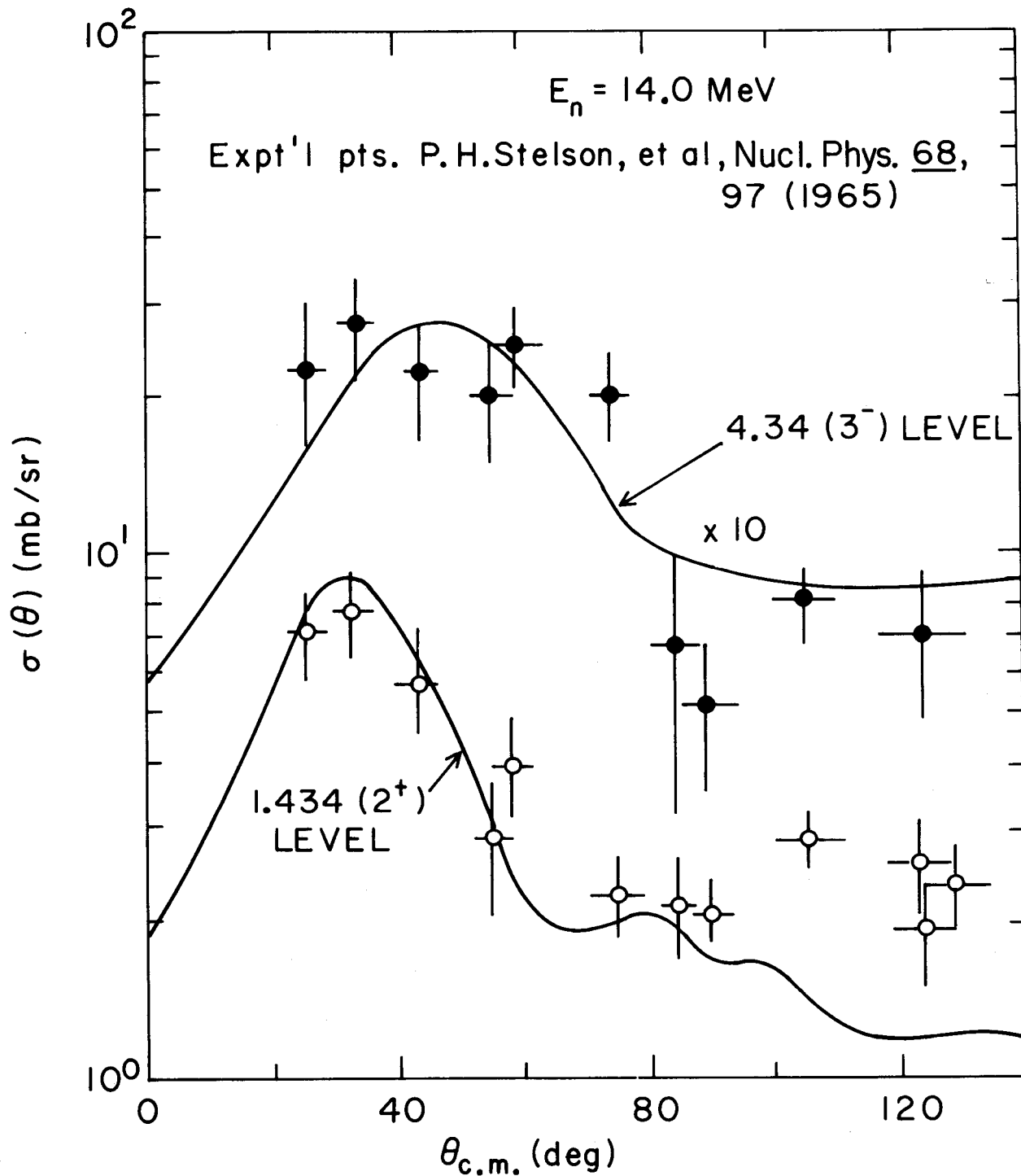
Figure 59.

REACTION CHAIN FOR ^{54}Cr(n,3n)
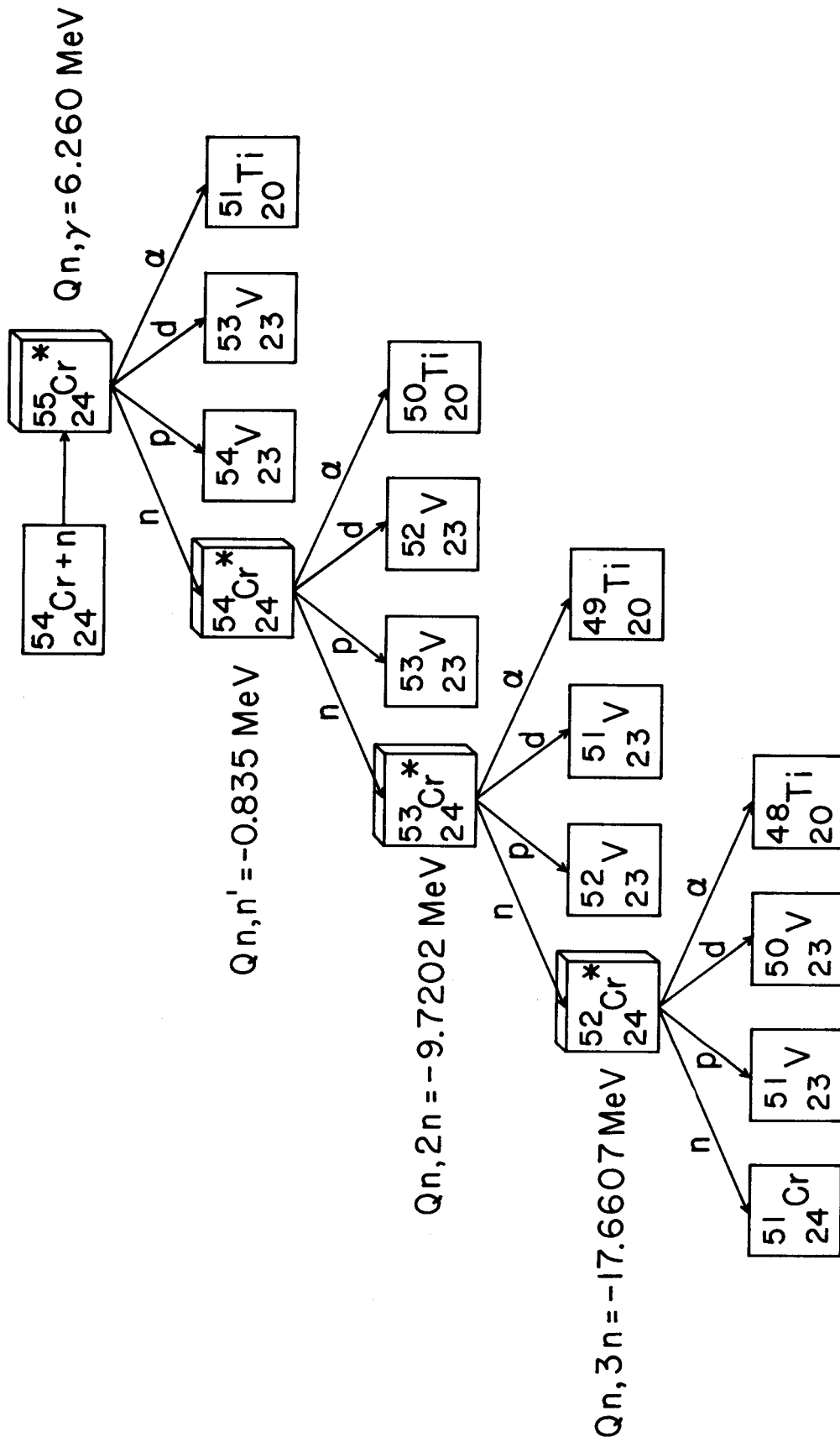
Figure 60.

(n,2n) CROSS SECTION FOR ^{50}Cr

- • Bormann. Priv. Comm. (Jan., 1965)
- ○ Mukherjee. Proc. Phys. Soc. (London) 77, 508 (1961)
- ■ Rayburn. Phys. Rev. 122, 168 (1961)
- □ Chittendon. Rept. (Arkansas, 1961)
- ▲ Khurana. Nucl. Phys. 28, 560 (1961)
- △ Araminowicz. INR-1464, 14 (1973)
- ▼ Qaim. Nucl. Phys. A185, 614 (1972)
- ▽ Holmberg. J. Inorg. Nucl. Chem. 36, 715 (1974)

^{50}Cr (n,2n)

CALCULATED

E_n (MeV)

$\sigma_{n,2n}$ (mb)
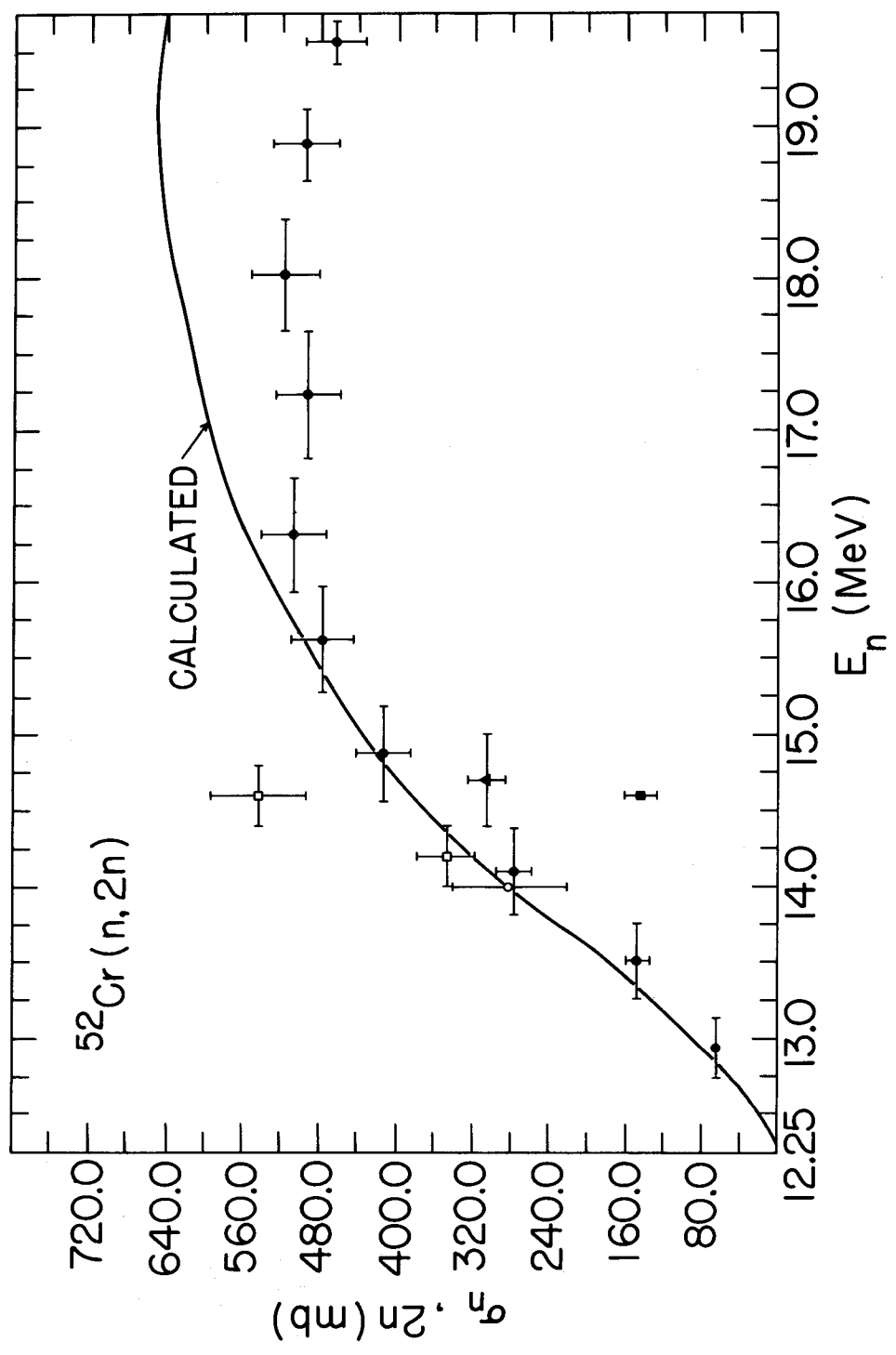
Figure 61.

Figure 62.

(n,2n) CROSS SECTION FOR NATURAL Cr.

• Frehaut and Mosinski.

Preprint – Trieste Conf. (Dec., 1975)
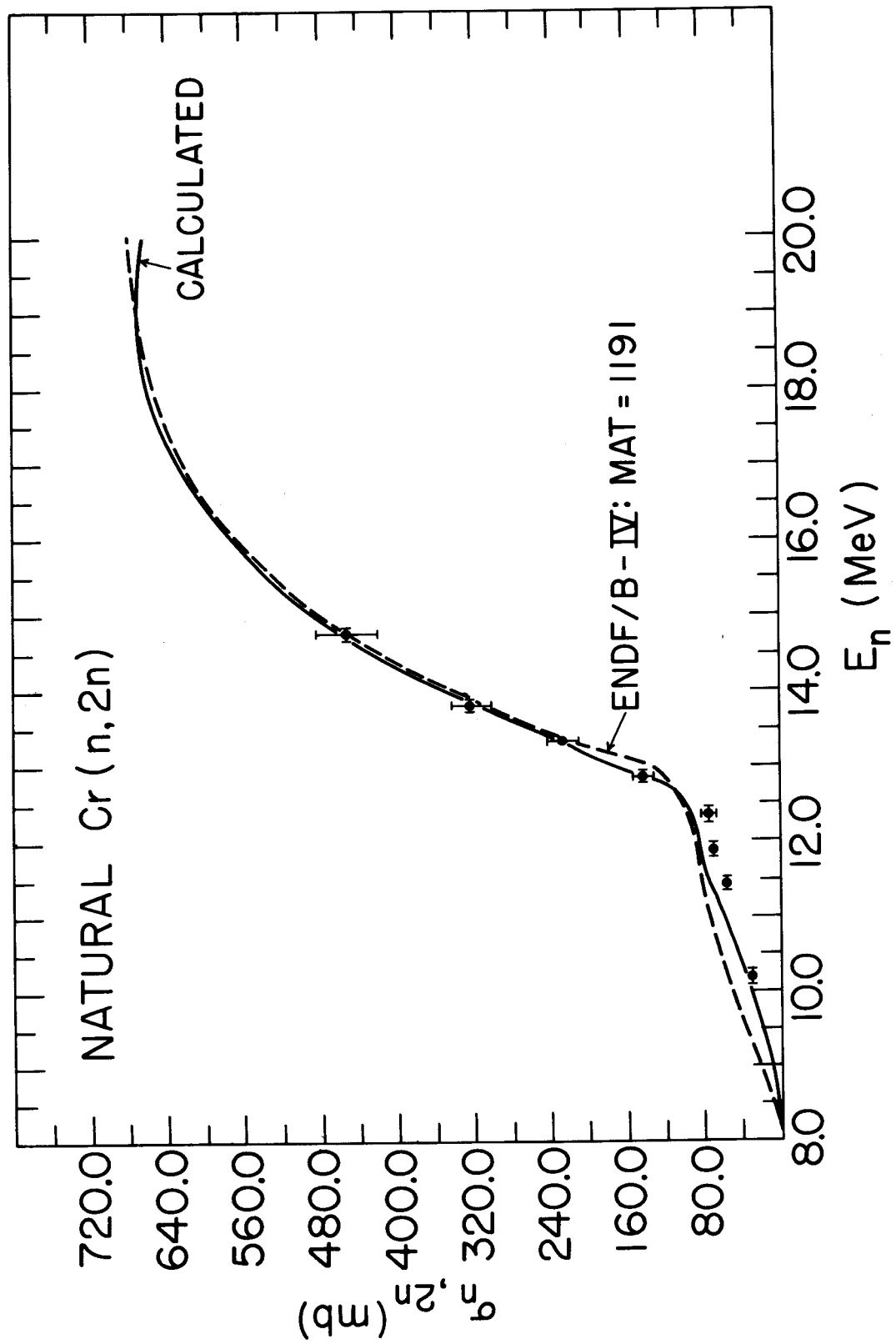
Figure 63.

(n,p) CROSS SECTION FOR ^{52}Cr

- • Kern. Nucl. Phys. <u>10</u>, 226 (1959)
- ○ I.G. Clator. Priv. Comm. from T. Clator (1969)
- ■ Paul. Can. J. Phys. <u>31</u>, 267 (1953)
- ▫ Husain. J. Inorg. Nucl. Chem. <u>29</u>, 2665 (1967)
- ▲ Chittenden. Rept. (Arkansas, 1961)
- △ Allan. Nucl. Phys. <u>24</u>, 274 (1961)
- ▼ Mitra. Nucl. Phys. <u>83</u>, 157 (1966)
- ▽ Mukherjee. Proc. Phys. Soc. (London) 77, 508 (1961)
- ✕ Dressler. INR-1464, 12 (1973)
- ▪ Khuruna. Nucl. Phys <u>69</u>, 153 (1965)
- ▫ Holmberg. J. Inorg. Nucl. Chem. <u>36</u>, 715 (1974)
- ◆ Aleksandrov. Sov. Atomic Energy <u>39</u>, 736 (1976)
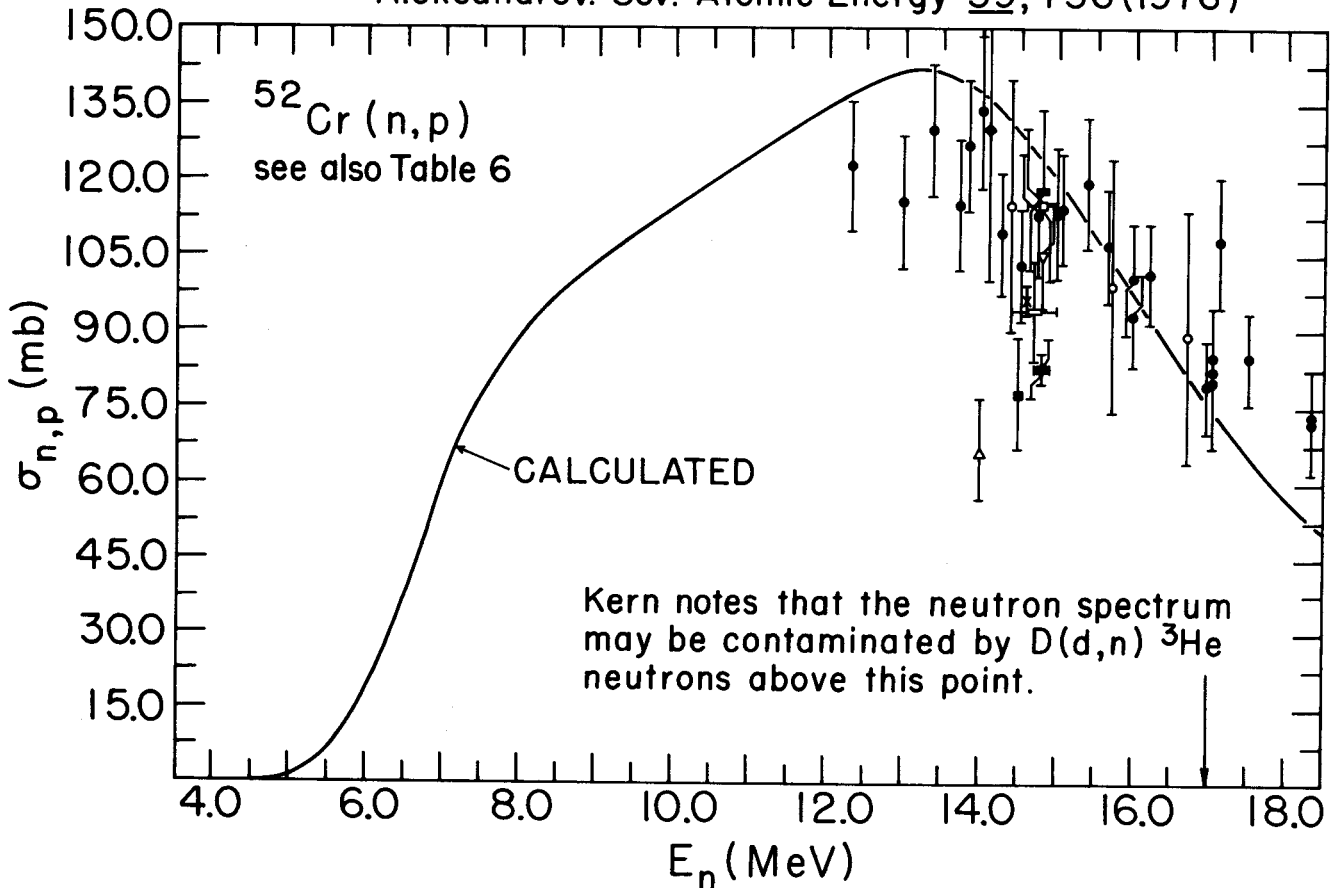
Figure 64.
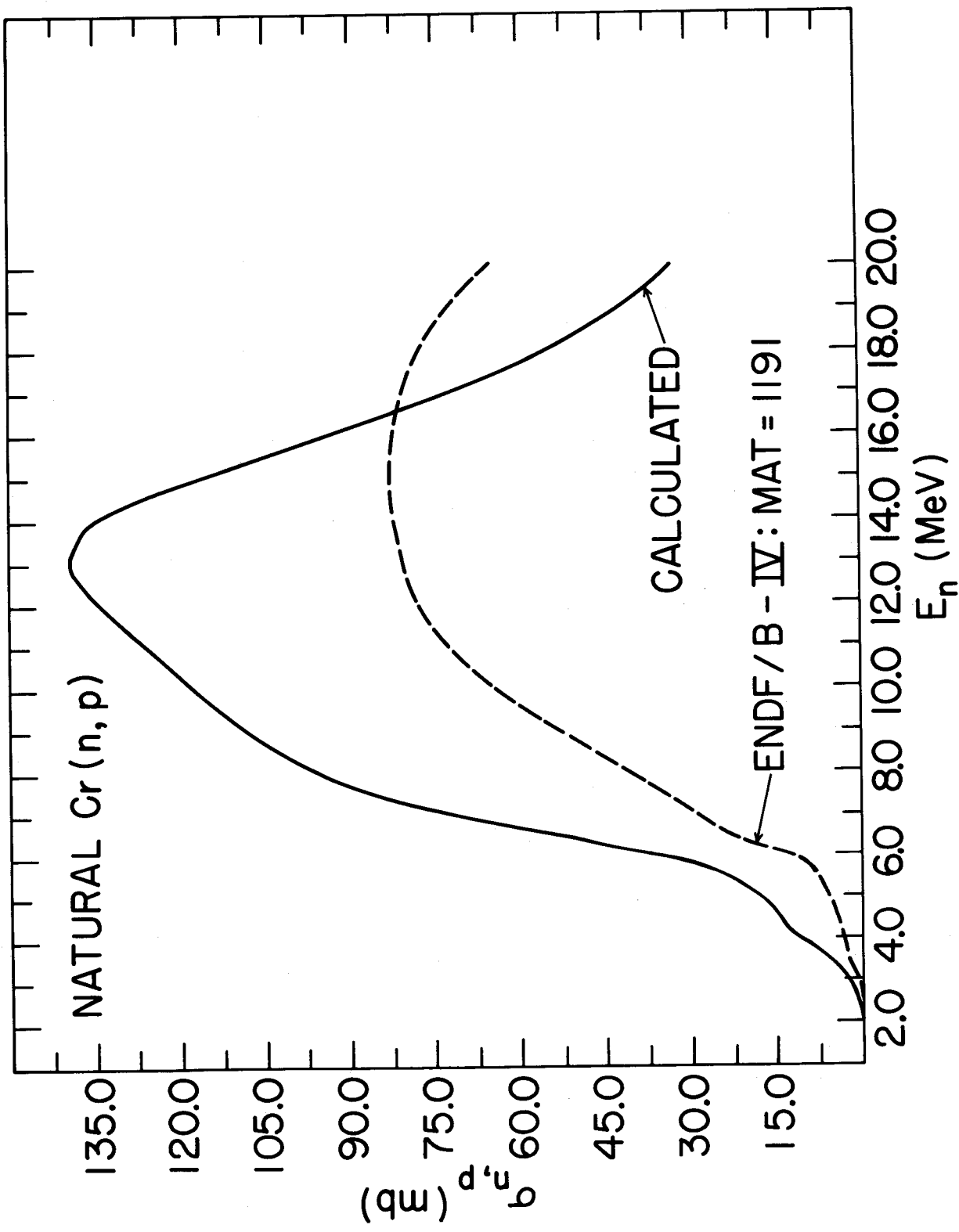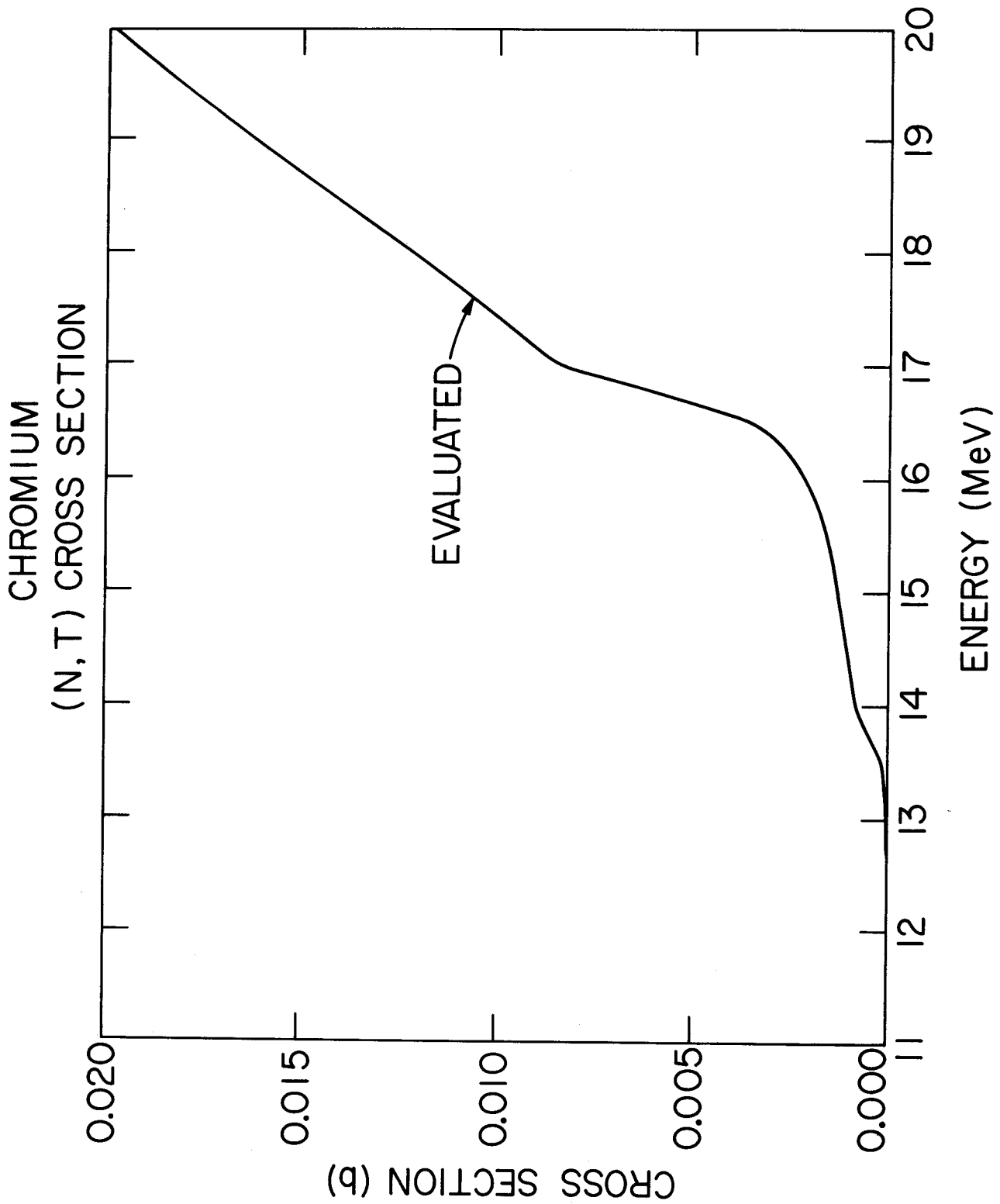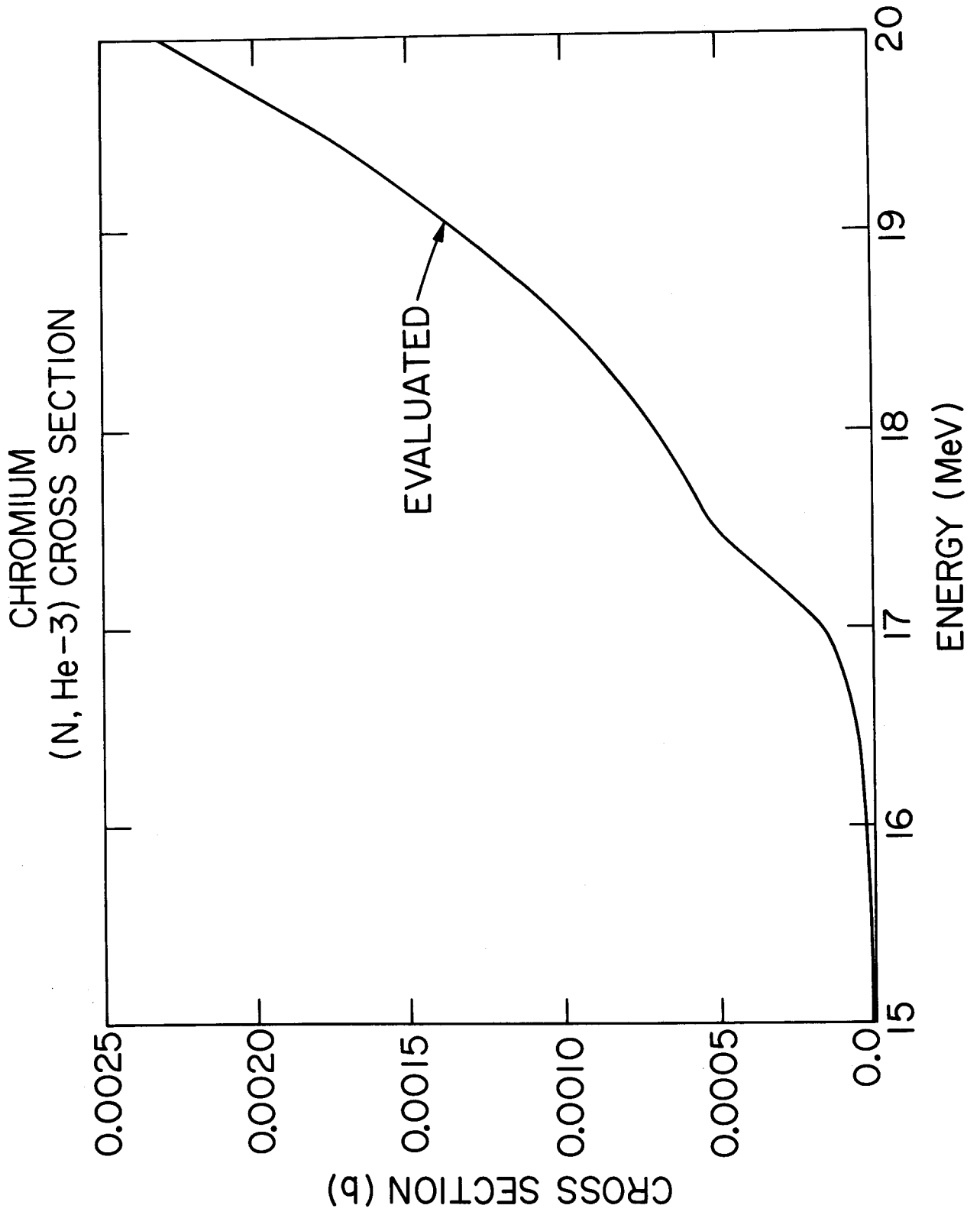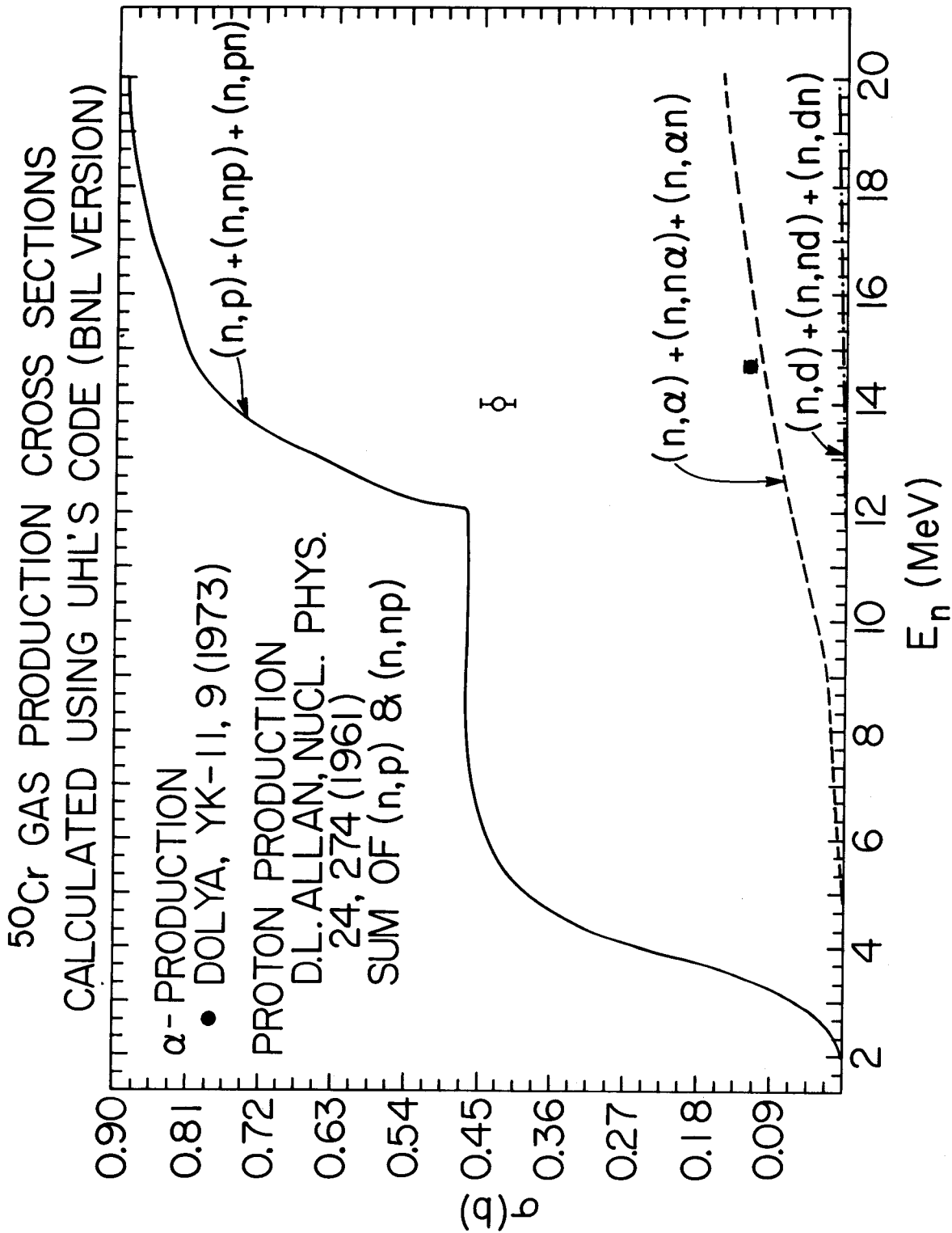
Figure 65.

CHROMIUM
(N,T) CROSS SECTION

Figure 66.

CHROMIUM
(N, He-3) CROSS SECTION

EVALUATED

Figure 67.

^{50}Cr GAS PRODUCTION CROSS SECTIONS
CALCULATED USING UHL'S CODE (BNL VERSION)

α- PRODUCTION
● DOLYA, YK-II, 9 (1973)
PROTON PRODUCTION
D.L. ALLAN, NUCL. PHYS.
24, 274 (1961)
SUM OF (n,p) & (n,np)

(n,p) + (n,np) + (n,pn)

(n,α) + (n,nα) + (n,αn)

(n,d) + (n,nd) + (n,dn)

E_n (MeV)

σ(b)

Figure 68.

- 83 -
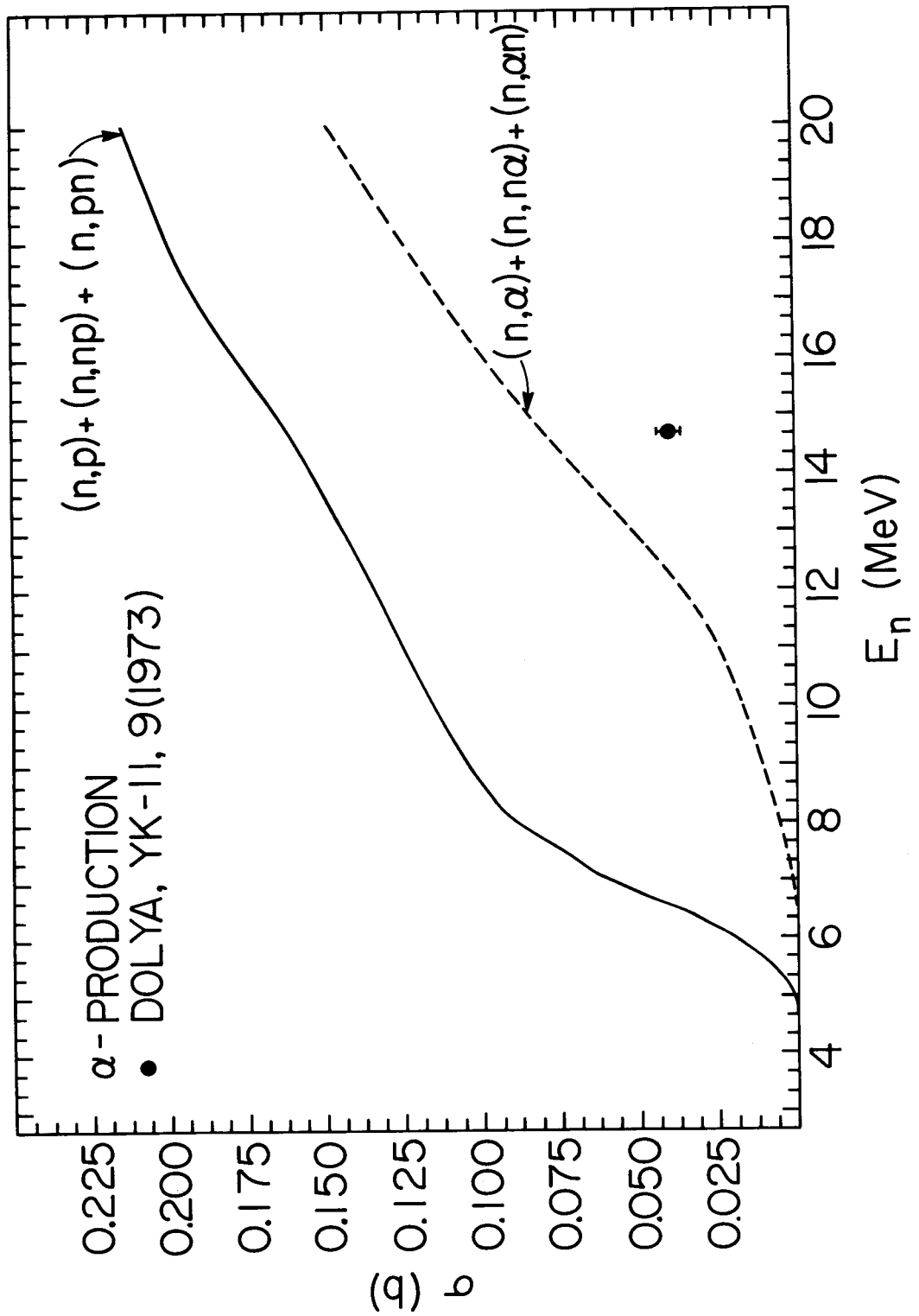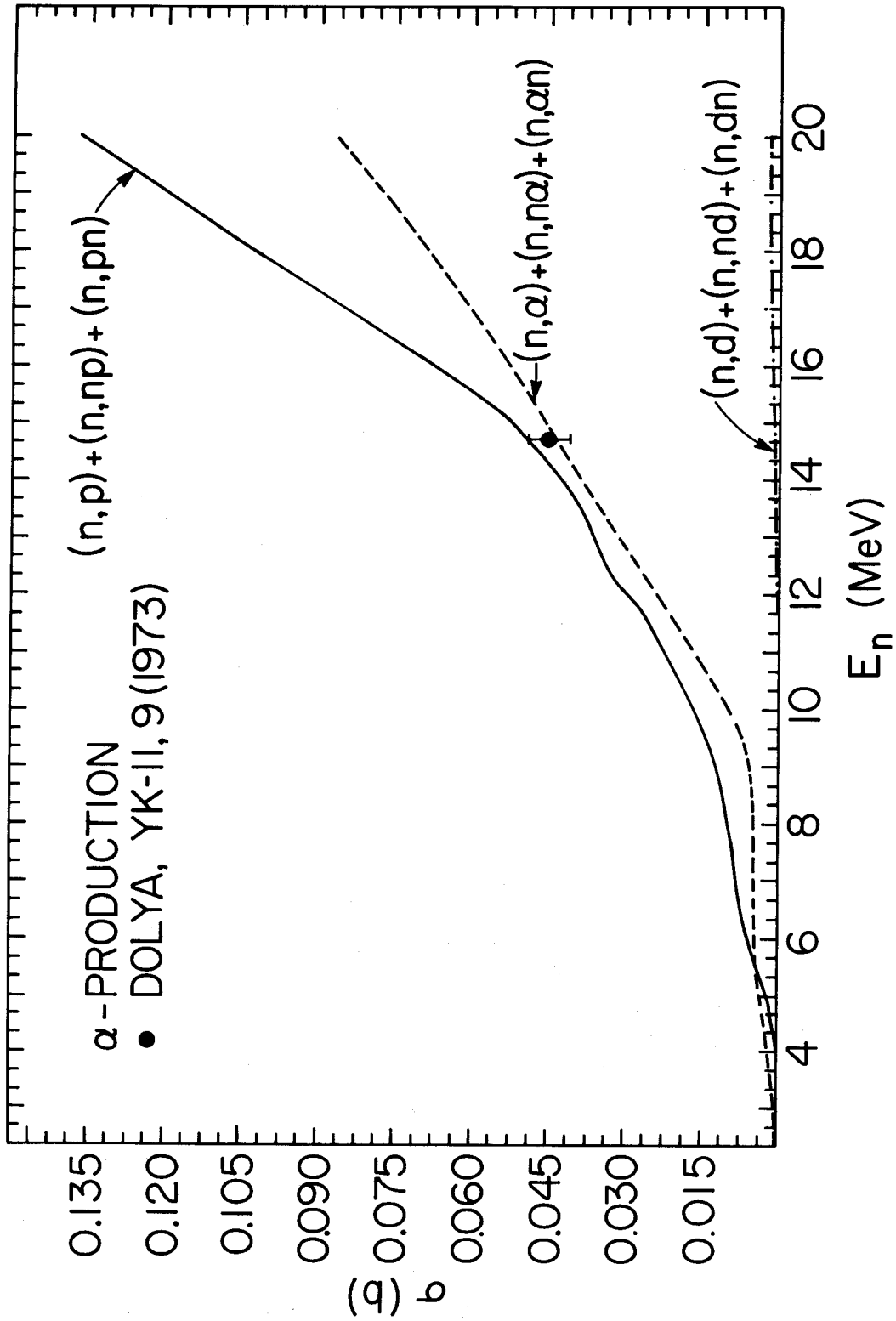
Figure 69.

Figure 70.

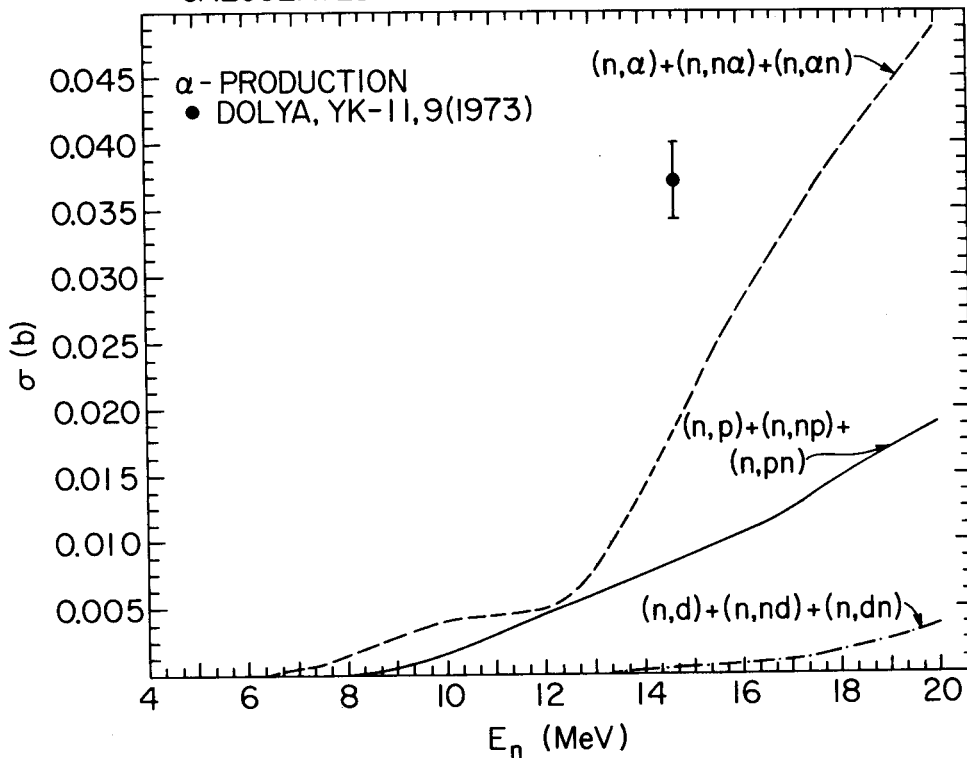**54GAS PRODUCTION CROSS SECTIONS CALCULATED USING UHL'S CODE (BNL VERSION)**

Figure 71.

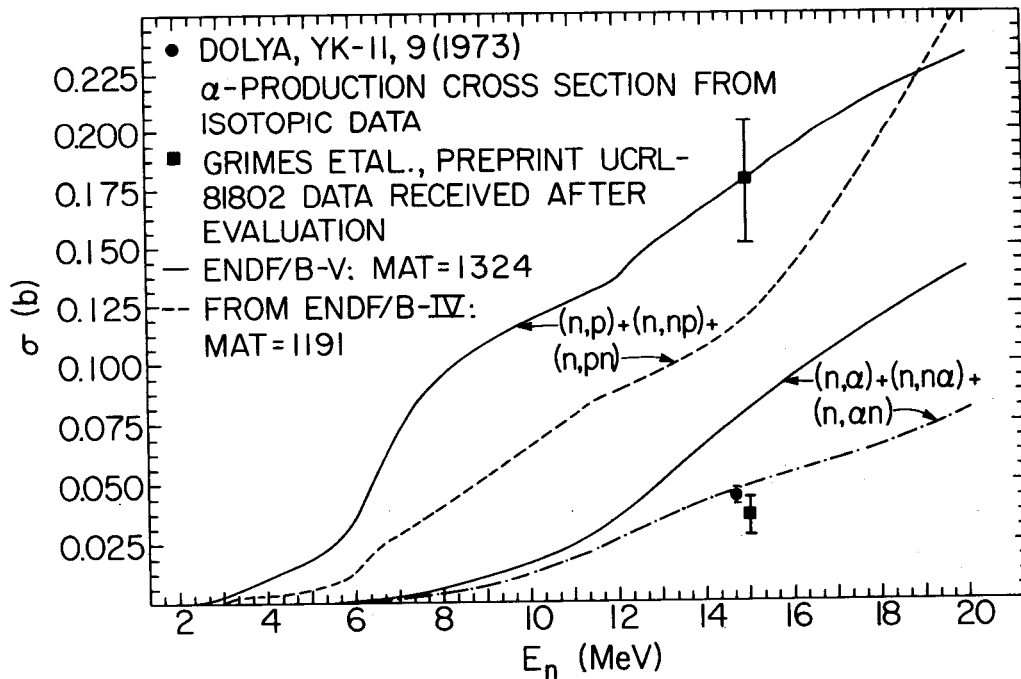**NATURAL CHROMIUM GAS PRODUCTION CROSS SECTIONS (BNL VERSION)**

Figure 72.